INSTITUT FÜR INFORMATIK

2D Signal Analysis by Generalized Hilbert Transforms

Oliver Fleischmann
Betreuer: Lennart Wietzke

Diplomarbeit
August 2008

CHRISTIAN-ALBRECHTS-UNIVERSITÄT

ZU KIEL

Erklärung

Hiermit versichere ich, die vorliegende Diplomarbeit ohne Hilfe Dritter und nur mit den angegebenen Quellen und Hilfsmitteln angefertigt zu haben. Alle Stellen, die aus den Quellen entnommen wurden, sind als solche kenntlich gemacht worden. Diese Arbeit hat in gleicher oder ähnlicher Form noch keiner Prüfungsbehörde vorgelegen.

Kiel, den 27. August 2008 Oliver Fleischmann

Danksagung

Am Ende meiner Diplomarbeit und meines Studiums möchte ich all jenen danken, die mich während der letzten Jahre unterstützt haben.
Dabei danke ich zunächst Prof. Gerald Sommer für seine fachliche Kompetenz und seine Unterstützung beim wissenschaftlichen Arbeiten an seinem Lehrstuhl. Von Beginn der Diplomarbeit an stand mir direkt am Lehrstuhl ein Platz in einem Büro zur Verfügung, der ein angnehmes Arbeiten in der Gruppe ermöglichte. Zu besonderem Dank bin ich meinem Betreuer Lennart Wietzke verpflichtet, der mir stets bei Fragen zur Seite stand und der in anregenden Diskussionen den Verlauf der Diplomarbeit förderte. Zudem danke ich allen weiteren Mitarbeitern am Lehrstuhl für Kognitive Systeme für das angenheme Arbeitsklima und die Integration in die Gruppe.
Prof. Thomas Wilke möchte ich dafür danken, dass ich während eines Großteils meiner Studienzeit an seinem Lehrstuhl als Techniker tätig sein konnte.
Von ganzem Herzen danke ich meinen Eltern für die moralische und finanzielle Unterstützung während des Studiums. Ferner gilt besonderer Dank meinem Bruder Lennart für das Korrekturlesen der Diplomarbeit.

Contents

1 Introduction **9**

2 Clifford Analysis **11**
2.1 Monogenic functions 11
2.2 Generalized Hilbert transforms 13
2.2.1 Cauchy integral formula 13
2.2.2 Riesz transforms 16
2.2.3 Plemelj-Sokhotzki formula 18

3 The Riesz transform in terms of the Radon transform **23**
3.1 Properties of the Radon transform 26
3.2 Analysis of i1D signals 28
3.3 Analysis of superposed i1D signals 32

4 The monogenic curvature tensor **37**
4.1 Basic differential geometry 37
4.2 Analysis of i1D signals 41
4.3 Analysis of superposed i1D signals 42
4.4 Second Order Riesz transform convolution kernels 46
4.5 Third Order Riesz transform convolution kernels 51
4.6 Discussion of the monogenic curvature tensor 54

5 The conformal monogenic signal **59**
5.1 Analysis of i1D signals 62
5.2 Analysis of superposed i1D signals 63
5.3 Analysis of circular signals 66
5.4 Phase analysis 72
5.5 The Hilbert transform on $\mathbb{S}^n$ 76
5.6 Application of the Hilbert transform on $\mathbb{S}^2$ 78
5.7 The Hilbert transform on $\mathbb{S}^3$ 83
5.8 Application: Normal and Gaussian curvature 85

6 Conclusion and outlook **91**

1 Introduction

This thesis deals with low-level image processing to analyze features such as orientation, phase and curvature of certain signal models. The analysis of low-level features is the building block to construct detectors for higher-level structures like corners and edges. Common edge and corner detectors are based on methods involving derivatives (see e.g. [22, 25, 33]). Since operators based on derivatives are often sensitive to noise and illumination changes one may focus on alternative techniques. One of these alternatives are operators contained in the class of so called *generalized Hilbert transforms*. These operators arise in the context of Clifford analysis as the non-tangential boundary values of the Cauchy-transform ([12, 5, 6]). The well known Hilbert transform and the Riesz transform are just two operators contained in this class. The Hilbert transform has widely been studied and used in one-dimensional signal processing. Dennis Gabor used the Hilbert transform to construct the so called analytic signal in order to obtain the local phase of one-dimensional signals [17].Michael Felsberg extended the idea of the analytic signal with a generalization of the Hilbert transform called the Riesz transform to construct the monogenic signal ([15, 14, 16]). The monogenic signal allows the determination of the orientation and local phase for intrinsically one-dimensional (i1D) image structures. Based on the monogenic signal Di Zang constructed a tensor pair with entries consisting of second and third order Riesz transforms which was supposed to determine differential geometric quantities such as the Gaussian and the mean curvature in addition to the features obtained by the monogenic signal [32].

Although the monogenic signal turned out to determine the local phase and orientation of i1D signals, it was a difficult task to understand what the Riesz transform was actually doing. This thesis focuses on the understanding of the Riesz transform via the Radon transform, the detailed study of the monogenic curvature tensor and higher order Riesz transforms and the construction and analysis of the lately introduced signal model called the conformal monogenic signal [30].

The mathematical basis is introduced in chapter 2 in the context of Clifford analysis. It provides the framework to generalize the Hilbert transform to arbitrary sufficiently smooth closed surfaces in $\mathbb{R}^n$. Furthermore it contains the theorems establishing the link between the generalized Hilbert transform in $\mathbb{R}^n$ and the Radon transform .

Based on this mathematical background chapter 3 establishes the link between the Radon transform and the Riesz transform to study and obtain a descriptive and imaginative understanding of the Riesz transform. This understanding is used to determine orientation, local phase and the apex angle of intrinsically one-dimensional signals and their superposition under certain constraints.

Using this knowledge the monogenic signal and the monogenic curvature tensor are analyzed in detail in chapter 4. Exact convolution kernels for the second and third order Riesz transforms are calculated in the Poisson scale space of the spatial domain to avoid

the calculation in the Fourier domain. It is shown that the monogenic curvature tensor does not represent any differential geometric quantities. Nonetheless it is proven that the tensor pair is able to obtain the orientation, phase and apex angle of i1D and superimposed i1D signals.
Following the idea of generalizing the Hilbert transform to higher dimensions the lately introduced conformal monogenic signal [30] is analyzed in detail in chapter 5. It projects a two-dimensional signal to the Riemann sphere in $\mathbb{R}^3$ in order to lift up the signal to a higher dimensional space. By applying the Riesz transform in $\mathbb{R}^3$ it is proven that the conformal monogenic signal contains the monogenic signal as a subset and furthermore provides additional information in terms of isophote curvature and an additional phase for plane waves in $\mathbb{R}^3$ which allows the analysis of a certain class of structures in $\mathbb{R}^2$.

2 Clifford Analysis

This chapter is intended to provide the mathematical background for this thesis. It gives a brief overview of Clifford analysis which includes differentiability properties and the fundamental integral theorems which are of interest in the following chapters.
The starting point is the construction of the universal *Clifford algebra* $\mathbb{R}_{0,n}$ over the vector space $\mathbb{R}^{0,n}$ which is the real vector space $\mathbb{R}^n$ equipped with a non-degenerate quadratic signature $(0,n)$. For an orthonormal basis $(e_1,...,e_n)$ of $\mathbb{R}^{0,n}$ the following multiplication rules arise in $\mathbb{R}_{0,n}$:

$$e_ie_j + e_je_i = -2\delta_{ij}, \quad \forall i,j \in \{1,..,n\} \tag{2.1}$$

In the following the notation $e_ie_j = e_{ij}$ is used. Now for a set $A = \{i_1,...,i_h\} \subseteq \{1,...,n\}$ with $1 \leq i_1 \leq ... \leq i_h \leq n$ and $e_A = e_{i_1}e_{i_2}...e_{i_h}$ the basis $(e_A : A \subseteq \{1...n\})$ forms a basis for the Clifford algebra $\mathbb{R}_{0,n}$. Therefore an element $a \in \mathbb{R}_{0,n}$ allows the representation $a = \sum_{k=0}^{n}[a]_k$ where $[a]_k = \sum_{|A|=k} a_Ae_A$ is called *k-vector*. Vectors $x = (x_1,...,x_n) \in \mathbb{R}^n$ are identified with one-vectors $x = \sum_{j=1}^{n} x_je_j$. The product of two vectors $x, y \in \mathbb{R}_{0,n}$ is then defined by

$$xy = - < x,y > + x \wedge y \tag{2.2}$$

where the *inner product*

$$x \bullet y = < x,y > = \sum_{i=1}^{n} x_iy_i = -\frac{1}{2}(xy + yx) \tag{2.3}$$

results in a scalar and the *wedge product* or *outer product*

$$x \wedge y = \sum_{i<j} e_ie_j(x_iy_j - x_jy_i) = -\frac{1}{2}(xy + yx) \tag{2.4}$$

results in a two-vector which is also known as a bivector. Furthermore the conjugation in $\mathbb{R}_{0,n}$ is given by $\overline{e_i} = -e_i$ and therefore the conjugation of a vector x results in $\overline{x} = -x$.

2.1 Monogenic functions

Let f be a C_1 function with values in the Clifford algebra $\mathbb{R}_{0,n+1}$. Under which conditions is f *differentiable*? This is the first question one has to answer to find an entry to the theory of functions in a Clifford analysis setting. In history different terminologies of complex- or hypercomplex- *differentiable* functions have been established. The terms *analytic*, *holomorphic* and *monogenic* are all used to describe the property of being *differentiable* in $\mathbb{R}_{0,n+1}$. To avoid confusion in the following the term *monogenic* will be

used. In order to define monogenecity the first order linear differential operator called *Dirac operator* is introduced as

$$\partial_x = \sum_{i=0}^{n} e_i \partial_{x_i}. \tag{2.5}$$

Due to the noncommutativity of the standard product in $\mathbb{R}_{0,n+1}$ the result of the Dirac operator can be applied from the left or from the right side to a function which will in general lead to different results.

Example 2.1.1. Consider $f(x) = f_1(x)e_{01}$ for $x \in \mathbb{R}^{0,2}$. Then

$$\partial_x f = (e_0\partial x_0 + e_1\partial x_1)f(x) = -\frac{\partial f_1(x)}{\partial_{x_0}}e_1 + \frac{\partial f_1(x)}{\partial_{x_1}}e_0 \tag{2.6}$$

but

$$f\partial_x = f(x)(e_0\partial x_0 + e_1\partial x_1) = \frac{\partial f_1(x)}{\partial_{x_0}}e_1 - \frac{\partial f_1(x)}{\partial_{x_1}}e_0 \tag{2.7}$$

With the Dirac operator a monogenic function can now be defined as the solution of a certain system of partial differential equations.

Definition 2.1.2. Let $G \subset \mathbb{R}^{0,n+1}$ be an open set and let f be a $C_1(G)$ function with values in $\mathbb{R}_{0,n+1}$. f is called left-/right-*monogenic* iff

$$\partial_x f = 0 \quad \text{respectively} \quad f\partial_x = 0 \tag{2.8}$$

holds.

Apart from being used to define monogenecity the Dirac operator factorizes the *Laplace* operator.

$$\Delta := \sum_{i=0}^{n} \partial_i^2 \tag{2.9}$$

as [11]

$$-\Delta = \partial_x^2. \tag{2.10}$$

Solutions of the differential equation $\Delta f = 0$ are called *harmonic* functions. As a result the component functions of a monogenic function $f = \sum_A f_A e_A$ f_A are harmonic with $\Delta f_A = 0$. The reader might notice the analogy to the complex case where every complex differentiable function f can be written as a sum $f = u(x,y) + iv(x,y)$ with $\Delta u = 0$ and $\Delta v = 0$. Furthermore setting $x = x_0 + x_1\overline{e_0}e_1$ and applying ∂_x to $f = f_0(x) + f_1(x)\overline{e_0}e_1$ results in

$$\partial_x f = \frac{\partial f_0}{\partial x_0}e_0 + \frac{\partial f_0}{\partial x_1}e_1 + \frac{\partial f_1}{\partial x_0}e_1 - \frac{\partial f_1}{\partial x_1}e_0. \tag{2.11}$$

It follows that $\partial_x f = 0$ is only fulfilled if

$$\frac{\partial f_0}{\partial x_0} e_0 - \frac{\partial f_1}{\partial x_0 1} e_0 = 0 \quad \text{and} \quad \frac{\partial f_0}{\partial x_1} e_1 + \frac{\partial f_1}{\partial x_0} e_1 = 0 \tag{2.12}$$

which are nothing else but the classical *Cauchy-Riemann-Equations* in the complex case. Therefore (2.1.2) can be considered as the higher dimensional analogue to the *Cauchy-Riemann-Equations*.

2.2 Generalized Hilbert transforms

The Hilbert transform of a one dimensional function has been used frequently in signal processing since Dennis Gabor proposed the *analytic signal* [17]. It rendered the possibility to determine the instantaneous phase and frequency of a given function. During the last years the image processing community has tried to generalize the analytic signal to two dimensions in order to determine an equivalent to the phase in the one dimensional case. Especially Michael Felsberg succeeded in this research area with the proposition of a two dimensional analogue called the *monogenic signal* [14]. Simultaneously to the research of generalized Hilbert transforms in image processing the Clifford analysis community has followed the same goal, although they had not the same applications in mind. Especially the Clifford Research group in Ghent has contributed fundamental work in this area ([12, 5, 6, 8, 7]).
Instead of introducing the analytic and monogenic signal first and discussing the features they are able to extract, this section starts with some basic integral theorems known from Clifford analysis. Part of these integral theorems is the *Plemelj-Sokhotzki formula* which is based on a generalized Hilbert transform in arbitrary dimensions. Having introduced this general Hilbert transform it will be shown that the analytic and the monogenic signal are just two special cases of the Plemelj-Sokhotzki formula for the dimensions $n = 1$ and $n = 2$.

2.2.1 Cauchy integral formula

The fundamental theorem this section is based on is the *Cauchy Integral Formula* which is well known from complex analysis and may be found in common complex analysis literature like [1]. The theorem can be generalized in the context of Clifford analysis and reads as follows (see e.g. [18]):

Theorem 2.2.1 (Cauchy integral theorem)**.** *Let $G \subset \mathbb{R}^{n+1}$ with sufficiently smooth boundary ∂G and let f be a left-monogenic function in $C_1(\bar{G})$. Then it holds that*

$$\int_{\partial G} E_n(x-y) f(y) n(y) dS(y) = \begin{cases} f(x), & x \in G, \\ 0, & x \in \mathbb{R}^{n+1} \setminus \bar{G} \end{cases} \tag{2.13}$$

where $n(y)$ is the outward pointing normal at y, dS is the surface element of ∂G and E is the *Cauchy kernel* defined by

$$E_n(x) = \frac{1}{A_{n+1}} \frac{\bar{x}}{|x|^{n+1}} \tag{2.14}$$

with the area A_{n+1} of the unit sphere $\mathbb{S}^n$.
It can be observed that a left-monogenic function in the given set is completely determined by its boundary values. Hence the Cauchy kernel is known to be a reproducing kernel generating a monogenic function from its boundary values. The integral used in the Cauchy integral formula defines a new operator called the *Cauchy transform* (see reference [8]):

Definition 2.2.2 (Cauchy transform)**.** Let $f \in L_2(G)$. Then its Cauchy transform is defined as

$$\mathcal{C}[f](x) = \int_{\partial G} E_n(x-y) f(y) n(y) dS(y), \quad x \notin \partial G \tag{2.15}$$

Applying the Cauchy transform to a function $f \in L_2(\partial G)$ will result in a function which is monogenic in G. This property is quite similar to an integral transform known from *harmonic analysis* called the *Poisson integral*. The Poisson integral reproduces a harmonic function in a given region from its boundary values by convolution with the so called *Poisson kernel* and the function describing the boundary values. The regions of interest in this case are the upper half space $\mathbb{R}^{n+1}_+$ and the ball $\mathbb{B}^n$. For these domains the Poisson kernels are explicitly known. Poisson kernels exist for other domains but it is often complicated to find a closed form expression. The Poisson integrals for the ball and the upper half space are defined as [2]:

Definition 2.2.3 (Poisson integral in the upper half space $\mathbb{R}^{n+1}_+$)**.**

$$\mathcal{P}[f](x) = (\mathcal{P}_{x_0} * f)(x) = \frac{1}{A_{n+1}} \int_{\mathbb{R}^n} \frac{2x_0}{|x_0 e_0 + x - y|^{n+1}} f(y) dV(y) \tag{2.16}$$

with the Poisson kernel in the upper half space

$$\mathcal{P}_{x_0}(x) = \frac{2x_0}{|x_0 e_0 + x|^{n+1}} \tag{2.17}$$

Definition 2.2.4 (Poisson integral in the ball $\mathbb{B}^n$)**.**

$$\mathcal{P}[f](x) = \frac{1}{A_{n+1}} \int_{\mathbb{S}^n} \frac{1-|x|^2}{|x-\xi|^{n+1}} f(\xi) dS(\xi) \tag{2.18}$$

with $x \in \mathbb{B}^n$ and the Poisson kernel in the ball

$$\mathcal{P}_{\mathbb{B}}(x,\xi) = \frac{1-|x|^2}{|x-\xi|^{n+1}} \tag{2.19}$$

Having defined the Poisson integral formula and the involved kernels it is now possible to solve the problem of finding the harmonic function in the set by evaluating the Poisson integral for the given boundary values. This problem is known as the *Dirichlet problem* [2].

Definition 2.2.5 (The Dirichlet problem for the upper half space)**.** Let $f \in L_1(\mathbb{R}^{n+1})$ and let $\mathcal{P}_{x_0}$ be the Poisson kernel for the upper half space. Then the function $u(x)$ defined by

$$u(x) = \begin{cases} \mathcal{P}[f](x), & x \in \mathbb{R}^{n+1} \\ f(x), & x \in \mathbb{R}^n \end{cases}, \tag{2.20}$$

is harmonic in $\mathbb{R}^{n+1}_+$.

In analogy to the Cauchy kernel the Poisson kernel generates a function from the values on the boundary of a given set but instead of generating a monogenic function a harmonic one is the result. According to definition 2.1.2 the components of a monogenic function are harmonic. In the light of the Dirichlet problem the question comes up if there is a connection between the Cauchy and the Poisson integral. This is indeed the case, but before the relation between the two transforms can be formulated the notion of the *generalized Hilbert transform* is required.
The Cauchy transform reproduces monogenic functions in a set G by the values on its boundary ∂G. According to the definition this only holds for values in $G \setminus \partial G$. But what happens with the integral (2.15) for values $x \in \partial G$? The integral turns into a strongly singular integral which can only be formulated as a *Cauchy principal value* integral and is called *generalized Hilbert transform* (see e.g. [12]):

Definition 2.2.6 (Generalized Hilbert transform)**.** Let $G \subset \mathbb{R}^{m+1}$ and $x \in \partial G$. The Hilbert transform on G reads:

$$H[f](x) = 2 \int_{\partial G} E_n(x-y) f(y) n(y) dS(y), \quad x \in \partial G \tag{2.21}$$

$$= \frac{2}{A_{n+1}} P.V. \int_{\partial G} \frac{\overline{y} - \overline{x}}{|y-x|^{n+1}} n(y) f(y) dS(y) \tag{2.22}$$

with $n(y)$ as the outward pointing normal at y and dS as the surface element of G.

Notice the subtle difference between (2.15) and (2.21): The integrals are quite similar but the points at which they are evaluated are *inside* of G in the case of the Cauchy transform and *on the boundary* ∂G in the case of the Hilbert transform. It has been shown in [8] that with these preliminaries the Cauchy transform can be written as the splitting

$$\mathcal{C}[f](x) = \frac{1}{2}\mathcal{P}[f](x) + \frac{1}{2}\mathcal{P}[H[f]](x) \tag{2.23}$$

where $\mathcal{P}[H(f)] = \mathcal{Q}[f]$ is also referred to as the *conjugate Poisson integral*.
This relation is important from two different points of view: On the one hand *given* a monogenic function f it can be expressed in terms of the Poisson integral and the Poisson integral of its Hilbert transform. But on the other hand a monogenic function can be *generated* by the Poisson integral and the Poisson integral of the Hilbert transform. This concept might already be known from complex analysis and is shown for the complex case in the followin example:

Example 2.2.7. To emphasise the analogy, the isomorphism $\mathbb{R}_{0,2} \cong \mathbb{C}$ is used again with the identification $i = \overline{e_0}e_1$. It is known that a function in $\mathbb{C}$ with values in $\mathbb{C}$ can be written as $f = u(x,y) + iv(x,y)$. Let f be monogenic, that is complex differentiable in this case. Then both component functions u and v are harmonic with

$$u = \mathcal{P}[f] \tag{2.24}$$

and

$$v = \mathcal{P}[H(f)] = \mathcal{Q}[f] \tag{2.25}$$

u and v are also called a pair of *conjugate harmonics*.

2.2.2 Riesz transforms

A special class of generalized Hilbert transforms arises for the upper half space $G = \mathbb{R}^{n+1}_+$ where $\mathbb{R}^{n+1}_+ = \{\underline{x} = (x, x_n) = (x_0, x_1, \ldots, x_n) : x_n > 0\}$. The outward pointing unit normal vector is then just $\overline{e_n}$ and the Hilbert transform is obtained as [12]:

$$H[f](x) = \frac{1}{A_{n+1}} P.V. \int_{\mathbb{R}^n} \frac{x-y}{|x-y|^{n+1}} \overline{e_m} f(y) dy \tag{2.26}$$

$$= \frac{1}{A_{n+1}} \overline{e_m} \left(\sum_{i=0}^{n-1} e_i P.V. \int_{\mathbb{R}^n} \frac{x_i - y_i}{|x-y|^{n+1}} f(y) dy \right) \tag{2.27}$$

with $x \in \partial G = \mathbb{R}^n$.
The component integrals are also known as *Riesz transforms* and can be expressed as n-dimensional convolutions

$$R_j[f](x) = \frac{1}{A_{n+1}} P.V. \int_{\mathbb{R}^n} \frac{x_i - y_i}{|x-y|^{n+1}} f(y) dy \tag{2.28}$$

$$= (r_j * f)(x) \tag{2.29}$$

with the so called *Riesz kernels* [29]:

$$r(x) = \frac{1}{A_{n+1}} \frac{x}{|x|^{n+1}} \tag{2.30}$$

Note that in the case of $n = 1$ the Riesz kernel r_1 is nothing else but the standard Hilbert kernel known from the real line

$$r_1(x) = \frac{1}{\pi}\frac{x}{|x|^2} = \frac{1}{\pi x}. \tag{2.31}$$

Riesz transforms were introduced by Marcel Riesz in [27] and further studied by Horváth in [20] as a class of singular integral kernels of the form

$$K = P.V.\frac{k(\omega)}{r^n}, \quad x = r\omega, x \in \mathbb{R}^n. \tag{2.32}$$

The functions $k(\omega)$ are supposed to have vanishing spherical means:

$$\int\limits_{\mathbb{S}^{n-1}} k(\omega)dS(\omega) = 0 \tag{2.33}$$

A a special class $k(\omega)$ of functions fulfilling this property is obtained from harmonic homogenouous polynomials

$$x^j = (x_0e_0 + x_1e_1 + \cdots + x_{n-1}e_{n-1})^j \tag{2.34}$$

and their restrictions to the sphere

$$k(\omega) = \frac{x^j}{|x|^{n+j}} = \frac{Y_j(\omega)}{r^n} \tag{2.35}$$

where Y_j are also known as spherical harmonics. Horváth called the vectorial distribution

$$H_j = \frac{1}{A_{n+1}}\frac{x^j}{|x|^{n+j}} \tag{2.36}$$

vectorial Hilbert transform. Under these conditions the components of the Riesz transform components turn out to be the components of the *vectorial Hilbert transforms* for $j = 1$ with the kernels

$$K_i = \frac{1}{A_{n+1}}\frac{x_i}{|x|^{n+1}} = \frac{1}{A_{n+1}}\frac{w}{r^n}, \quad k_i(\omega) = \frac{1}{A_{n+1}}\omega_i \tag{2.37}$$

Horváth showed in [20] that the Riesz kernels have a defined Fourier transform and act as multipliers in the Fourier space denoted by

$$\mathcal{F}[r_j](x) = -i\frac{x_j}{|x|}. \tag{2.38}$$

Furthermore there exists a close connection between the Riesz transform and the partial derivatives of a function described by the properties

$$\frac{\partial^2}{\partial_{ij}}f = -R_iR_j[\Delta f] \tag{2.39}$$

where Δ is the Laplace operator (see [9]).

The Riesz transform was one of the first attempts to generalize the Hilbert transform to $\mathbb{R}^{n+1}_+$. In the context of this thesis Riesz transforms are of special interest. They are the basis for the analytic, the monogenic, and the conformal signal which are discussed in detail in the next chapter.

2.2.3 Plemelj-Sokhotzki formula

The general Hilbert transform has been introduced, up to a factor of two, as the Cauchy transform for values on the boundary. Given the splitting in (2.23), what happens if the evaluation point x moves more and more towards the boundary? To be more precise, how does the limit of the splitting (2.23) behave for points moving non-tangentially towards the boundary? The answer to this question is given by the *Plemelj-Sokhotzki formula* [18]:

Theorem 2.2.8 (Plemelj-Sokhotzki formula)**.** *Let $G \subset \mathbb{R}^{n+1}$ and let f be Holder continuous on the sufficiently smooth boundary ∂G. Then for every $x \in \partial G$*

$$\lim_{t \to x} \mathcal{C}[f](t) = \frac{1}{2} f(x) + \frac{1}{2} H[f](x) \tag{2.40}$$

where the limit is non-tangential.

The non-tangential boundary value of the Cauchy transform $\mathcal{C}[f]$ is therefore a composition of the function f and its Hilbert transform $H[f]$. Note that although the Cauchy transform generates a monogenic function, the non-tangential boundary value of the Plemelj-Sokhotzki formula is in general *not* monogenic.

The Plemelj-Sokhotzki formula is the generalization of what is called the *analytic signal* for $n = 1, G = \mathbb{R}^2$ and the *monogenic signal* for $n = 2, G = \mathbb{R}^3$. To emphasize the importance of this relationship these special cases are treated in detail.

Example 2.2.9 (Analytic Signal)**.** Let $n = 1$ and $G = \mathbb{R}^2_+$. Consider a function f defined on the boundary ∂G which is just the real line $\mathbb{R}$ in this case. To apply the Plemelj-Sokhotzki formula the generalized Hilbert transform of f has to be known. For the given boundary and $n(y) = \overline{e_1}$ as the outward pointing normal the Hilbert transform (2.21) reads:

$$H[f](x) = 2\int_{\partial G} E_n(x-y)f(y)n(y)dS(y), \quad x \in \partial G \tag{2.41}$$

$$= \frac{2}{2\pi} P.V. \int_{\mathbb{R}} \frac{\overline{y}-\overline{x}}{|y-x|^2} e_0\overline{e_1} f(y)dS(y) \tag{2.42}$$

$$= \frac{1}{\pi} P.V. \int_{y=-\infty}^{+\infty} \frac{\overline{y}-\overline{x}}{|y-x|^2} e_0\overline{e_1} f(y)dy \tag{2.43}$$

$$= e_0\overline{e_1}\frac{1}{\pi} P.V. \int_{y=-\infty}^{+\infty} \frac{1}{x-y}\overline{e_1} f(y)dy \tag{2.44}$$

Identifying $e_0\overline{e_1}$ again with the imaginary unit i by virtue of the isomorphism $\mathbb{R}_{0,1} \cong \mathbb{C}$ the result just reads:

$$H[f](x) = i\mathcal{H}[f](x) \tag{2.45}$$

where $\mathcal{H}[f](x)$ is the classical Hilbert transform on the real line. Together with the original function f the Plemelj-Sokhotzki formula is obtained as:

$$\lim_{t\to x} \mathcal{C}[f](t) = \frac{1}{2}f(x) + \frac{1}{2}i\mathcal{H}[f](x) \tag{2.46}$$

which is up to the factor $\frac{1}{2}$ the analytic signal introduced by Dennis Gabor in [17].

Example 2.2.10 (Monogenic Signal)**.** Let $n = 2$ and $G = \mathbb{R}^3_+$. The boundary ∂G where the values of f reside is the plane $\mathbb{R}^2$. Working in the upper half space of $\mathbb{R}^3$ the outward pointing normal is the directional vector along the negative e_2 axis $n(y) = \overline{e_2}$. The Hilbert transform (2.21) is obtained as:

$$H[f](x) = 2\int_{\partial G} E_n(x-y)f(y)n(y)dS(y), \quad x \in \partial G \tag{2.47}$$

$$= \frac{2}{4\pi^2} P.V. \int_{\mathbb{R}^2} \frac{\overline{y}-\overline{x}}{|y-x|^3}\overline{e_2} f(y)dS(y) \tag{2.48}$$

$$= \frac{1}{2\pi^2} P.V. \int_{\mathbb{R}^2} \frac{\overline{y_0}-\overline{x_0}}{|y-x|^3} e_0\overline{e_2} f(y)dy \tag{2.49}$$

$$+ \frac{1}{2\pi^2} P.V. \int_{\mathbb{R}^2} \frac{\overline{y_1}-\overline{x_1}}{|y-x|^3} e_1\overline{e_2} f(y)dy \tag{2.50}$$

The component integrals can be expressed in terms of the Riesz transform introduced in (2.28) as two-dimensional convolutions with the Riesz kernels

$$R_j[f](x) = \frac{1}{2\pi^2} P.V. \int_{\mathbb{R}^2} \frac{\overline{y_j} - \overline{x_j}}{|y-x|^3} f(y)dy \tag{2.51}$$

$$= (r_j * f)(x) \tag{2.52}$$

resulting in the generalized Hilbert transform

$$H[f](x) = \overline{e_2}\,(e_0(r_0 * f) + e_1(r_1 * f)) \tag{2.53}$$

$$= \overline{e_2} \sum_{i=0}^{1} e_i R_i[f](x) \tag{2.54}$$

and the according Plemelj-Sokhotzki formula:

$$\lim_{t \to x} \mathcal{C}[f](t) = \frac{1}{2} f(x) + \frac{1}{2} H[f](x) \tag{2.55}$$

$$= \frac{1}{2} f(x) + \frac{1}{2} \overline{e_2} \sum_{i=0}^{1} e_i R_i[f](x) \tag{2.56}$$

This result coincides with the monogenic signal introduced by Michael Felsberg in [15].

It has already been mentioned above that the non-tangential boundary value of the Plemelj-Sokhotzki formula is in general not monogenic. Therefore the names analytic and monogenic signal are often confusing. Since they are non-tangential boundary values of the Cauchy transform their results are in general neither analytic nor monogenic although their names allow these assumptions.
One can conclude that the Riesz transform, itself being a generalization of the Hilbert transform on the real line to $\mathbb{R}^{n+1}_+$, is just a special case of the generalized Hilbert transform obtained in the Clifford analysis framework. While in the signal and image processing community the signal representations, such as the analytic and the monogenic signal, have been developed independently they were already included in the Cauchy transform and the Plemelj-Sokhotzki formula. Furthermore the framework includes a scale space concept known as the *Poisson scale space*. In conjunction with the monogenic signal Felsberg introduced this scale space in [16] as an alternative to the standard *Gaussian scale space* known from image processing (see e.g. [28]). He defined the Poisson scale space representation of the monogenic signal as the convolution of the monogenic signal with the Poisson kernel for $\mathbb{R}^3_+$:

$$\mathcal{P}[f](x) + \mathcal{P}[\sum_{i=0}^{1} R_i[f]](x) = \mathcal{P}[f](x) + \mathcal{P}[H[f]](x) \tag{2.57}$$

which is up to the factor 1/2 nothing else but the Cauchy transform identified by the splitting introduced in (2.23). This relation is fundamental. First the Cauchy transform

and its non-tangential boundary value which results in the generalized Hilbert transform are therefore the entry to image analysis in the framework of Clifford analysis. It naturally provides the concept of the Poisson scale space and contains the already known analytic and monogenic signal as a subset. Second it is the entry to complex function theory in higher dimensions. Since the Cauchy transform generates monogenic functions we deal with such functions only if we work in the Poisson scale space. Important theorems known from Clifford analysis depending on monogenic functions can therefore be applied. This is not the case if the analysis is carried out in the standard Gaussian scale space.
This chapter has introduced the generalized Hilbert transform as a part of the non-tangential boundary value of the Cauchy transform. The generalized Hilbert transform is able to operate on the suffciently smooth boundary ∂G of arbitrary connected sets $G \subset \mathbb{R}^{n+1}$. These boundaries might for example be plane curves, space curves, and closed surfaces. Therefore the generalized Hilbert transform is not restricted to the boundary of the upper half space $\mathbb{R}^{n+1}_+$ as it is the case with the Riesz transform. As a special class of generalized Hilbert transforms the Riesz transforms have been introduced as a Hilbert transform on the boundary $\partial G = \mathbb{R}^{n+1}_+$. Classical signal representations such as the analytic signal and the monogenic signal are based on the Riesz transform. These representations which are combinations of the original signal and its Riesz transform turned out to be special cases of the Plemelj-Sokhotzki formula. Since the Clifford analysis framework provides the possibility to apply the Hilbert transform on more complex boundaries than the upper half spaces, the question arises how these Hilbert transforms could be used in image processing. The next chapters provide an overview of the existing signal representations, the features they are able to extract, and their drawbacks. New signal representation involving the generalized Hilbert transform on manifolds different from the boundary of the upper half spaced are introduced and discussed.

3 The Riesz transform in terms of the Radon transform

While the last chapter has introduced the formal concepts of the Cauchy transform and the generalized Hilbert transform, their interpretation and application in the context of image processing has not been discussed yet. The primary goal is the extraction of certain features from a signal. To use the introduced Hilbert transform for feature extraction one has to understand what it actually does if it is applied to a signal. In addition one has to understand and mathematically model the features that are supposed to be extracted.
In the following, *signals* are considered which are functions $f(\mathbf{x})$ from $\Omega \subset \mathbb{R}^2$ to $\mathbb{R}$ with $f \in \mathrm{L}^2(\mathbb{R}^2, \mathbb{R})$ and $f \in \mathrm{C}^2(\mathbb{R}^2, \mathbb{R})$.
Subscripts of the form f_{i0D}, f_{i1D} and f_{i2D} will represent the *intrinsic dimension* of the function which is defined according to [14] for a local neighbourhood $N \subset \Omega$ as:

$$f \in \begin{cases} i0D_N, & f(x_i) = f(x_j)\ \forall x_i, x_j \in N \\ i1D_N, & f(x_1, x_2) = g(x_1\ \cos(\theta) + x_2\ \sin(\theta))\ \forall (x_1, x_2) \in N, \\ & g : \mathbb{R} \to \mathbb{R} \wedge\ g \notin i0D_N \\ i2D_N, & else \end{cases} \tag{3.1}$$

θ_{Main} will denote their main *orientation*. In the case of f_{i2D} signals, which are superpositions of two i1D signals, θ_1, θ_2 are the orientations of corresponding i1D signals. φ_1, φ_2 will denote their *local phases* respectively.
The $nD-$Fourier transform of a function f will be denoted by $\mathcal{F}$ and is defined as

$$\mathcal{F}[f](u) = \int_{\mathbb{R}^n} f(x)\ e^{-i2\pi <x,u>} dx\ , u \in \mathbb{R}^2 \tag{3.2}$$

The analytic signal The last chapter has introduced the analytic signal as a special case of the Plemelj-Sokhotzki formula and therefore as the non-tangential boundary value of the Cauchy transform for $G = \mathbb{R}^2_+$ and $\partial G = \mathbb{R}$. Although the Plemelj-Sokhotzki formula generalizes the analytic signal, it provides no interpretation of its effect on an input function. Omitting the factor $1/2$ found in the Plemelj-Sokhotzki formula (2.46) in example 2.2.9 the analytic signal has been defined as

$$2 \lim_{t \to x} \mathcal{C}[f](t) = f_a(x) = f(x) + i\mathcal{H}[f](x) \tag{3.3}$$

To interpret the analytic signal $f : \mathbb{R} \to \mathbb{R}$ is assumed to be a cosine function

$$f(x) = k(x)\ cos(\omega x + \phi), \quad \omega > 0, k \in \mathbb{R} \tag{3.4}$$

where $k = k(x)$ is called the *amplitude*, the argument $arg(f(x)) = \omega x + \phi$ is called *instantaneous phase* or just *phase* and $d/dx\, arg(f(x))$ is called *instantaneous frequency*. Since

the Hilbert transform of f reads $\mathcal{H}[f](x) = k\sin(\omega x+\phi)$ its analytic signal representation is the function

$$f_a(x) = k\cos(\omega x + \phi) + ik\sin(\omega x + \phi). = k(x)e^{i(\omega x+\phi)} \tag{3.5}$$

defined in the complex plane. The function

$$|f_a(x)| = \sqrt{f(x)^2 + \mathcal{H}[f](x)^2} \tag{3.6}$$

is also known as the *amplitude envelope* or *instantaneous amplitude*.
The instantaneous phase is obtained by the arc tangent as

$$\omega x + \phi = \arctan\left(\frac{\mathcal{H}[f](x)}{f(x)}\right) = \left(\frac{\sin(\omega x + \phi)}{\cos(\omega x + \phi)}\right). \tag{3.7}$$

Note that the instantaneous phase is only exactly determined for a single cosine or sine function. For the phase of an arbitrary function $f \in L_2(\mathbb{R}, \mathbb{R})$ consider their Fourier series representation

$$f(x) = \sum_{m=-\infty}^{\infty} c_m e^{imx} \tag{3.8}$$

with the Fourier coefficients

$$c_m = \frac{1}{2\pi}\int_{-\pi}^{\pi} f(x)e^{-imx}dx \tag{3.9}$$

Then due to the linearity of the Hilbert transform the expression

$$\arctan\left(\frac{\mathcal{H}[f](x)}{f(x)}\right) = \arctan\left(\frac{\mathcal{H}[\sum_{m=-\infty}^{\infty} c_m e^{imx}](x)}{\sum_{m=-\infty}^{\infty} c_m e^{imx}}\right) \tag{3.10}$$

$$= \arctan\left(\frac{\sum_{m=-\infty}^{\infty} \mathcal{H}[c_m e^{imx}](x)}{\sum_{m=-\infty}^{\infty} c_m e^{imx}}\right) \tag{3.11}$$

is just the average of the component function phases. Hence for arbitrary L_2 functions the term *phase* is only significant if the function is prefiltered in such a way, that only *one* frequency is obtained.

The monogenic signal One dimensional functions $f \in L_2(\mathbb{R}, \mathbb{R})$ can be analyzed in terms of the instantaneous phase, frequency and amplitude with the one dimensional Hilbert transform. To generalize the Hilbert transform from the real line $\mathbb{R}$ to the plane $\mathbb{R}^2$ for functions $f \in L_2(\mathbb{R}^2, \mathbb{R})$, the Hilbert transform on $\partial G = \mathbb{R}^2$ as the boundary of the upper half space $\mathbb{R}^3_+$ is used. The outward pointing normal is then denoted by $\overline{e_2}$ pointing down the negative e_2 axis. It has already been mentioned that the generalized Hilbert transform for the upper half space corresponds to the Riesz transform. In conjunction

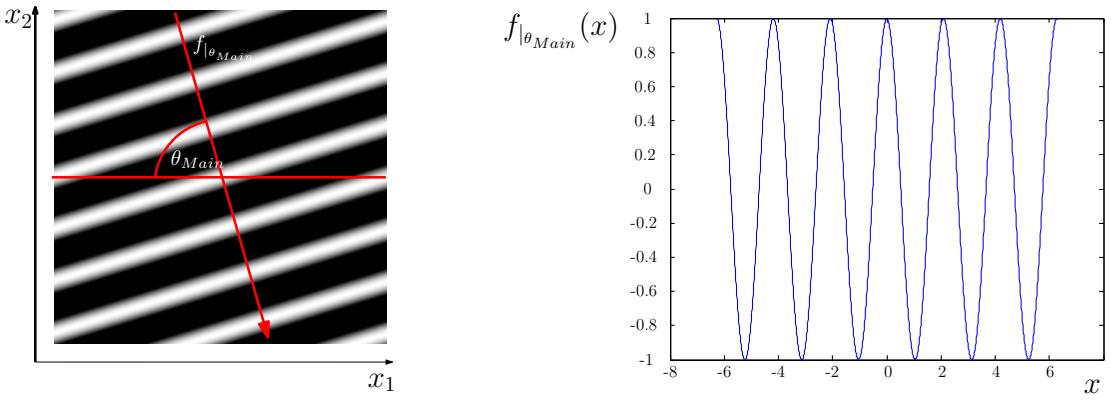

Figure 3.1: Left: Basic i1D signal. Right: One-dimensional signal obtained by restricting the original signal along its orientation

with the original function f its Riesz transform leads to the Plemelj-Sokhotzki-formula which is also known as the monogenic signal:

$$f_m(x) = 2 \lim_{t \to x} \mathcal{C}[f](t) \tag{3.12}$$

$$= f(x) + H[f](x) \tag{3.13}$$

$$= f(x) + \overline{e_2} \sum_{i=0}^{1} e_i R_i[f](x) \tag{3.14}$$

Problems arise if one tries to interpret the monogenic signal in terms of the phase since there is no exact definition of a two dimensional phase. Nonetheless, a motivation can be given if the underlying signal model is assumed to be a cosine function depending on the scalar product of the two dimensional input coordinates $x \in \mathbb{R}^2$ and a given *orientation vector* $u = (\cos\theta, \sin\theta)^T$.

$$f(x) = k \cos(\omega < x, u > +\varphi), \quad \omega > 0, k \in \mathbb{R} \tag{3.15}$$

which is the real part of so called *plane wave* functions

$$f_p(x) = k \, e^{i(\omega < x, u > +\varphi)}. \tag{3.16}$$

Note that f is intrinsically one-dimensional since it is constant along the line perpendicular to u.
For plane wave functions a phase can be defined according to the one dimensional definition as

$$arg(f(x)) = \omega < x, u > +\varphi \tag{3.17}$$

In contrast to the one-dimensional case this phase function additonally depends on the orientation u. If the orientation u is known, then the phase function can be determined by applying the concepts of the analytic signal from the previous section to the one-dimensional function obtained by the restriction of f to a straight line *along* u. Furthermore, with the knowledge of u one would obtain the orientation angle θ of the plane wave which is important for orientation analysis of certain image structures.
The Riesz transform is able to obtain the orientation angle θ of plane waves and therefore their phase. To understand the functionality of the Riesz transform, its close link with the Radon transform is exploited. First a few preliminaries concerning the Radon transform are necessary. Working in a Clifford analysis setting, the Radon transform of functions with values in $\mathbb{R}_{0,n}$ is considered which is discussed in detail in [7].

Definition 3.0.11. Let $f(x) \in L_2(\mathbb{R}^n, \mathbb{R}_{0,n})$, $u \in \mathbb{S}^{n-1}$ and $s \in \mathbb{R}$. Then the *Radon transform* $\mathcal{R} : \mathbb{R}^n \to \mathbb{S}^{n-1} \times \mathbb{R}$ of f is defined as:

$$\mathcal{R}[f](u,s) = \int\limits_{x \in \mathbb{R}^n} f(x)\, \delta_0(< x, u > -s) dy \tag{3.18}$$

where δ_0 ist the Dirac-Delta distribution.

The Radon transform integrates over all possible hyperplanes $\mathbb{R}^n$ described by the unit vector u and the minimal distance s from the origin. Of interest are the cases $n = 2$ and $n = 3$. For $n = 2$ the set of all possible hyperplanes in $\mathbb{R}^2$ are all possible straight lines. In $\mathbb{R}^3$ $n-$dimensional hyperplanes correspond to ordinary planes in $\mathbb{R}^3$. In this scenario the Radon transform is of special interest since it decomposes a given function into its plane waves and is therefore also known under the name *plane wave decomposition*. If the input function consists of a single plane wave like (3.15) it will be transformed into a one-dimensional function in the new parameter space called *Radon space* (see Figure 3.2). The Radon space parameterizes the new one-dimensional functions depending on the orientation described by u for each given plane waves. Since $u \in \mathbb{S}^{n-1}$, it can be described by $n-1$ angles in spherical coordinates. The Radon parameter space is spanned by these $n-1$ angles and the distance parameter s. One-dimensional functions in the Radon space along s for a given u are also referred to as *slices*.

3.1 Properties of the Radon transform

The Radon transform shares some properties which will be used in the following. It is invertible and its inversion will be denoted by (see [10])

$$f(x) = \mathcal{R}^{-1}[\mathcal{R}[f]](x) = \int\limits_{|u|=1} h(u, < x, u >) du \tag{3.19}$$

where

$$h(u,t) = \left\{ \begin{array}{ll} a_n \frac{\partial^{n-1}}{\partial t^{n-1}} \mathcal{R}[f](u,t), & \text{for odd } n \\ a_n \mathcal{H}\left[\frac{\partial^{n-1}}{\partial p^{n-1}} \mathcal{R}[f](u,p)\right](t), & \text{for even } n \end{array} \right\} \tag{3.20}$$

and

$$a_n = \left\{ \begin{array}{ll} \frac{i^{n-1}}{2(2\pi)^{n-1}}, & \text{for odd } n \\ \frac{i^n}{2(2\pi)^{n-1}}, & \text{for even } n \end{array} \right\}. \tag{3.21}$$

Hence it is possible to reconstruct a function from its plane wave decomposition. Furthermore, both the Radon transform and its inverse are linear integral transforms with

$$\mathcal{R}[f](u,s) = \mathcal{R}\left[\sum_A e_A f_A\right](u,s) = \sum_A e_A \mathcal{R}[f_A](u,s). \tag{3.22}$$

Shifting a function in the spatial domain by a vector $v \in \mathbb{R}^n$ results in a shift in the Radon space along the s axis:

$$\mathcal{R}[f(x+t)](u,s) = \mathcal{R}[f(x)](u, s+ < t, u >). \tag{3.23}$$

Of special interest is the close connection between the Radon transform and the Fourier transform:

Theorem 3.1.1 (Fourier slice theorem or central slice theorem)**.** *Let u be a unit vector in $\mathbb{R}^n$ and $t, s \in \mathbb{R}$. Then the following holds:*

$$\mathcal{F}[f(x)](tu) = \mathcal{F}_{t\to s}[\mathcal{R}[f](u,t)](s) \tag{3.24}$$

where $\mathcal{F}_{t\to s}$ denotes the one-dimensional Fourier transform along the slice at u evaluated at s.

The Fourier slice theorem relates the n-dimensional Fourier transform of a function f to the *one*-dimensional Fourier transform along the slice at the orientation described by u. All points in the Fourier domain located along a given orientation u belong to the same slice in the Radon domain and therefore to the same plane wave. The Fourier slice theorem is the central theorem to establish the link between the generalized Hilbert transform and the Radon transform which reads

Theorem 3.1.2 (Connection between the generalized Hilbert and the Radon transform)**.**

$$\mathcal{R}[\mathcal{H}[f]](u,s) = i\overline{e_0} u \mathcal{H}_{t\to s}[\mathcal{R}[f](u,t)](s) \tag{3.25}$$

where $\mathcal{H}_{t\to s}$ denotes the one-dimensional Hilbert transform along the slice located at u evaluated at s.

A proof for an arbitrary dimension n of the connection above using the Fourier slice theorem may be found in [7]. Applying the inverse Radon transform to (3.25) results in

$$\mathcal{H}[f](x) = \mathcal{R}^{-1}[i\overline{e_0} u \mathcal{H}_{t\to s}[\mathcal{R}[f](u,t)](s)](x) \tag{3.26}$$

Similar to the Fourier slice theorem the equation above states that the generalized Hilbert transform of a function in $\mathbb{R}^n$ evaluated at point (u,s) is the same as the inverse Radon

transform of the *one-dimensional* Hilbert transform along the slice described by the direction u in the Radon space. Therefore every generalized Hilbert transform on $\partial G = \mathbb{R}^n_+$ reduces to a one-dimensional Hilbert transform along the corresponding slices in the Radon domain. This general link between the Hilbert and the Radon transform is the basis for the following analysis of plane waves in $\mathbb{R}^2$. For these types of functions the integral involved in the inverse Radon transform can be simplified to reveal the orientation of the plane wave.

3.2 Analysis of i1D signals

Single plane waves in $\mathbb{R}^2$ are equivalent to intrinsically one dimensional functions. Since they depend on the scalar product of the desired direction vector u and the coordinate vector x it is constant at every x along the direction perpendicular to $u = (\cos(\theta), \sin(\theta))^T$ which is the definition of a i1D function. In the following these functions are denoted by f_{i1D}.
The Radon transform has been introduced as a plane wave decomposition. If it is applied to a single plane wave function there is actually nothing to decompose since only one plane wave is present. As a result the Radon transform of a plane wave is only a single one-dimensional function along one slice at its orientation described by u. At all other slices the resulting functions are constant:

Lemma 3.2.1. *Let f_{i1D} be a i1D function and let $\theta_{Main} \in [0, \pi)$ be its main orientation with respect to the x_1-axis. Then for all $t_1, t_2 \in \mathbb{R}$ and for all $u = (\cos\theta, \sin\theta)^T, \theta \in [0, \pi] \setminus \{\theta_{Main}\}$ the following holds:*

$$\mathcal{R}[f](u, t_1) = \mathcal{R}[f](u, t_2) \tag{3.27}$$

Proof. Consider two straight lines l_1, l_2 in $\mathbb{R}^2$ described by their orientation angle θ with respect to the x_1-axis an their distances t_1, t_2 from the origin. Now consider a point x_1 on l_1 and the corresponding value $f(x_1)_{i1D}$. l_1 and l_2 are parallel, since they have the same orientation angle but only differing distances from the origin. By definition the function f_{i1D} is a i1D function so it is constant along one orientation ϕ in the spatial domain. But then x_1 has a corresponding bijective projection on l_2 along that orientation ϕ namely $\mathbf{x_2}$ with $f(x_1)_{i1D} = f(x_2)_{i1D}$. □

Corollary 3.2.2. *Let f_{i1D} be a i1D function and let $\theta_{Main} \in [0, \pi)$ be its main orientation with respect to the x_1-axis. Then for all $u = (\cos\theta, \sin\theta)^T, \theta \in [0, \pi] \setminus \{\theta_{Main}\}$ and for all $t \in \mathbb{R}$:*

$$\mathcal{R}[f](u, t) = c \tag{3.28}$$

where $c \in \mathbb{R}$ is some constant.

This constancy property at all slices different from the slice at the angle θ_{Main} is a key property for the determination of the orientation u with the Riesz transform. Using

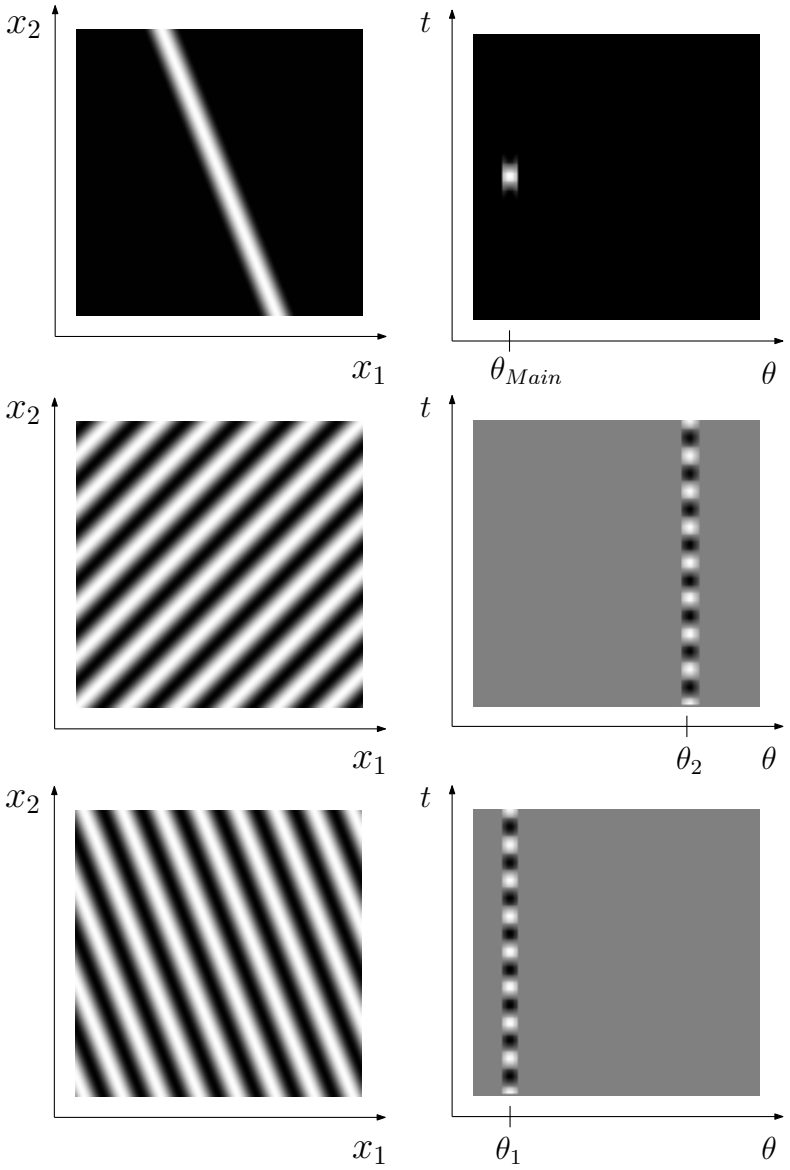

Figure 3.2: Left column: Original i1D signals in the spatial domain. Right column: The corresponding Radon transformations. The Radon transform of i1D signals has only non-constant values at $\theta = \theta_{Main}$

the definition of the inverse Radon transform (3.19) for $n = 2$ leads to the explicit two-dimensional inversion formula

$$f(x) = \mathcal{R}^{-1}[\mathcal{R}[f]](x) = \frac{1}{2\pi^2} \int\limits_{|u|=1} \mathcal{H}_{t\to s}[\frac{\partial}{\partial t}\mathcal{R}[f](u,t)](< x,u >)du \tag{3.29}$$

In conjunction with the relation (3.26) the link between the Radon and the Hilbert transform, which is the Riesz transform in this case, reads:

$$\begin{aligned}\mathcal{H}[f](x) &= i\overline{e_0}\mathcal{R}^{-1}\left\{\begin{pmatrix}\cos\,\theta\\ \sin\,\theta\end{pmatrix}\mathcal{H}_{t\to s}[\mathcal{R}\{f\}(u,t)](s)\right\}(x)\\ &= -\frac{i\overline{e_0}}{2\pi^2}\int\limits_{|u|=1}\begin{pmatrix}\cos\,\theta\\ \sin\,\theta\end{pmatrix}\mathcal{H}_{t\to s}[\mathcal{H}_{t\to s}[\frac{\partial}{\partial t}\mathcal{R}[f](u,t)]](<x,u>)du\\ &= \frac{i\overline{e_0}}{2\pi^2}\int\limits_{|u|=1}\begin{pmatrix}\cos\,\theta\\ \sin\,\theta\end{pmatrix}\frac{\partial}{\partial t}\mathcal{R}[f](u,<x,u>)du. \end{aligned} \tag{3.30}$$

The Riesz transforms are just the components

$$\begin{pmatrix}R_{x_1}[f](x)\\ R_{x_2}[f](x)\end{pmatrix} = \frac{1}{2\pi^2}\int\limits_{|u|=1}\begin{pmatrix}\cos\,\theta\\ \sin\,\theta\end{pmatrix}\frac{\partial}{\partial t}\mathcal{R}[f](u,<x,u>)du. \tag{3.31}$$

Having established the link between the generalized Hilbert transform and the Radon transform, this concept can now be used to analyze single plane waves f_{i1D} in $\mathbb{R}^2$. It has been shown in (3.28) that the Radon transform of a i1D signal, which is the real part of a plane wave, is only non-constant along one single slice in the Radon domain. This slice corresponds to the orientation angle θ_{Main} of the signal. At every other slice the one dimensional function along that slice is constant. Now imagine the inverse Radon transform of such a signal. Since the inverse Radon transform involves partial derivatives along each slice according to (3.31), these derivatives will vanish at all slices different from θ_{Main}. As a result the integration over all angles θ is just the slice function at θ_{Main}. Hence with $u_{Main} = (\cos\theta_{Main}, \sin\theta_{Main})^T$ the Riesz transforms read:

$$\begin{pmatrix}R_{x_1}[f_{i1D}](x)\\ R_{x_2}[f_{i1D}](x)\end{pmatrix} = \frac{1}{2\pi^2}\begin{pmatrix}\cos\,\theta_{Main}\\ \sin\,\theta_{Main}\end{pmatrix}\frac{\partial}{\partial t}\mathcal{R}[f_{i1D}](u_{Main},<x,u_{Main}>). \tag{3.32}$$

With the abbrevation

$$s(\theta_{Main}) = \frac{1}{2\pi^2}\frac{\partial}{\partial t}\mathcal{R}[f_{i1D}](u_{Main},<x,u_{Main}>) \tag{3.33}$$

the Riesz transform components along the x_1 and the x_2 axis read

$$\begin{pmatrix}R_{x_1}[f_{i1D}](0,0)\\ R_{x_2}[f_{i1D}](0,0)\end{pmatrix} = s(\theta_{Main})\begin{pmatrix}\cos\,\theta_{Main}\\ \sin\,\theta_{Main}\end{pmatrix}. \tag{3.34}$$

which allow the determination of the main orientation θ_{Main} as:

$$\frac{\mathrm{R}_{x_2}[f_{i1D}](0,0)}{\mathrm{R}_{x_1}[f_{i1D}](0,0)} = \frac{s(\theta_{Main})\sin\,\theta_{Main}}{s(\theta_{Main})\cos\,\theta_{Main}} = \tan\,\theta_{Main} \tag{3.35}$$

$$\theta_{Main} = \arctan\left(\frac{\mathrm{R}_{x_2}[f_{i1D}](0,0)}{\mathrm{R}_{x_1}[f_{i1D}](0,0)}\right) \tag{3.36}$$

With the main orientation of the signal f_{i1D} it is now possible to calculate the phase of the signal by evaluating the one dimensional Hilbert transform along u_{Main} from the origin. But even this step can be expressed in terms of the Riesz transform. It turns out that the one-dimensional Hilbert transform along u_{Main} is exactly the same as the inverse Radon transform of the one-dimensional Hilbert transform along each slice in the Radon domain:

Theorem 3.2.3 (Hilbert transform in the Radon domain)**.**

$$\mathcal{R}^{-1}[\mathcal{H}_{t\to s}[\mathcal{R}[f_{i1D}](u,t)]](s)_{s=<x,u>}](x) = \mathcal{H}_{t\to s}[f_{i1D}(t\cos\theta_{Main}, t\sin\theta_{Main})](s). \tag{3.37}$$

Proof. Define $r(t,\theta) = \mathcal{R}[f](t,\theta)$.

$$\begin{aligned}
&\mathcal{R}^{-1}[h(t) * \mathcal{R}[f_{i1D}](0,0)\\
&= \mathcal{R}^{-1}\left[\frac{1}{\pi}\int_{\tau=-\infty}^{\infty}\frac{r(\tau+t,\theta)}{-\tau}d\tau\right](0,0)\\
&= \frac{1}{2\pi^3}\int_{\theta=0}^{\pi}\int_{t=-\infty}^{\infty}\frac{1}{-t}\left[\frac{\partial}{\partial t}\int_{\tau=-\infty}^{\infty}\frac{r(\tau+t)}{-\tau}d\tau\right]dtd\theta\\
&= \frac{1}{\pi}\int_{\tau=-\infty}^{\infty}\frac{1}{-\tau}\left[\frac{1}{2\pi^2}\int_{\theta=0}^{\pi}\int_{t=-\infty}^{\infty}\frac{1}{(0\,\cos\theta + 0\,\sin\theta) - t}\frac{\partial}{\partial t}r(\tau+t,\theta)dtd\theta\right]d\tau\\
&= \frac{1}{\pi}\int_{\tau=-\infty}^{\infty}\frac{g(\tau+0)}{-\tau}d\tau\\
&= (h*g)(0)\\
&= h(0) * \mathcal{R}^{-1}[r(t,\theta)](0,0)\\
&= (h * f_{i1D_{\theta_{Main}}})(0)\\
&= \frac{-1}{\pi}\int_{\tau=-\infty}^{\infty}\frac{f_{i1D}(\tau\,\cos\,\theta_{Main}, \tau\,\sin\,\theta_{Main})}{\tau}d\tau
\end{aligned}$$

□

In conjunction with (3.31) the phase at the origin can now be expressed in terms of the Riesz transforms as

Theorem 3.2.4 (Phase of i1D signals)**.**

$$\varphi = \arctan 2(\sqrt{R_{x_1}[f_{i1D}](0,0)^2 + R_{x_2}[f_{i1D}](0,0)^2}, f(0,0)) \tag{3.38}$$

Proof. With the abbrevation

$$s(x) = \mathcal{R}^{-1}[\mathcal{H}_{t\to s}[\mathcal{R}[f](u,t)]](s)_{s=<x,u>}](x) \tag{3.39}$$

one has

$$\sqrt{R_{x_1}[f_{i1D}](0,0)^2 + R_{x_2}[f_{i1D}](0,0)^2} = \sqrt{s^2(0,0)\cos^2\theta_{Main} + s^2(0,0)\sin^2\theta_{Main}} \tag{3.40}$$

$$= s(0,0). \tag{3.41}$$

Using theorem 3.2.3 the assumption follows.

□

3.3 Analysis of superposed i1D signals

The transformation of a signal via the Radon transform and its inverse revealed the possibility of determining the main orientation and the phase of a i1D signal in a descriptive manner. The question arises if it is possible to use the Radon transform and its inverse in a similar manner for i2D signals. A starting point will be i2D signals which are a superposition of two i1D signals.

Definition 3.3.1. Let f_{i1D_1} and f_{i1D_2} be two i1D signals with main orientations θ_1 and θ_2. Then the i2D signals in the section will be of the form:

$$f_{i2D} = f_{i1D_1} + f_{i1D_2}$$

$\theta_{Main} = \frac{\theta_1+\theta_2}{2}$ will denote the main orientation of the i2D signal.

Proceeding analogous to the last section the Riesz transform of a f_{i2D} function using (3.30) is obtained as:

$$\begin{aligned}
\begin{pmatrix} R_{x_1}[f_{i2D}](x) \\ R_{x_2}[f_{i2D}](x) \end{pmatrix} &= \begin{pmatrix} R_{x_1}[f_{i1D_1} + f_{i1D_2}](x) \\ R_{x_2}[f_{i1D_1} + f_{i1D_2}](x) \end{pmatrix} \\
&= \mathcal{R}^{-1}\left\{ \begin{pmatrix} \cos\theta \\ \sin\theta \end{pmatrix} \mathcal{H}_{t\to s}[\mathcal{R}[f_{i1D_1} + f_{i1D_2}](u,t)](s)_{s=<x,u>} \right\}(x) \\
&= \mathcal{R}^{-1}\left\{ \begin{pmatrix} \cos\theta \\ \sin\theta \end{pmatrix} \mathcal{H}_{t\to s}[\mathcal{R}[f_{i1D_1}](u,t)](s)_{s=<x,u>} \right\}(x) + \\
&\quad \mathcal{R}^{-1}\left\{ \begin{pmatrix} \cos\theta \\ \sin\theta \end{pmatrix} \mathcal{H}_{t\to s}[\mathcal{R}[f_{i1D_2}](u,t)](s)_{s=<x,u>} \right\}(x) \\
&= \frac{1}{2\pi^2} \begin{pmatrix} \cos\theta_1 \\ \sin\theta_1 \end{pmatrix} \frac{\partial}{\partial t}\mathcal{R}[f_{i1D_1}](u_{\theta_1},t)_{t=<x,u_{\theta_1}>} + \\
&\quad \frac{1}{2\pi^2} \begin{pmatrix} \cos\theta_2 \\ \sin\theta_2 \end{pmatrix} \frac{\partial}{\partial t}\mathcal{R}[f_{i1D_2}](u_{\theta_2},t)_{t=<x,u_{\theta_2}>}
\end{aligned}$$

With

$$s(x,\theta) := \frac{1}{2\pi^2}\frac{\partial}{\partial t}\mathcal{R}[f_{i1D}](u_\theta,t)_{t=<x,u_\theta>}$$

the above result shortens to

$$\begin{pmatrix} R_{x_1}[f_{i2D}](x) \\ R_{x_2}[f_{i2D}](x) \end{pmatrix} = s(x,\theta_1)\begin{pmatrix} \cos\,\theta_1 \\ \sin\,\theta_1 \end{pmatrix} + s(x,\theta_2)\begin{pmatrix} \cos\,\theta_2 \\ \sin\,\theta_2 \end{pmatrix} \tag{3.42}$$

In general $s(\theta_1) \neq s(\theta_2)$ which prohibits the approach we used in Eq. (3.36). To derive the main orientation from this equation either demands that we know θ_1, θ_2 in advance or further assumptions about the two i1D signals are required. In the following it is assumed that the two i1D functions f_{i1D_1} and f_{i1D_2} have the same but an arbitrary phase.

Theorem 3.3.2 (Main orientation of i2D signals with same but arbitrary phase)**.** *Let f_{i1D_1} and f_{i1D_2} be two i1D signals with arbitrary but same phase. Then the main orientation θ_{Main} of $f_{i2D} = f_{i1D_1} + f_{i1D_2}$:*

$$\theta_{Main} = \frac{\theta_1+\theta_2}{2} = \arctan\left(\frac{R_{x_2}[f_{i1D}](0,0)}{R_{x_1}[f_{i2D}](0,0)}\right) \tag{3.43}$$

Proof. If the two i1D signals are assumed to have an arbitrary but the same phase, the integrals $s(\theta_1)$ and $s(\theta_2)$ will be equal and lead to:

$$\begin{pmatrix} R_{x_1}[f_{i2D}](0,0) \\ R_{x_2}[f_{i2D}](0,0) \end{pmatrix} = s(\theta_1)\begin{pmatrix} \cos\,\theta_1 \\ \sin\,\theta_1 \end{pmatrix} + s(\theta_2)\begin{pmatrix} \cos\,\theta_2 \\ \sin\,\theta_2 \end{pmatrix} \tag{3.44}$$

$$= \begin{pmatrix} \cos\,\theta_1 + \cos\,\theta_2 \\ \sin\,\theta_1 + \sin\,\theta_2 \end{pmatrix} s. \tag{3.45}$$

This directly reveals the main orientation in the same manner as in Eq. (3.36) □

Note that the main orientation is equal to the average of the i1D signal orientations for two or more superposed i1D signals.
In addition to the main orientation it is possible to determine the apex angle $|\theta_1 - \theta_2|$ of the two superposed i1D signals. With the knowledge of the main orientation and the apex angle the two orientation angles θ_1 and θ_2 can be calculated.

Theorem 3.3.3. *Let f_{i1D_i} and f_{i1D_2} be two i1D signals with arbitrary but same phase and amplitude and main orientations θ_1, θ_2. Further define:*

$$\begin{aligned} s &:= s(x,\theta_1) = s(x,\theta_2) \\ q_1 &:= (\cos\,\theta_1 + \cos\,\theta_2)s \\ q_2 &:= (\sin\,\theta_1 + \sin\,\theta_2)s \end{aligned}$$

Then the apex angle $\theta_1 - \theta_2$ of $f_{i2D} = f_{i1D_1} + f_{i1D_2}$ can be determined by:

$$\theta_1 - \theta_2 = \arccos\left(\frac{q_1^2 + q_2^2}{2s^2} - 1\right) \tag{3.46}$$

Proof. According to the identities of the trigonometric functions one gets:

$$\begin{aligned} q_1^2 &= (s(\cos\ \theta_1 + \cos\ \theta_2))^2 \\ &= \left(2s\ \sin\left(\frac{\theta_1 + \theta_2}{2}\right)\cos\left(\frac{\theta_1 - \theta_2}{2}\right)\right)^2 \end{aligned}$$

and

$$\begin{aligned} q_2^2 &= (s(\cos\ \theta_1 + \cos\ \theta_2))^2 \\ &= \left(2s\ \cos\left(\frac{\theta_1 + \theta_2}{2}\right)\cos\left(\frac{\theta_1 - \theta_2}{2}\right)\right)^2 \end{aligned}$$

Therefore:

$$\begin{aligned} \frac{q_1^2 + q_2^2}{2s^2} - 1 &= \frac{4s^2\cos\left(\frac{\theta_1-\theta_2}{2}\right)\left(\sin^2\left(\frac{\theta_1+\theta_2}{2}\right) + \cos^2\left(\frac{\theta_1+\theta_2}{2}\right)\right)}{2s^2} - 1 \\ &= 2\cos^2\left(\frac{\theta_1 - \theta_2}{2}\right) - 1 \\ &= \cos(2\frac{\theta_1 - \theta_2}{2}) \\ &= \cos(\theta_1 - \theta_2) \end{aligned}$$

□

To extend the phase calculation for i1D signals seen in (3.38) to i2D structures, it is again assumed that the signal f_{i2D} is a superposition of two f_{i1D} signals with same but arbitrary phase. Furthermore, the orientations θ_1, θ_2 are assumed to be known.

Theorem 3.3.4. *Let f_{i2D} be the superposition of two f_{i1D} signals with same but arbitrary phase. Let θ_1, θ_2 be their main orientations. Then the Hilbert transform along θ_1, θ_2 is obtained as:*

$$\mathcal{H}_{\theta_1}[f_{i2D}(t\cos\theta_1, t\sin\theta_1)](0) = \mathcal{H}_{\theta_2}[f_{i2D}(t\cos\theta_1, t\sin\theta_1)](0) \tag{3.47}$$

$$= \frac{R_{x_1}[f_{i2D}](0,0)}{\cos(\theta_1) + \cos(\theta_2)} \tag{3.48}$$

$$= \frac{R_{x_2}[f_{i2D}](0,0)}{\sin(\theta_1) + \sin(\theta_2)} \tag{3.49}$$

where $\mathcal{H}_\theta$ is the one-dimensional partial Hilbert transform along θ.

Proof. Evaluating the Riesz transform along the x_1-axis using (3.42) and using the definition (3.33) for $s(\theta)$ leads to

$$R_{x_1}[f_{i2D}](0,0) = \cos(\theta_1)s(\theta_1) + \cos(\theta_2)s(\theta_2) \tag{3.50}$$

Since the two i1D signals have the same phase it follows that $s(\theta_1) = s(\theta_2)$. Using (3.37) the Riesz transform becomes

$$\begin{aligned} R_{x_1}[f_{i2D}](0,0) &= s(\theta_{1/2})(\cos(\theta_1) + \cos(\theta_2)) && (3.51)\\ &= (\cos(\theta_1) + \cos(\theta_2))\mathcal{H}_{\theta_1}[f_{i2D}(t\cos\theta_1, t\sin\theta_1)](0) && (3.52)\\ &= (\cos(\theta_1) + \cos(\theta_2))\mathcal{H}_{\theta_2}[f_{i2D}(t\cos\theta_1, t\sin\theta_1)](0). && (3.53) \end{aligned}$$

□

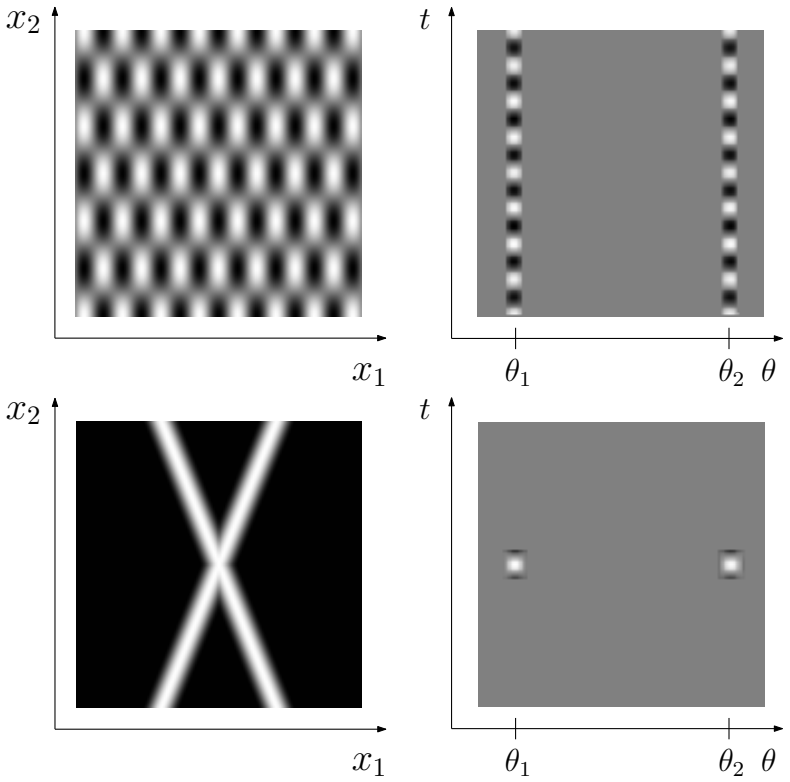

Figure 3.3: Left column: Original i2D signals which are superpositions of two i1D signals in the spatial domain. Right column: The corresponding Radon transformations. As it has already been stated, the Radon transform of i1D signals has only non-constant values at θ_1, θ_2

The goal of this section was an imaginative description of the generalized Hilbert transform on the boundary $\partial G = \mathbb{R}^2$ of $G = \mathbb{R}^3_+$ which coincides with the Riesz transform.

Using the relation between the Riesz transfrom and the Radon transform it was possible to show that the Riesz transform is just a one-dimensional Hilbert transform in the Radon domain. With this knowledge, certain properties such as orientation and phase of i1D signals (plane waves) and i2D signals which are a superposition of i1D signals have been determined. Since the monogenic signal representation consists of the Riesz transform and generalizes the analytic signal to plane wave analysis in $\mathbb{R}^2$, it provides the framework for the achieved results. Nevertheless, it is limited to the analysis of plane waves and therefore i1D structures.

4 The monogenic curvature tensor

Since the monogenic signal is limited to the analysis of i1D functions, there have been attempts to further extend the monogenic signal in order to analyze arbitrary i2D signals. One attempt is the monogenic curvature signal introduced by Di Zang in [32]. The main idea is to interpret the given signal as a Monge patch surface in $\mathbb{R}^3$ to connect the monogenic signal with curvature invariants known from differential geometry. Based on the Hessian matrix, a tensor pair consisting of the second order derivatives and its Riesz transform is constructed.
Although the idea of coupling differential geometry with the monogenic signal might lead to a framework for the analysis of i2D structures, the monogenic curvature tensor is limited. It is shown how to extract the properties like orientation, apex angle and phase with the monogenic curvature tensor.

4.1 Basic differential geometry

Before the monogenic curvature tensor is covered in detail, some differential geometric basics are introduced. They will serve as a basis for the comparison between the entities the monogenic curvature tensor is supposed to and the quantities it actually does determine.
The geometric object of interest is the *Monge patch* embedding of an input signal $f : \mathbb{R}^2 \to \mathbb{R}$ in $\mathbb{R}^3$ given by:

$$S(x_1, x_2) = x_1 e_1 + x_2 e_2 + f(x_1, x_2) e_3. \tag{4.1}$$

Given this embedding one can study differential geometric invariants of the surface. The subject of interest in this case are the *Gaussian* and mean curvature which are based on the *Gauss map*. To every surface point p the Gauss map assigns its oriented unit normal

$$N(p) = \frac{S_{x_1}(p) \times S_{x_2}(p)}{|S_{x_1}(p) \times S_{x_2}(p)|} \tag{4.2}$$

where $\times$ is the cross product in $\mathbb{R}^3$.
Therefore it is a map from the surface to the unit sphere $\mathbb{S}^2$. The differential of the Gauss map dN is a linear map from the tangent space $T_p(S)$ of the surface at the point p to the tangent space $T_{N(p)}(\mathbb{S}^2)$ of the unit sphere. Using the basis $\{S_{x_1}, S_{x_2}\}$ it may be written as a matrix

$$A = \begin{pmatrix} a_{11} & a_{21} \\ a_{12} & a_{22} \end{pmatrix} \tag{4.3}$$

with

$$a_{11} = \frac{fF - eG}{EG - F^2} \quad a_{12} = \frac{gF - fG}{EG - F^2} \tag{4.4}$$

$$a_{21} = \frac{eF - fE}{EG - F^2} \quad a_{22} = \frac{fF - gE}{EG - F^2} \tag{4.5}$$

where E, G, F are the coefficients of the first and e, g, f are the coefficients of the second fundamental form. The matrix A is also known as the Weingarten map and the equations of its entries are known as the Weingarten equations [13]. It is a well known fact that the coefficients for a Monge patch are given by

$$E = 1 + f_{x_1}^2, e = \frac{f_{x_1x_1}}{\sqrt{1 + f_{x_1}^2 + f_{x_2}^2}} \tag{4.6}$$

$$F = f_{x_1} f_{x_2}, f = \frac{f_{x_1x_2}}{\sqrt{1 + f_{x_1}^2 + f_{x_2}^2}} \tag{4.7}$$

$$G = 1 + f_{x_2}^2, g = \frac{f_{x_2x_2}}{\sqrt{1 + f_{x_1}^2 + f_{x_2}^2}} \tag{4.8}$$

$$\tag{4.9}$$

The Gaussian and mean curvature are then obtained as

$$K = det(A) = \frac{f_{x_1x_1} f_{x_2x_2} - f_{x_1x_2}^2}{(1 + f_{x_1}^2 + f_{x_2}^2)^2} \tag{4.10}$$

$$H = \frac{1}{2} \frac{(1 + f_{x_1}^2) f_{x_2x_2} - 2 f_{x_1} f_{x_2} f_{x_1x_2} + (1 + f_{x_2})^2 f_{x_1x_1}}{(1 + f_{x_1}^2 + f_{x_2}^2)^{3/2}}. \tag{4.11}$$

These two curvatures can be used to obtain the two principal curvatures κ_1, κ_2 which are the eigenvalues of the Weingarten map. They correspond to the eigenvectors pointing along directions with maximum and minimum normal curvature, also known as principal directions, which are the two principal curvatures. They are obtained as

$$\kappa_{1/2} = H \pm \sqrt{H^2 - K} \tag{4.12}$$

In image processing Gaussian and the mean are of interest since it is possible to classify surfaces based on the sign of their Gaussian and mean curvature [13]. Surfaces with $K > 0$ correspond to elliptic patches and can further be classified as convex ($H > 0$) and concave patches ($H < 0$). Negative Gaussian curvature indicates a hyperbolic patch. These different surface types are used to distinguish between i1D and different i2D regions in the target image. This classification possibility serves as the main idea to couple differential geometry with the monogenic signal to extend it in order to analyze i2D regions.
As a starting point to construct the monogenic curvature tensor, Di Zang uses the Hessian matrix

$$H_M = \begin{bmatrix} \frac{\partial^2}{\partial x_1^2} f(x) & \frac{\partial^2}{\partial x_1 x_2} f(x) \\ \frac{\partial^2}{\partial x_1 x_2} f(x) & \frac{\partial^2}{\partial x_2^2} f(x) \end{bmatrix}. \tag{4.13}$$

Switching to the Fourier domain and using polar coordinates

$$u^T = (r\ \cos(\theta), r\ \sin(\theta))^T \tag{4.14}$$

the entries of the Fourier transformed Hessian matrix read:

$$\begin{array}{lll} \mathcal{F}[f_{x_1x_1}](u) & = (i\ r\ \cos(\theta))^2\ \mathcal{F}[f](u) & = -r^2\ \cos^2(\theta)\ \mathcal{F}[f](u) \\ \mathcal{F}[f_{x_1x_2}](u) & = (i\ r\ \cos(\theta))(i\ r\ sin(\theta))\ \mathcal{F}[f](u) & = -r^2\ \sin(\theta)\cos(\theta)\ \mathcal{F}[f](u) \\ \mathcal{F}[f_{x_2x_1}](u) & = -(\mathcal{F}[f_{x_2x_1}](u)) & \\ \mathcal{F}[f_{x_2x_2}](u) & = (i\ r\ sin(\theta))^2\ \mathcal{F}[f](u) & = -r^2\ sin^2(\theta)\ \mathcal{F}[f](u) \end{array}$$

The so called even tensor part is constructed by ignoring the radial factors r^2 in the Fourier domain:

$$H_e = \begin{bmatrix} \cos^2(\theta)\mathcal{F}[f] & -\cos(\theta)\sin(\theta)\ \mathcal{F}[f]e_{12} \\ \cos(\theta)\sin(\theta)\ \mathcal{F}[f]e_{12} & \sin^2(\theta)\mathcal{F}[f] \end{bmatrix} \tag{4.15}$$

The ignorance of the radial factors in the Fourier domain has a crucial consequence for the entries in the tensor. Although they are supposed to represent second order derivatives in Fourier domain, the entries are just the second order Riesz transforms in the Fourier domain. To point out this fact consider the second order Riesz kernels in the Fourier domain

$$\begin{array}{lll} \mathcal{F}[R_{x_1}\ R_{x_1}](u) & = \left(\frac{i\ u_1}{|u|}\right)^2 & = -\frac{r^2\ \cos^2(\theta)}{r^2} \quad = -\cos^2(\theta) \\ \mathcal{F}[R_{x_1}\ R_{x_2}](u) & = \left(\frac{i\ u_1}{|u|}\right)\left(\frac{i\ u_2}{|u|}\right) & = -\frac{r^2\ \cos(\theta)sin(\theta)}{r^2} \quad = -\cos(\theta)sin(\theta)\ . \\ \mathcal{F}[R_{x_2}\ R_{x_2}](u) & = \left(\frac{i\ u_2}{|u|}\right)^2 & = -\frac{r^2\ sin^2(\theta)}{r^2} \quad = -sin^2(\theta) \end{array} \tag{4.16}$$

As one can see these are exactly the factors used in the even tensor entries. Therefore, the even tensor part can be written in terms of the second order Riesz transforms as

$$T_e = \begin{bmatrix} R_{x_1x_1}[f] & -R_{x_1x_2}[f]e_{12} \\ R_{x_1x_2}[f]e_{12} & R_{x_2x_2}[f] \end{bmatrix}. \tag{4.17}$$

The odd tensor part in the spatial domain is constructed by applying the Riesz transform again to the even tensor entries.
The terms *even* and *odd* in conjunction with the tensor parts are related to the argument of the sine and cosine functions which serve as basis functions. While the even tensor consists of even basis functions of order 0 and 2, the odd part consists of odd basis functions. Since the Riesz kernels have their origin in the study of kernels derived from

spherical harmonics as it has been shown in (2.35), the sine and cosine functions in this case are also referred to as spherical harmonics on the unit sphere $\mathbb{S}$ in $\mathbb{R}^2$.
Now that the two tensor parts have been expressed in terms of the Riesz transform, the single tensor entries can be interpreted in terms of the Radon transform. In the last chapter the relation between the Riesz and the Radon transform has been introduced. Applying the link (3.30) between the two transforms to the single tensor entries results in the following representation in the Radon domain:

$$\begin{aligned}
R_{x_1x_1}[f] &= \mathcal{R}^{-1}[\cos(\theta)\,\mathcal{H}[\mathcal{R}[\mathcal{R}^{-1}[\cos(\theta)\,\mathcal{H}[\mathcal{R}[f]]]]]] && (4.18)\\
&= \mathcal{R}^{-1}[\cos(\theta)\,\mathcal{H}[\cos(\theta)\,\mathcal{H}[\mathcal{R}[f]]]] && (4.19)\\
&= \mathcal{R}^{-1}[-\cos^2(\theta)\mathcal{R}[f]] && (4.20)\\
R_{x_1x_2}[f] &= R_{x_2x_1}[f] && (4.21)\\
&= \mathcal{R}^{-1}[\cos(\theta)\,\mathcal{H}[\mathcal{R}[\mathcal{R}^{-1}[\sin(\theta)\,\mathcal{H}[\mathcal{R}[f]]]]]] && (4.22)\\
&= \mathcal{R}^{-1}[\cos(\theta)\,\mathcal{H}[\sin(\theta)\,\mathcal{H}[\mathcal{R}[f]]]] && (4.23)\\
&= \mathcal{R}^{-1}[-\cos(\theta)\sin(\theta)\mathcal{R}[f]] && (4.24)\\
R_{x_2x_2}[f] &= \mathcal{R}^{-1}[\sin(\theta)\,\mathcal{H}[\mathcal{R}[\mathcal{R}^{-1}[\sin(\theta)\,\mathcal{H}[\mathcal{R}[f]]]]]] && (4.25)\\
&= \mathcal{R}^{-1}[\sin(\theta)\,\mathcal{H}[\sin(\theta)\,\mathcal{H}[\mathcal{R}[f]]]] && (4.26)\\
&= \mathcal{R}^{-1}[-\sin^2(\theta)\mathcal{R}[f]] && (4.27)
\end{aligned}$$

where the property $\mathcal{H}[\mathcal{H}[f]] = -f$ of the Hilbert transform has been used. Using these components the even tensor in terms of the Radon transform reads

$$T_e = \begin{bmatrix} \mathcal{R}^{-1}[\cos^2(\theta)\mathcal{R}[f]] & \mathcal{R}^{-1}[-\cos(\theta)\sin(\theta)\mathcal{R}[f]]e_{12} \\ \mathcal{R}^{-1}[\cos(\theta)\sin(\theta)\mathcal{R}[f]]e_{12} & \mathcal{R}^{-1}[\sin^2(\theta)\mathcal{R}[f]] \end{bmatrix}. \tag{4.28}$$

Proceeding in the same way as above, relating the odd tensor to the Radon transform results in

$$T_o = \begin{bmatrix} T_{o11} & T_{o21} \\ T_{o12} & T_{o22} \end{bmatrix} \tag{4.29}$$

with

$$\begin{aligned}
T_{o11} &= \mathcal{R}^{-1}[\cos^3(\theta)\mathcal{H}[\mathcal{R}[f]]] + \mathcal{R}^{-1}[\cos^2(\theta)\sin(\theta)\mathcal{H}[\mathcal{R}[f]]]e_{12} && (4.30)\\
T_{o12} &= \mathcal{R}^{-1}[\cos^2(\theta)\sin(\theta)\mathcal{H}[\mathcal{R}[f]]]e_{12} + \mathcal{R}^{-1}[\cos(\theta)\sin^2(\theta)\mathcal{H}[\mathcal{R}[f]]]e_{12} && (4.31)\\
T_{o21} &= \mathcal{R}^{-1}[-\cos^2(\theta)\sin(\theta)\mathcal{H}[\mathcal{R}[f]]]e_{12} + \mathcal{R}^{-1}[\cos(\theta)\sin^2(\theta)\mathcal{H}[\mathcal{R}[f]]]e_{12} && (4.32)\\
T_{o22} &= \mathcal{R}^{-1}[\sin^3(\theta)\mathcal{H}[\mathcal{R}[f]]]e_{12} + \mathcal{R}^{-1}[\cos(\theta)\sin^2(\theta)\mathcal{H}[\mathcal{R}[f]]] && (4.33)\\
& && (4.34)
\end{aligned}$$

The above representation allows the splitting into the x_1 and x_2 components as

$$T_o = T_{o_{x_1}} + T_{o_{x_2}} \tag{4.35}$$

with

$$T_{o_{x_1}} = \begin{bmatrix} \mathcal{R}^{-1}[\cos^3(\theta)\mathcal{H}[\mathcal{R}[f]]] & \mathcal{R}^{-1}[\cos^2(\theta)\sin(\theta)\mathcal{H}[\mathcal{R}[f]]] \\ \mathcal{R}^{-1}[\cos^2(\theta)\sin(\theta)\mathcal{H}[\mathcal{R}[f]]] & \mathcal{R}^{-1}[\cos(\theta)\sin^2(\theta)\mathcal{H}[\mathcal{R}[f]]] \end{bmatrix} \tag{4.36}$$

and

$$T_{o_{x_2}} = \begin{bmatrix} \mathcal{R}^{-1}[\cos^2(\theta)\sin(\theta)\mathcal{H}[\mathcal{R}[f]]] & \mathcal{R}^{-1}[\cos(\theta)\sin^2(\theta)\mathcal{H}[\mathcal{R}[f]]] \\ \mathcal{R}^{-1}[\cos(\theta)\sin^2(\theta)\mathcal{H}[\mathcal{R}[f]]] & \mathcal{R}^{-1}[\sin^3(\theta)\mathcal{H}[\mathcal{R}[f]]] \end{bmatrix} \tag{4.37}$$

With the constructed tensor pairs the monogenic curvature signal according to [32] is defined as:

Definition 4.1.1 (Monogenic curvature signal)**.**

$$f_{i2D} = det(T_e)e_3 + det(T_o)e_1 = det(T_e)e_3 + det(T_{o_{x_1}})e_1 + det(T_{o_{x_2}})e_2 \tag{4.38}$$

4.2 Analysis of i1D signals

Before discussing the differential geometric entities the signal is supposed to represent, it will be shown that the monogenic curvature signal is as powerful as the monogenic signal in terms of determining main orientation, phase and apex angle of i1D and two superposed i1D signals with the same but arbitrary phase and amplitude.

Theorem 4.2.1. *Let f_{i1D} be a i1D signal with main orientation θ_{Main}. Then the main orientation is obtained by:*

$$\theta_{Main} = \arctan\left(\sqrt{\frac{T_{e_{22}}}{T_{e_{11}}}}\right) = \arctan\left(\sqrt{\frac{T_{e_{12}}}{T_{e_{11}}}}\right) = \arctan\left(\sqrt{\frac{T_{e_{22}}}{T_{e_{12}}}}\right) \tag{4.39}$$

Proof. Since the target signal is a i1D signal its corresponding Radon transform has only one non-constant slice function located at θ_{Main}. Therefore, according to the orientation determination with the monogenic signal in (3.36), it is legitimate to move the sine and cosine terms out of the inverse Radon transform integral as it has already been done in the last chapter. This results in

$$\arctan\left(\sqrt{\frac{T_{e_{22}}}{T_{e_{11}}}}\right) = \arctan\left(\sqrt{\frac{\mathcal{R}^{-1}[\sin^2(\theta)\mathcal{R}[f_{i1D}]]}{\mathcal{R}^{-1}[\cos^2(\theta)\mathcal{R}[f_{i1D}]]}}\right) \tag{4.40}$$

$$= \arctan\left(\sqrt{\frac{\sin^2(\theta_{Main})\mathcal{R}^{-1}[\mathcal{R}[f_{i1D}]]}{\cos^2(\theta_{Main})\mathcal{R}^{-1}[\mathcal{R}[f_{i1D}]]}}\right) \tag{4.41}$$

$$= \arctan\left(\frac{sin(\theta_{Main})}{cos(\theta_{Main})}\right) \tag{4.42}$$

□

In addition it is possible to determine the local phase of the i1D signal.

Theorem 4.2.2. *Let f_{i1D} be a i1D signal with main orientation θ_{Main}. Then the local phase is given by:*

$$\varphi = \arctan\left(\frac{trace(T_{o_{x_2}})}{sin(\theta_{Main})trace(T_e)}\right) \tag{4.43}$$

Proof. Using (3.37) and moving again the sine and cosine terms out of the inverse Radon transform integral one obtains

$$\begin{aligned}\frac{trace(T_{o_{x_2}})}{sin(\theta_{Main})trace(T_e)} &= \frac{\mathcal{R}^{-1}[\cos^2(\theta)\sin(\theta)\mathcal{H}[\mathcal{R}[f_{i1D}]]] + \mathcal{R}^{-1}[\sin^3(\theta)\mathcal{H}[\mathcal{R}[f_{i1D}]]]}{\sin(\theta_{Main})\ (\mathcal{R}^{-1}[\cos^2(\theta)\mathcal{R}[f_{i1D}]] + \mathcal{R}^{-1}[\sin^2(\theta)\mathcal{R}[f_{i1D}]])} &(4.44)\\ &= \frac{\sin(\theta_{Main})\mathcal{R}^{-1}[\mathcal{H}[\mathcal{R}[f_{i1D}]]]}{\sin(\theta_{Main})\ \mathcal{R}^{-1}[\mathcal{R}[f_{i1D}]]} &(4.45)\\ &= \frac{\mathcal{H}_{t\to s}[f_{i1D}(t\cos\theta_{Main}, t\sin\theta_{Main})](s)}{f_{i1D}}. &(4.46)\end{aligned}$$

□

4.3 Analysis of superposed i1D signals

Proceeding analogously to the previous section, the monogenic curvature signal is used to determine the main orientation, the apex angle, and the phase of two superposed i1D signals

$$f_{i2D} = f_{i1D_1} + f_{i1D_2} \tag{4.47}$$

The main orientations of the two i1D signals are denoted by θ_1, θ_2 and the local phases by φ_1, φ_2. Further on the following abbreviations will be used:

$$a := \cos(\theta_1), b := \cos(\theta_2), c := \sin(\theta_1), d := \sin(\theta_2) \tag{4.48}$$

$$s(\theta_{(1/2)}) = \mathcal{R}^{-1}[\mathcal{H}[\mathcal{R}[f]]]. \tag{4.49}$$

With these abbrevations the even and odd tensors for a f_{i2D} signal as it has been defined above read:

$$T_e = f_{i2D}\begin{bmatrix} a^2+b^2 & ca+db \\ ca+db & c^2+d^2 \end{bmatrix} \tag{4.50}$$

$$T_o = s(\theta_{1/2})\begin{bmatrix} (a^2c+b^2d)e_{12}+a^3+b^3 & -(ca^2+db^2)e_{12}+c^2a+d^2b \\ ca^2+db^2)e_{12}-(c^2a+d^2b) & (c^2a+d^2)e_{12}+bc^3+d^3 \end{bmatrix} \tag{4.51}$$

The determinant is then obtained as:

$$e_1 det(T_o) = e_1 s^2(\theta_{1/2})\,(a^3d^2b + b^3c^2a - ca^2d^3 - db^2c^3 - 2ca^2db^2 + 2c^2ad^2b) \tag{4.52}$$
$$+ e_2 s^2(\theta_{1/2})\,(a^3d^3 + b^3c^3 - db^2c^2a - ca^2d^2b) \tag{4.53}$$
$$= e_1 det(T_{o_{x_1}}) + e_2 det(T_{o_{x_2}}). \tag{4.54}$$

With the determinants of the tensor parts $T_{o_{x_1}}$ and $T_{o_{x_2}}$ the main orientation of i2D signals can be calculated.

Theorem 4.3.1. *Let $f_{i2D} = f_{i1D_1} + f_{i1D_2}$ be the superposition of two i1D signals with main orientations θ_1, θ_2. Then the main orientation θ_{Main} of f_{i2D} is obtained by:*

$$\theta_{Main} = \frac{1}{2}\arctan\left(\frac{det(T_{o_{x_2}})}{det(T_{o_{x_1}})}\right) \tag{4.55}$$

Proof. $det(T_{o_{x_1}})$ and $det(T_{o_{x_2}})$ can be written as:

$$det(T_{o_{x_1}}) = s(\theta_{1/2})^2(a^3d^2b + b^3c^2a - ca^2d^3 - db^2c^3 - 2ca^2db^2 + 2c^2ad^2b) \tag{4.56}$$
$$= s(\theta_{1/2})^2(a^2d^2(ab - cd) + b^2c^2(ab - cd) - 2abcd(ab - cd)) \tag{4.57}$$
$$= s(\theta_{1/2})^2((ab - cd)(a^2d^2 + b^2c^2 - 2abcd)) \tag{4.58}$$

and

$$det(T_{o_{x_2}}) = s(\theta_{1/2})^2(a^3d^3 + b^3c^3 - ab^2c^2a - ca^2d^2b) \tag{4.59}$$
$$= s(\theta_{1/2})^2((ad + bc)(a^2d^2 - abcd + b^2c^2) - abcd(ad + bc)) \tag{4.60}$$
$$= s(\theta_{1/2})^2((ad + bc)a^2d^2 + (ad + bc)b^2c^2 - 2abcd(ad + bc)) \tag{4.61}$$
$$= s(\theta_{1/2})^2((ad + bc)(a^2d^2 + b^2c^2 - 2abcd)) \tag{4.62}$$

therefore:

$$\frac{B}{C} = \frac{(ad - cd)(a^2d^2 + b^2c^2 - 2abcd)}{(ad + bc)(a^2d^2 + b^2c^2 - 2abcd)} \tag{4.63}$$
$$= \frac{ab - cd}{ad + bc} \tag{4.64}$$
$$= \frac{\cos(\theta_1)\cos(\theta_2) - \sin(\theta_1)\sin(\theta_2)}{\cos(\theta_1)\sin(\theta_2) + \cos(\theta_2)\sin(\theta_1)} \tag{4.65}$$
$$= \frac{\cos(\theta_1 + \theta_2)}{\sin(\theta_1 + \theta_2)} \tag{4.66}$$
$$= \frac{1}{\tan(\theta_1 + \theta_2)} \tag{4.67}$$

and

$$\arctan\left(\frac{det(T_{o_{x_1}})}{det(T_{o_{x_2}})}\right) = \arctan(\frac{1}{\tan(\theta_1+\theta_2)}) \tag{4.68}$$

$$= \frac{\pi}{2} - \arctan(\tan(\theta_1+\theta_2)) \tag{4.69}$$

$$= \frac{\pi}{2} - (\theta_1+\theta_2) \tag{4.70}$$

□

Apart from the main orientation and the local phase, two superposed i1D signals provide an additional feature: the apex angle of the two i1D structures. The previous section already introduced the apex angle calculation in terms of first order Riesz transforms. Now the apex angle is determined in terms of second order Riesz transforms following an approach from differential geometry which first appeared in [31]. The two superposed i1D signals are assumed to have the same but arbitrary phase and amplitude. Analysis of the signal is performed at the origin $(0,0)^T$. Furthermore, the signal is embedded in $\mathbb{R}^3$ as a Monge patch $S(x) = x_1e_1 + x_2e_2 + f(x)e_3$. From differential geometry it is known that the normal curvatures along the two orientations θ_1, θ_2 of the two i1D signals at the origin is equal to 0 since the radius of the osculating circle at that point is infinite. Additionally the signal is assumed to be rotated in such a way, that the maximum curvature direction n_{k_1} points along the x_1 axis and the minimum curvature direction points along the x_2 axis. The problem of determining the apex angle α reduces to the determination of the angle between the maximum curvature direction and θ_1. According to Meusnier's and Eueler's theorem the normal curvature along $\frac{\alpha}{2}$ reads

$$k(\frac{\alpha}{2}) = \cos^2(\frac{\alpha}{2}) + \sin^2(\frac{\alpha}{2}). \tag{4.71}$$

Solving for $k(\frac{\alpha}{2}) = 0$

$$\alpha = 2\arctan\left(\sqrt{\frac{|k_1|}{|k_2|}}\right) \tag{4.72}$$

expresses the apex angle α in terms of the principal curvatures k_1, k_2. The principal curvatures have been introdued as the eigenvalues of the Weingarten map and allow the representation in terms of the mean and Gaussian curvature of the Monge patch embedding as

$$k_{1/2} = H \pm \sqrt{H^2 - K}. \tag{4.73}$$

Recalling the defintions (4.10) for the curvatures H, K on an notice that first order derivatives are involved. Due to the nature of the underlying signal model which is the superposition of the plane waves, the first order derivatives vanish at the origin $(0,0)^T$ at which the evaluation takes place. Hence for this special signal model the mean and

Gaussian curvature can be represented as the trace and the determinant of the Hessian matrix

$$H(0,0) = trace(H_M)(0,0) = f_{x_1x_1}(0,0) + f_{x_2x_2}(0,0) \tag{4.74}$$
$$K(0,0) = det(H_M)(0,0) = f_{x_1x_1}(0,0) f_{y_1y_1}(0,0) - f^2_{x_1x_2}(0,0) \tag{4.75}$$

The question arises, if one can proceed accordingly involving quantities, that is second order Riesz transforms, from the even monogenic curvature tensor, which is answered by the following theorem:

Theorem 4.3.2. *Let $f_{i2D} = f_{i1D_1} + f_{i1D_2}$ be the superposition of two i1D signals with main orientations θ_1, θ_2. Further define:*

$$H := \frac{1}{2} trace(T_e) = s\frac{1}{2}(a^2 + b^2 + c^2 + d^2) = s \tag{4.76}$$
$$K := det(T_e) = s^2(a^2d^2 + b^2c^2 - 2abcd) \tag{4.77}$$

Then the apex angle $\theta_1 - \theta_2$ of f_{i2D} is obtained by:

$$\theta_1 - \theta_2 = 2 \arctan \sqrt{\left| \frac{H - \sqrt{H^2 - K}}{H + \sqrt{H^2 - K}} \right|} \tag{4.78}$$
$$= 2 \arctan \sqrt{\left| \frac{s(1 - \sqrt{1 - (a^2d^2 + b^2c^2 - 2abcd)})}{s(1 + \sqrt{1 - (a^2d^2 + b^2c^2 - 2abcd))} \right|} \tag{4.79}$$

Proof.

$$1 - \sqrt{1 - det(T_e)} = 1 - \sqrt{1 - a^2d^2 + b^2c^2 - 2abcd} \tag{4.80}$$
$$= 1 - \sqrt{1 - (bc - ad)^2} \tag{4.81}$$
$$= 1 - \sqrt{1 - (\cos(\theta_2)\sin(\theta_1) - \cos(\theta_1)\sin(\theta_2))^2} \tag{4.82}$$
$$= 1 - \sqrt{1 - \sin^2(\theta_1 - \theta_2)} \tag{4.83}$$
$$= 1 - \cos(\theta_1 - \theta_2) \tag{4.84}$$

equivalently

$$1 + \sqrt{1 + det(T_e)} = 1 + \cos(\theta_1 - \theta_2) \tag{4.85}$$

Therefore the following holds:

$$\frac{1 - \sqrt{1 - det(T_e)}}{1 + \sqrt{1 - det(T_e)}} = \frac{1 - \cos(\theta_1 - \theta_2)}{1 + \cos(\theta_1 - \theta_2)} \tag{4.86}$$
$$= \frac{\sqrt{2}\sin^2(\frac{\theta_1 - \theta_2}{2})}{\sqrt{2}\cos^2(\frac{\theta_1 - \theta_2}{2})} \tag{4.87}$$
$$= \tan^2(\frac{\theta_1 - \theta_2}{2}) \tag{4.88}$$

From the above formula follows

$$\arctan\left(\sqrt{\tan^2(\frac{\theta_1-\theta_2}{2})}\right) = \left|\frac{\theta_1-\theta_2}{2}\right| \tag{4.89}$$

□

In (3.47) it has been shown how the phase of two superposed i1D signals with arbitrary but same phase could be determined via the Riesz transform and the assumption, that the main orientations θ_1, θ_2 are known. We will now state the result in terms of the monogenic curvature tensor. Using the definitions from above for $T_{o_{x_1}}, T_{o_{x_2}}$ and defining further

$$\begin{aligned} det(T_e) &= f_{i2D}^2\left[(a^2+b^2)(c^2+d^2)-(ca+db)^2\right] && (4.90)\\ &= f_{i2D}^2\left[a^2d^2+b^2c^2-2abcd\right] && (4.91)\end{aligned}$$

leads to:

$$\begin{aligned} \frac{\sqrt{det(T_{o_{x_1}})^2+det(T_{o_{x_2}})^2}}{det(T_e)} &= \frac{\sqrt{(h(t)*f_{i2D})^2(a^2b^2+c^2+d^2+a^2d^2+c^2b^2)}}{f_{i2D}^2} && (4.92)\\ &= \frac{\sqrt{(h(t)*f_{i2D})^2(\cos^2(\theta_1)+sin^2(\theta_1))}}{f_{i2D}^2} && (4.93)\\ &= \frac{(h(t)*f_{i2D})^2}{f_{i2D}^2} && (4.94)\end{aligned}$$

4.4 Second Order Riesz transform convolution kernels

The features of i1D and superposed i1D signals in terms of the monogenic curvature tensor use the second order Riesz transforms. These transforms are obtained by convolution with the appropriate kernels in the spatial domain. Convoluting in the spatial domain overcomes the calculation in the Fourier domain. Nonetheless, the convolution kernels have to be determined first. For the first order Riesz transforms in $\mathbb{R}^2$ these kernels have already been introduced as

$$r_1 = \frac{x_1}{|x|^3}, r_2 = \frac{x_2}{|x|^3} \tag{4.95}$$

To obtain the kernels for the second order Riesz transforms, the Hilbert-transform like operator

$$\mathcal{H}^{(m)}[f](z) = \frac{-|m|}{2\pi}\int_{\mathbb{C}} \frac{f(\xi)}{(z-\xi)^m|z-\xi|^{2-m}}d\xi \tag{4.96}$$

with $z \in \mathbb{C}$ which has been introduced in [21] is considered. For $m = 1$ the operator $\mathcal{H}^1[f](z)$ evaluates to:

$$\mathcal{H}^{(1)}[f](z) = \frac{-1}{2\pi} \int_{\mathbb{C}} \frac{f(\xi)}{(z-\xi)|z-\xi|} d\xi \tag{4.97}$$

$$= \frac{-1}{2\pi} \int_{\mathbb{C}} \frac{f(\xi)((z_1-\xi_1) - i(z_2-\xi_2))}{((z_1-\xi_1) - i(z_2-\xi_2))((z_1-\xi_1) + i(z_2-\xi_2))|z-\xi|} d\xi \tag{4.98}$$

$$= \frac{-1}{2\pi} \int_{\mathbb{C}} \frac{f(\xi)(z_1-\xi_1) - i(z_2-\xi_2))}{|z-\xi|^2|z-\xi|} d\xi \tag{4.99}$$

$$= \frac{-1}{2\pi} \int_{\mathbb{C}} \frac{f(\xi)(z_1-\xi_1)}{|z-\xi|^3} d\xi + \frac{i}{2\pi} \int_{\mathbb{C}} \frac{f(\xi)(z_2-\xi_2)}{|z-\xi|^3} d\xi \tag{4.100}$$

$$= -R_{x_1}[f](z) + iR_{x_2}[f](z) \tag{4.101}$$

which is nothing else but a complex operator representing the first order Riesz transform in terms of the already known convolution integrals. In the case of $m = 2$ the operator results in the Beurling-Ahlfors transform [21] with the Fourier multiplier (see [4]):

$$\mathcal{F}[\mathcal{H}^{(2)}[f]](\xi) = -\frac{\overline{\xi}}{\xi} \tag{4.102}$$

which will be used to prove the following theorem which establishes the link between the Beurling-Ahlfors transform and the second order Riesz transforms:

Theorem 4.4.1.

$$\mathcal{H}^{(2)}[f](z) = -R_{11}[f](z) + R_{22}[f](z) + 2iR_{12}[f](z) \tag{4.103}$$

Proof. Switching to the Fourier domain and using the Fourier multipliers of the Riesz transforms

$$\mathcal{F}[r_j] = i\frac{\xi_j}{|\xi|} \tag{4.104}$$

one obtains:

$$\mathcal{F}[R_{x_1x_1}[f] - R_{x_2x_2}[f] - 2iR_{x_1x_2}[f]](\xi) = -\frac{\xi_1^2}{|\xi|^2} + -\frac{\xi_2^2}{|\xi|^2} + 2i\frac{\xi_1\xi_2}{|\xi|^2} \tag{4.105}$$

$$= -\frac{(\xi_1 - i\xi_2)^2}{|\xi|^2} \tag{4.106}$$

$$= \frac{\overline{\xi}^2}{\xi\overline{\xi}} = -\frac{\overline{\xi}}{\xi} = \mathcal{F}[\mathcal{H}^2[f]](\xi) \tag{4.107}$$

□

Since the Beurling-Ahlfors transform is an operator consisting of second order Riesz transforms the convolution integral is now split up into its components to obtain the convolution kernels:

$$\mathcal{H}^{(2)}[f](z) = \frac{-2}{2\pi}\int\limits_{\mathbb{C}} \frac{f(\xi)}{(z-\xi)^2}d\xi \tag{4.108}$$

$$= \frac{-2}{2\pi}\int\limits_{\mathbb{C}} \frac{f(\xi)}{((z_1-\xi_1)+i(z_2-\xi_2))^2}d\xi \tag{4.109}$$

$$= \frac{-2}{2\pi}\int\limits_{\mathbb{C}} \frac{f(\xi)}{(z_1-\xi_1)^2+2i(z_1-\xi_1)(z_2-\xi_2)-(z_2-\xi_2)^2}d\xi \tag{4.110}$$

$$= \frac{-2}{2\pi}\int\limits_{\mathbb{C}} \frac{f(\xi)((z_1-\xi_1)^2-2i(z_1-\xi_1)(z_2-\xi_2)-(z_2-\xi_2)^2)}{\begin{array}{c}((z_1-\xi_1)^2+2i(z_1-\xi_1)(z_2-\xi_2)-(z_2-\xi_2)^2)\\((z_1-\xi_1)^2-2i(z_1-\xi_1)(z_2-\xi_2)-(z_2-\xi_2)^2)\end{array}}d\xi \tag{4.111}$$

$$= \frac{-2}{2\pi}\int\limits_{\mathbb{C}} \frac{f(\xi)((z_1-\xi_1)^2-2i(z_1-\xi_1)(z_2-\xi_2)-(z_2-\xi_2)^2)}{((z_1-\xi_1)^2-(z_2-\xi_2)^2)^2+4(z_1-\xi_1)^2(z_2-\xi_2)^2}d\xi \tag{4.112}$$

$$= \frac{-2}{2\pi}\int\limits_{\mathbb{C}} \frac{f(\xi)(z_1-\xi_1)^2}{((z_1-\xi_1)^2-(z_2-\xi_2)^2)^2+4(z_1-\xi_1)^2(z_2-\xi_2)^2}d\xi \tag{4.113}$$

$$+ \frac{2}{2\pi}\int\limits_{\mathbb{C}} \frac{f(\xi)(z_2-\xi_2)^2}{((z_1-\xi_1)^2-(z_2-\xi_2)^2)^2+4(z_1-\xi_1)^2(z_2-\xi_2)^2}d\xi \tag{4.114}$$

$$+ \frac{4i}{2\pi}\int\limits_{\mathbb{C}} \frac{f(\xi)(z_1-\xi_1)(z_2-\xi_2)}{((z_1-\xi_1)^2-(z_2-\xi_2)^2)^2+4(z_1-\xi_1)^2(z_2-\xi_2)^2}d\xi \tag{4.115}$$

$$= R_{x_1x_1}[f](z) - R_{x_2x_2}[f](z) - 2iR_{x_1x_2}[f](z) \tag{4.116}$$

Therefore the convolution kernels read:

$$r_{11} = \frac{1}{\pi}\frac{x_1^2}{(x_1^2-x_2^2)^2+4x_1^2x_2^2} = \frac{x_1^2}{|x|^4}\frac{1}{\pi} \tag{4.117}$$

$$r_{22} = \frac{1}{\pi}\frac{x_2^2}{(x_1^2-x_2^2)^2+4x_1^2x_2^2} = \frac{x_2^2}{|x|^4}\frac{1}{\pi} \tag{4.118}$$

$$r_{12} = \frac{1}{\pi}\frac{x_1x_2}{(x_1^2-x_2^2)^2+4x_1^2x_2^2} = \frac{x_1x_2}{|x|^4}\frac{1}{\pi} \tag{4.119}$$

According to the first order Riesz transforms the convolutions are singular integrals which only exist as Cauchy principal values. In order to use them in the Poisson scale space concept their Poisson transforms are of interest. They are obtained by convoluting the kernels with the Poisson kernel in the spatial domain. Using the Fourier convolution theorem this convolution corresponds to a multiplication in the Fourier domain.

Using the Fourier multipliers of the Beurling-Ahlfors transform operator and the Poisson kernel

$$\mathcal{F}[\mathcal{P}_s](u) = e^{-2\pi|u|s} = e^{-2\pi rs}, u \in \mathbb{R}^2, s \in \mathbb{R}_+ \tag{4.120}$$

$$\mathcal{F}[\mathcal{H}^{(2)}[f]](\xi) = -\frac{\overline{\xi}}{\xi} \tag{4.121}$$

the convolution kernel in the spatial domain is obtained by applying the inverse Fourier transform in polar coordinates to the product of the Poisson- and the Beurling-Ahlfors multiplier in the Fourier domain with $x \in \mathbb{C}, x = ke^{i\varphi}$:

$$\mathcal{F}^{-1}[-e^{-2\pi rs}e^{-i2\theta}](x) = (2\pi)\int_0^\infty\int_0^{2\pi} -e^{-2\pi rs}e^{-i2\theta}e^{i2\pi kr\cos(\theta-\varphi)}rd\theta dr \tag{4.122}$$

$$= (2\pi)\int_0^\infty\int_0^{2\pi} -e^{-2\pi rs}e^{-i2(\theta+\varphi)}e^{i2\pi kr\cos(\theta)}rd\theta dr \tag{4.123}$$

$$= -(2\pi)e^{-i2\varphi}\int_0^\infty e^{-2\pi rs}\int_0^{2\pi} e^{-i2\theta}e^{i2\pi kr\cos(\theta)}rd\theta dr \tag{4.124}$$

$$= -(2\pi)e^{-i2\varphi}\int_0^\infty e^{-2\pi rs}J_2(2\pi kr)rdr \tag{4.125}$$

where J_2 is a Bessel function of the first kind and order 2. In the following the abbrevations $\alpha = 2\pi s$ and $\beta = 2\pi k$ will be used. J_2 can be written due to the recurrence relation for Bessel functions as

$$J_2(2\pi kr) = J_2(\beta r) = \frac{2}{\beta r}J_1(\beta r) - J_0(\beta r) \tag{4.126}$$

which leads to

$$- (2\pi)e^{-i2\varphi} \int_0^\infty e^{-\alpha r} J_2(\beta r) r dr \tag{4.127}$$

$$= -(2\pi)e^{-i2\varphi} \int_0^\infty e^{-\alpha r} \frac{2}{\beta r} J_1(\beta r) r dr \tag{4.128}$$

$$- -(2\pi)e^{-i2\varphi} \int_0^\infty e^{-\alpha r} J_0(\beta r) r dr \tag{4.129}$$

$$= -(2\pi)e^{-i2\varphi} \left(\frac{2}{\beta} \int_0^\infty e^{-\alpha r} J_1(\beta r) dr - e^{-i2\varphi} \int_0^\infty e^{-\alpha r} J_0(\beta r) r dr \right) \tag{4.130}$$

$$\tag{4.131}$$

According to common integral tables like [23], one obtains the evaluation of the two Bessel integrals as

$$\int_0^\infty e^{-\alpha r} \frac{2}{\beta} J_1(\beta r) dr = \frac{4(\sqrt{\alpha^2 + \beta^2} - \alpha)}{\beta^2 \sqrt{\alpha^2 + \beta^2}} \tag{4.132}$$

and

$$\int_0^\infty e^{-\alpha r} J_0(\beta r) r dr = \frac{2\alpha\Gamma(\frac{3}{2})}{\sqrt{\pi}(\alpha^2 + \beta^2)^{3/2}} = \frac{2\alpha\frac{\sqrt{\pi}}{2}}{\sqrt{\pi}(\alpha^2 + \beta^2)^{3/2}} \tag{4.133}$$

Applying these results to the equations above results in

$$- (2\pi)e^{-i2\varphi} \int_0^\infty e^{-\alpha r} J_2(2\pi k r) r dr \tag{4.134}$$

$$= -(2\pi)e^{-i2\varphi} \left(\frac{2}{\beta} \frac{2\sqrt{\alpha^2+\beta^2} - \alpha}{\beta\sqrt{\alpha^2+\beta^2}} - \frac{2\alpha\frac{\sqrt{\pi}}{2}}{\sqrt{\pi}(\alpha^2+\beta^2)^{(3/2)}} \right) \tag{4.135}$$

$$= -(2\pi)e^{-i2\varphi} \left(\frac{2\sqrt{\pi}(\alpha^2+\beta^2)^{(3/2)} - 2\sqrt{\pi}\alpha(\alpha^2+\beta^2) - \alpha\beta^2\sqrt{\pi}}{\sqrt{\pi}\beta^2(\alpha^2+\beta^2)^{(3/2)}} \right) \tag{4.136}$$

$$= -(2\pi)e^{-i2\varphi} \left(\frac{(-2\alpha^3 - 2\alpha\beta^2 - \alpha\beta^2) + 2(\alpha^2+\beta^2)^{(3/2)}}{\beta^2(\alpha^2+\beta^2)^{(3/2)}} \right) \tag{4.137}$$

$$= -(2\pi)e^{-i2\varphi} \left(\frac{2(\alpha^2+\beta^2)^{(3/2)} - \alpha(2\alpha^2+3\beta^2)}{\beta^2(\alpha^2+\beta^2)^{(3/2)}} \right) \tag{4.138}$$

$$= -e^{-i2\varphi} \left(\frac{2(s^2+k^2)^{(3/2)} - s(2s^2+3k^2)}{(2\pi)k^2(s^2+k^2)^{(3/2)}} \right) \tag{4.139}$$

$$= (x_1 - ix_2)^2 \left(\frac{s(2s^2+3k^2) - 2(s^2+k^2)^{(3/2)}}{(2\pi)k^4(s^2+k^2)^{(3/2)}} \right) \tag{4.140}$$

$$= (x_1^2 - 2ix_1x_2 - x_2^2) \left(\frac{s(2s^2+3k^2) - 2(s^2+k^2)^{(3/2)}}{(2\pi)k^4(s^2+k^2)^{(3/2)}} \right) \tag{4.141}$$

which leads to the three convolution kernels (see figure 4.1).

$$R_{x_1x_1} = x_1^2 \left(\frac{s(2s^2+3k^2) - 2(s^2+k^2)^{(3/2)}}{(2\pi)k^4(s^2+k^2)^{(3/2)}} \right) \tag{4.142}$$

$$R_{x_1x_2} = -x_1x_2 \left(\frac{s(2s^2+3k^2) - 2(s^2+k^2)^{(3/2)}}{(2\pi)k^4(s^2+k^2)^{(3/2)}} \right) \tag{4.143}$$

$$R_{x_2x_2} = -x_2^2 \left(\frac{s(2s^2+3k^2) - 2(s^2+k^2)^{(3/2)}}{(2\pi)k^4(s^2+k^2)^{(3/2)}} \right) \tag{4.144}$$

4.5 Third Order Riesz transform convolution kernels

To obtain the convolution kernels in the Poisson scale space for the third order Riesz transforms, the operator $\mathcal{H}^{(3)}$ is studied accordingly to (4.122) in the Fourier domain. Its multiplier reads $\mathcal{F}[\mathcal{H}^{(3)}] = e^{-i3\varphi}$. Following (4.122) one obtains the inverse Fourier transform

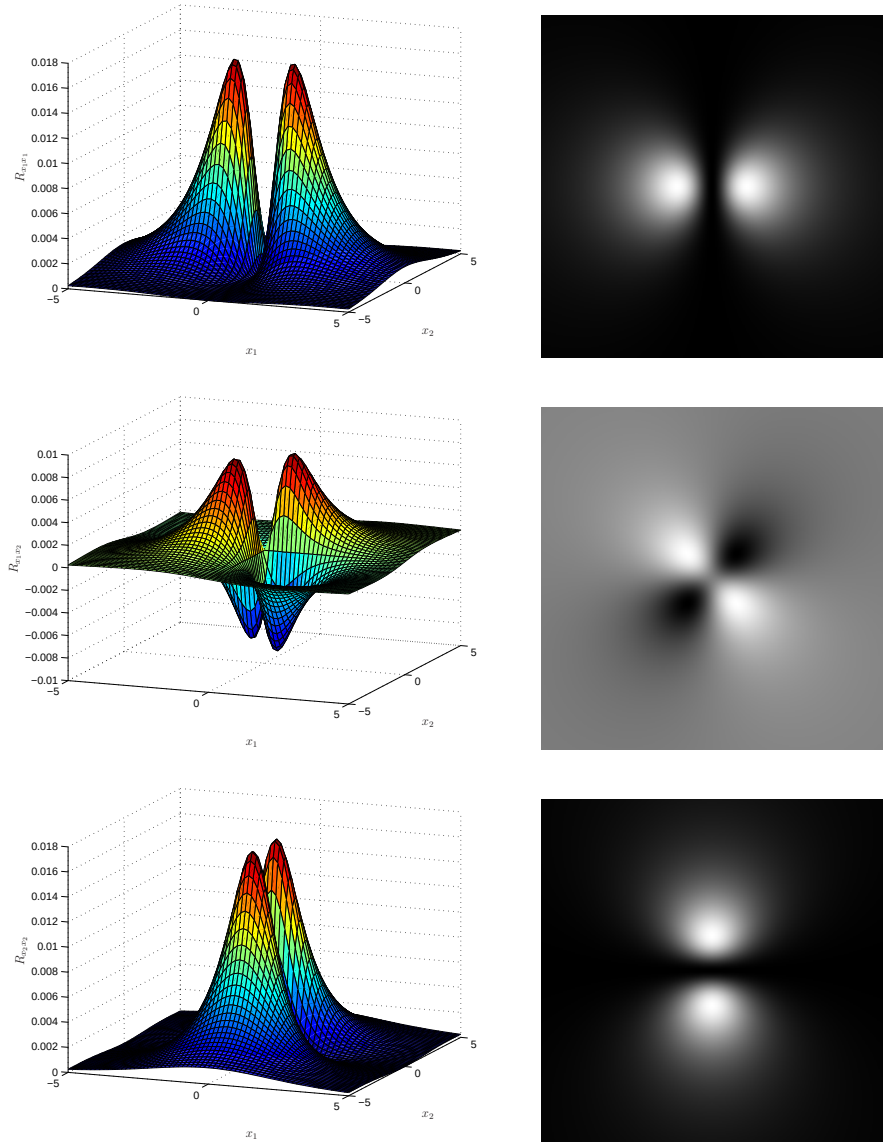

Figure 4.1: 3D and density plots of the second order Riesz transform convolution kernels in the Poisson scale space with scale parameters fine=1.1 and coarse=1.5

$$\mathcal{F}^{-1}[-e^{-2\pi rs}e^{-i3\theta}](x) = (2\pi)\int_0^{\infty}\int_0^{2\pi} -e^{-2\pi rs}e^{-i3\theta}e^{i2\pi kr\cos(\theta-\varphi)}rd\theta dr \tag{4.145}$$

$$= (2\pi)\int_0^{\infty}\int_0^{2\pi} -e^{-2\pi rs}e^{-i3(\theta+\varphi)}e^{i2\pi kr\cos(\theta)}rd\theta dr \tag{4.146}$$

$$= -(2\pi)e^{-i3\varphi}\int_0^{\infty} e^{-2\pi rs}\int_0^{2\pi} e^{-i2\theta}e^{i2\pi kr\cos(\theta)}rd\theta dr \tag{4.147}$$

$$= -(2\pi)e^{-i3\varphi}\int_0^{\infty} e^{-2\pi rs}J_3(2\pi kr)rdr \tag{4.148}$$

Using the recurrence relation

$$J_3(2\pi kr) = J_3(\beta r) = \frac{4}{\beta r}J_2(\beta r) - J_1(\beta r) \tag{4.149}$$

leads to

$$-(2\pi)e^{-i3\varphi}\int_0^{\infty} e^{-\alpha r}J_3(2\pi kr)rdr \tag{4.150}$$

$$= -(2\pi)e^{-i3\varphi}\left(4\frac{(\sqrt{\alpha^2+\beta^2}-\alpha)^2}{\beta^3\sqrt{\alpha^2+\beta^2}} - \frac{\beta}{(\alpha^2+\beta^2)^{(3/2)}}\right) \tag{4.151}$$

$$= -(2\pi)e^{-i3\varphi}\left(\frac{4(\alpha^2+\beta^2)^2 - 8\alpha(\alpha^2+\beta^2)^{(3/2)} + 4\alpha^2(\alpha^2+\beta^2) - \beta^4}{\beta^3(\alpha^2+\beta^2)^{(3/2)}}\right) \tag{4.152}$$

$$= -(2\pi)e^{-i3\varphi}\left(\frac{8\alpha^4 + 12\alpha^2\beta^2 + 3\beta^4 - 8\alpha(\alpha^2+\beta^2)^{(3/2)}}{\beta^3(\alpha^2+\beta^2)^{(3/2)}}\right) \tag{4.153}$$

$$= -(2\pi)(x-iy)^3\left(\frac{8k^4 + 12k^2s^2 + 3s^4 - 8k(k^2+s^2)^{(3/2)}}{s^6(k^2+s^2)^{(3/2)}}\right) \tag{4.154}$$

$$=: R_{K_3} \tag{4.155}$$

which allows the decomposition into the four third order convolution kernels (see figure 4.2).

$$R_{x_1x_1x_1} = x_1^3 R_{K_3} \tag{4.156}$$
$$R_{x_1x_1x_2} = -3x_1^2 x_2 R_{K_3} \tag{4.157}$$
$$R_{x_1x_2x_2} = -3x_1 x_2^2 R_{K_3} \tag{4.158}$$
$$R_{x_2x_2x_2} = x_2^3 R_{K_3} \tag{4.159}$$

4.6 Discussion of the monogenic curvature tensor

So far the monogenic curvature tensor has been able to extract the same information as the monogenic signal. As it has been mentioned in the introduction of the chapter the goal of the monogenic curvature tensor is an extension of the monogenic signal. This extension is supposed to be achieved by the coupling of the monogenic signal and concepts from differential geometry. In addition, the traces and determinants of the even and odd tensors are supposed to represent the Gaussian and the mean curvature of the Monge patch embedding to allow a further analysis and detection of i2D structures which is not limited to the case of two superposed i1D signals with same but arbitrary phase. In the following the differential geometric properties obtained from the tensor parts are analyzed and compared with the Gaussian and mean curvature.
It has already been shown in (4.16) that the second order Riesz transforms were obtained by the ignorance of the second order derivative radial factors in the Fourier domain. As a consequence the monogenic curvature tensor pair does not represent any partial derivatives and is therefore *not* able to describe curvature properties of the Monge patch embedding. This drawback can be overcome by using the connection between the second order partial derivatives and the second order Riesz transforms described by the identity

$$\frac{\partial^2 f}{\partial_{ij}} = -R_{ij}[\Delta f]. \tag{4.160}$$

where $i, j \in \{x_1, x_2\}$ and Δ is the Laplace operator [29]. Built upon this identity the Hessian matrix and hence the even tensor part can be rewritten in terms of the Riesz transform:

$$\hat{T}_e = \begin{bmatrix} -R_{x_1x_1}[\Delta f](x) & -R_{x_2x_1}[\Delta f](x) \\ -R_{x_1x_2}[\Delta f](x) & -R_{x_2x_2}[\Delta f](x) \end{bmatrix} \tag{4.161}$$

to obtain an even tensor consisting of the second order derivatives.
According the the original tensor pair the odd counterpart can be constructed by applying the Riesz transform to T_e resulting in:

$$\hat{T}_o = \begin{bmatrix} R_{x_1x_1x_1}[\Delta f] + R_{x_1x_1x_2}[\Delta f]e_{12} & R_{x_1x_1x_2}[\Delta f]e_{12} - R_{x_1x_2x_2}[\Delta f] \\ -R_{x_1x_1x_2}[\Delta f]e_{12} + R_{x_1x_2x_2}[\Delta f] & R_{x_1x_2x_2}[\Delta f] + R_{x_2x_2x_2}[\Delta f]e_{12} \end{bmatrix} \tag{4.162}$$

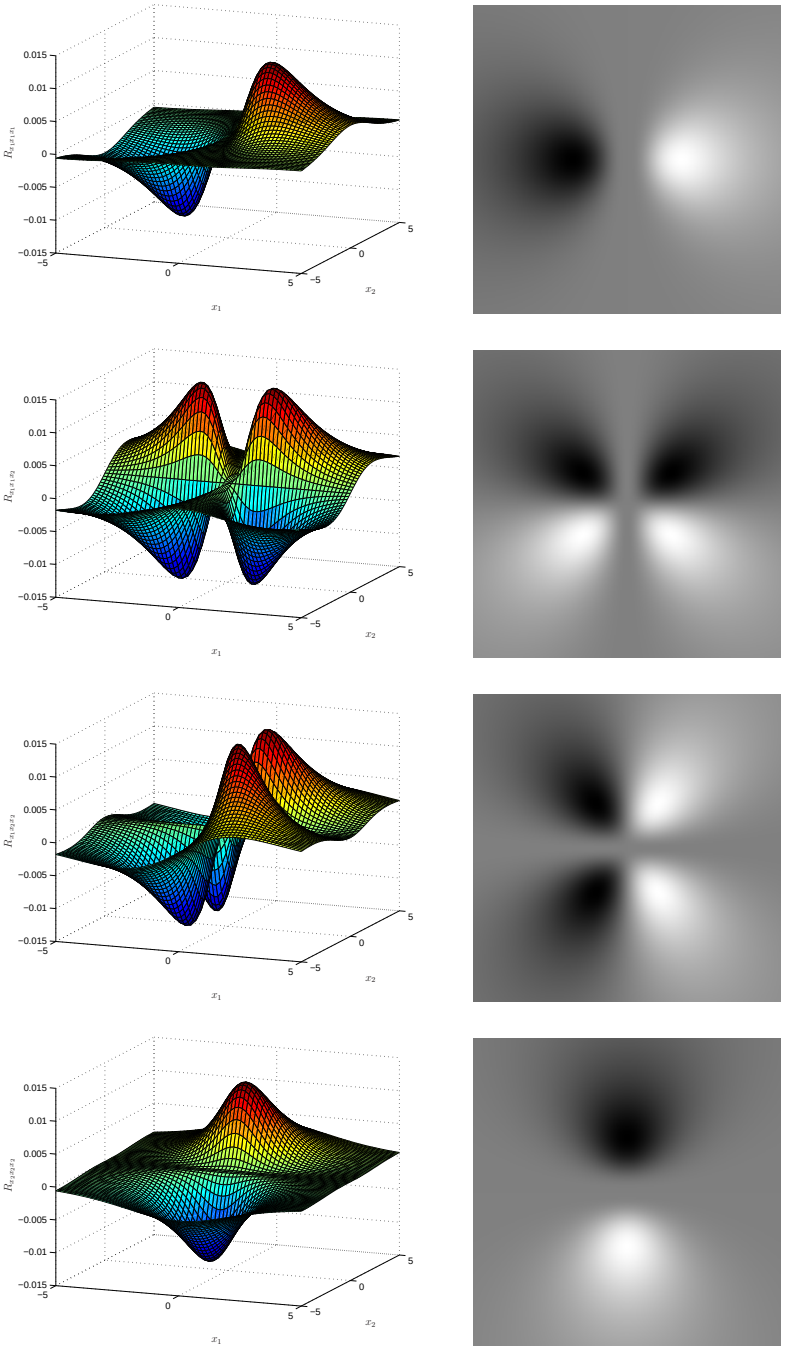

Figure 4.2: 3D and density plots of the third order Riesz transform convolution kernels in the Poisson scale space with scale parameters fine=1.1 and coarse=1.5

Examining the determinant of the even tensor part

$$det(\hat{T}_e) = R_{x_1x_1}[\Delta f]R_{x_2x_2}[\Delta f] - R_{x_1x_2}[\Delta f]^2 \tag{4.163}$$

$$= \frac{\partial^2 f}{\partial x_1^2}\frac{\partial^2 f}{\partial x_2^2} - \frac{\partial^2 f}{\partial x_1 x_2}\frac{\partial^2 f}{\partial x_2 x_1} \tag{4.164}$$

one can notice that it is up to the factor $(1 + f_x^2 + f_y^2)^2$ equal to the Gaussian curvature of a Monge patch defined in (4.10). Comparing the curvature representation of the new tensor pair with the one introduced by Di Zang

$$K_{T_e} = det(T_e) = R_{xx}\{f\}R_{yy}\{f\} - R_{xy}\{f\}^2$$

it is obvious that the quantity K_{T_e} does not represent the Gaussian curvature of the considered Monge patch. Due to the ignorance of the radial factors in the Fourier domain, the Laplace operator disappears. $\hat{T}_e$ serves as the correct alternative to the proposed even tensor which obviously is not related to the second order derivatives.
Nonetheless, one may ask if the proposed techniques to determine the orientation, the phase and the apex angle of i1D and superposed i1D structures stay valid in conjunction with the new tensor pair. This is indeed the case. Using the Radon transform of the Laplace operator applied to f one obtains (see [10]):

$$\mathcal{R}[\Delta f](x) = |u|^2 \frac{\partial^2 \mathcal{R}[f](p,u)}{\partial p^2} = \frac{\partial^2 \mathcal{R}[f](p,u)}{\partial p^2} \tag{4.165}$$

The Laplace operator acts as a second order partial derivative along each slice in the Radon domain and only affects each single slice. Therefore all the proposed methods can be applied according to the old tensor pair.
But even with the new proposed tensor pair the determinant of the even tensor differs from the Gaussian curvature of a Monge patch by the area element $1/(1 + f_x^2 + f_y^2)^2$. Only in the case of the evaluation at a point with vanishing first order derivatives the two terms would coincide. By consequently neglecting the area element factor containing the first order derivatives the following situation is assumed:
From differential geometry it is known that an infinitely small neighbourhood U of a point p on a regular surface S may be parameterized as $z = h(x_1, x_2)$ [13]. This is done by choosing a coordinate system in $\mathbb{R}^3$ in such a way that the origin of the coordinate system is the point p and the z-axis is directed along the positive normal of S at p. As a consequence, the first order derivatives at the origin of the chosen coordinate system vanish with $h(0,0) = h_{x_1}(0,0) = h_{x_2}(0,0) = 0$. The Gaussian curvature in terms of the new parametrization at the origin then reads

$$K_{U(p)}(0,0) = h_{x_1x_1}(0,0)h_{x_2x_2}(0,0) - h_{x_1x_2}^2(0,0) \tag{4.166}$$

which is identical quantity $K_{\hat{T}_e}$ evaluated at the origin. Due to the abscence of the first order derivatives, $K_{\hat{T}_e}$ always assumes a local coordinate system chosen in the way

described above. But if a new coordinate system is chosen, the parameterization of the local Monge patch has to be adjusted. The same transformation operation that is applied to retrieve the new coordinate system has to be applied to the point where the curvature is supposed to be evaluated. This fact is not taken into consideration in the calculation of $K_{\hat{T}_e}$.
As a result of this section one can summarize that the tensor pair $\hat{T}_e, \hat{T}_o$ serves as the correct alternative to the pair introduced by Di Zang in terms of representing second order derivatives. But neither $det(T_e)$ nor $det(\hat{T}_e)$ are able to represent the correct Gaussian curvature of a Monge patch in Euclidean space due to the lack of the area element factor. Nonetheless, the elliptic(i2D), hyperbolic(i2D), parabolic(i1D) and planar(i0D) surface types are characterized by the sign of the Gaussian and mean curvature[13]. Since the factor $(1/(1+f_x^2+f_y^2)^2)$ is always positive, it has no effect on the sign of the determinants $det(T_e)$ and $det(\hat{T}_e)$. Therefore it is possible to determine the shape type with new even tensor $det(\hat{T}_e)$. The question comes up if it might also be possible to determine the shape type by the determinant of the old even tensor T_e. This would be the case if

$$R_{x_1x_1}[f]R_{x_2x_2}[f] - R_{x_1x_2}[f]^2 \circ 0 \Leftrightarrow f_{x_1x_1}f_{x_2x_2} - f_{xy}^2 \circ 0 \tag{4.167}$$

holds where $\circ \in \{<, >, =\}$. To show that (4.167) the identity (4.160) is used again to rewrite the above equation as:

$$R_{x_1x_1}[f]R_{x_2x_2}[f] - R_{x_1x_2}[f]^2 \circ 0 \Leftrightarrow R_{x_1x_1}[\Delta f]R_{x_2x_2}[\Delta f] - R_{x_1x_2}[\Delta f]^2 \circ 0. \tag{4.168}$$

The two sides of the inequality differ only by the usage of the Laplace operator. At this point the interpretation of the Riesz transform in the Radon domain is considred in conjunction with (4.165) to express the second order derivatives as:

$$f_{x_1x_1} = R_{x_1x_1}[\Delta f] = \mathcal{R}^{-1}[\cos^2(\theta)\,\frac{\partial^2}{\partial p^2}\mathcal{R}[f]] \tag{4.169}$$

$$f_{x_1x_2} = f_{x_2x_2} = R_{x_1x_1}[\Delta f] = \mathcal{R}^{-1}[\cos(\theta)\sin(\theta)\,\frac{\partial^2}{\partial p^2}\mathcal{R}[f]] \tag{4.170}$$

$$f_{x_2x_2} = R_{x_1x_1}[\Delta f] = \mathcal{R}^{-1}[\sin^2(\theta)\,\frac{\partial^2}{\partial p^2}\mathcal{R}[f]] \tag{4.171}$$

Speaking in terms of the Radon transform the second order Riesz transforms and the second order derivatives differ by second order differentiation along the p-axis at each one-dimensional slice in the Radon domain. Since the derivation is a linear approximation inequality (4.167) indeed holds. It is therefore possible to determine the sign of the Gaussian and mean curvatures with T_e and $\hat{T}_e$.
Now that it is known that the determinants of T_e and T_o provide no curvature information, the amplitude of the monogenic curvature signal has to be reinterpreted, since it has been used to detect certain i2D features in terms of curvature information.
Using the monogenic curvature signal

$$\begin{aligned} f_{i2D} &= det(T_e)e_3 + det(T_o)e_1 \\ &= (R_{x_1x_1}R_{x_2x_2} - R_{x_1x_2}^2)e_3 \\ &+ (R_{x_1x_1x_1}R_{x_1x_2x_2} - R_{x_1x_1x_2}R_{x_2x_2x_2} - R_{x_1x_1x_2}^2 + R_{x_1x_2x_2}^2)e_1 \\ &+ (R_{x_1x_1x_2}R_{x_1x_2x_2} + R_{x_1x_1x_1}R_{x_2x_2x_2} - 2R_{x_1x_1x_2}R_{x_1x_2x_2})e_2 \\ &= Ae_3 + Be_1 + Ce_2 \end{aligned}$$

its amplitude reads:

$$|f_{i2D}| = \sqrt{A^2 + B^2 + C^3}. \tag{4.172}$$

Using again the interpretation of the Riesz transform in the Radon domain for a i1D signal it is possible to show that the indices in a product of Riesz transforms may be exchanged arbitrarily. The following holds:

$$\begin{aligned} R_{x_1x_1}[f_{i1D}]R_{x_2x_2}[f_{i1D}] &= \mathcal{R}^{-1}[\cos^2(\theta_{Main})\mathcal{R}[f_{i1D}]]\ \mathcal{R}^{-1}[\sin^2(\theta_{Main})\mathcal{R}[f_{i1D}]] \\ &= \cos^2(\theta_{Main})\mathcal{R}^{-1}[\mathcal{R}[f_{i1D}]]\sin^2(\theta_{Main})\mathcal{R}^{-1}[\mathcal{R}[f_{i1D}]] \\ &= \cos^2(\theta_{Main})s(\theta_{Main})\ \sin^2(\theta_{Main})s(\theta_{Main}) \\ &= \cos(\theta_{Main})\sin(\theta_{Main})\ s(\theta_{Main})\cos(\theta_{Main})\sin(\theta_{Main})\ s(\theta_{Main}) \\ &= R_{x_1x_2}[f_{i1D}]R_{x_1x_2}[f_{i1D}] \end{aligned}$$

It follows that the determinant of the even tensor is 0 for i1D signals. The same holds for the determinant of the odd tensor which can be seen by applying the above rule to (4.38). As soon as there is more than one non-constant slice function in the Radon domain the above does not hold. The energy will be non-zero. It can be concluded that the energy measures the amount of non-constant slice functions in the Radon domain and therefore the intrinsic dimensionality.

5 The conformal monogenic signal

In the previous sections the Riesz transform and its interpretation via the Radon transform in $\mathbb{R}^2$ has been used to analyze i1D and i2D signals. The interpretation in the Radon domain played an important role to determine features such as orientation, phase, and the apex angle of two superposed i1D signals with same but arbitrary phase. Nonetheless it was limited in the sense of analyzing plane waves and their superpositions. In this chapter the conformal monogenic signal introduced in [30] is discussed. It provides an extension of the concepts from the last chapters in $\mathbb{R}^2$ to $\mathbb{R}^3$ by inverse stereographically projecting the signal on the unit sphere and applying the Riesz transform in $\mathbb{R}^3$. It is shown that this concept contains the monogenic signal as a subset and further extends it by the possibility to analyze circles and therefore the isophote curvature of signals. Furthermore, it is shown that for certain signal models the concept is equivalent to the generalized Hilbert transform on the unit sphere in $\mathbb{R}^4$.
The basis for the analysis of signals $f : \mathbb{R}^2 \to \mathbb{R}$ is the inverse stereographic projection to the sphere $\mathbb{S}_R$ with center $(0, 0, \frac{1}{2})$ and radius $\frac{1}{2}$ (see [18]):

Definition 5.0.1 (Stereographic projection on $\mathbb{S}^2_R$)**.** The stereographic projection $\mathcal{S}^{-1} : \mathbb{R}^2 \to \mathbb{S}_R$ and its inverse mapping $\mathcal{S} : \mathbb{S}_R \to \mathbb{R}^2$ are defined as:

$$\mathcal{S} : (x, y, z) \mapsto (\frac{x}{1-z}, \frac{y}{1-z}) \tag{5.1}$$

and

$$\mathcal{S}^{-1} : (x, y) \mapsto (\frac{x}{1+x^2+y^2}, \frac{y}{1+x^2+y^2}, \frac{x^2+y^2}{1+x^2+y^2}) \tag{5.2}$$

The whole plane $\mathbb{R}^2$ is mapped conformally to the sphere. $\mathcal{S}^{-1}$ shares some important properties which are of special interest throughout the whole chapter:

- angles are preserved
- circles in the plane are mapped to circles on the sphere
- straight lines in the plane are mapped to circles passing through the northpole
- straight lines through the origin in the plane are mapped to great circles passing through the northpole

With the inverse stereographic projection the signal f is embedded into $\mathbb{R}^3$ as $f_S(x)$ with

$$f_S(x) = \begin{cases} f(\mathcal{S}(x)), & x \in \mathbb{S}_R \\ 0, & else \end{cases} \tag{5.3}$$

taking only values on the sphere. This embedding allows the application of the Riesz transform in three dimensions to the mapped signal f_S. According to (2.28) the Riesz transforms in $\mathbb{R}^3$ read

$$R_j[f](x) = \frac{1}{A_4} P.V. \int_{\mathbb{R}^3} \frac{x_i - y_i}{|x-y|^{n+1}} f(y) dy = \frac{1}{A_4} (\frac{x_j}{|x|^4} * f)(x) \tag{5.4}$$

To continue the concept from the last chapters in order to interpret the Riesz transform in an imaginative and descriptive way, its relation to the Radon transform is used. Therefore the Radon transform in $\mathbb{R}^3$ has to be investigated in first. It has already been mentioned that the Radon transform integrates over all hyperplanes in the target space. In the case of $\mathbb{R}^2$ the hyperplanes were described by straight lines. In $\mathbb{R}^3$ hyperplanes are described by planes in $\mathbb{R}^3$. Compared to straight lines in $\mathbb{R}^2$, which are described by one orientation angle of its normal θ and the distance from the origin, planes in $\mathbb{R}^3$ have an additional angle describing their orientation. The plane equation for a plane P in $\mathbb{R}^3$ in Hessian normal form reads

$$< n, p >= -d \tag{5.5}$$

where $n = (\cos(\theta)\sin(\varphi), \sin(\theta)\sin(\varphi), \cos(\varphi))^T$ is the unit normal of the plane, p is an arbitrary point on P and d is its distance from the origin. Equation (3.25) describes the link between the Riesz and the Radon transform for an arbitrary dimension n. In the case of $n = 3$ this relationship takes the following form:

Theorem 5.0.2 (Relation between the Riesz and the Radon transform in $\mathbb{R}^3$)**.**

$$f_R(x) = (R_{x_1}[f](x), R_{x_2}[f](x), R_{x_3}[f](x))^T \tag{5.6}$$
$$= \mathcal{R}^{-1}[u\mathcal{H}[\mathcal{R}[f](u,t)]_{t=<x,u>}](x) \tag{5.7}$$
$$= -\frac{1}{2}\Delta \int_{|u|=1} u\mathcal{H}[\mathcal{R}[f](u,t)]_{t=<x,u>} du \tag{5.8}$$

where $x \in \mathbb{R}^3$, $u \in \mathbb{S}^2$ *with* $u = (\cos(\theta)\sin(\varphi), \sin(\theta)\sin(\varphi), \cos(\varphi))^T$.

Proof. Let $F(su) = \mathcal{F}[f](x)$ denote the three-dimensional Fourier transform of f and $F_R(su) = \mathcal{F}[f_R](x)$ the three-dimensional Fourier transform of f_R with $s \in \mathbb{R}$ and $u = (\cos(\theta)\sin(\varphi), \sin(\theta)\sin(\varphi), \cos(\varphi))^T$. Consider the inverse three-dimensional Fourier transform:

$$\begin{aligned} f_R(x) &= \mathcal{F}^{-1}[F_R](su) \\ &= \int_0^\infty s^2 ds \int_{|u|=1} F(qu) e^{is(<x,u>)} du \end{aligned}$$

Since we know that the Radon transform is symmetric with respect to the t axis and $\mathcal{F}[\mathcal{R}[f](u,t)] = F$, we can replace the integral over q from 0 to ∞ with one-half of the integral from $-\infty$ to ∞. Rearranging the integrands results in:

$$\begin{aligned}
f_R(\mathbf{x}) &= \frac{1}{2} \int\limits_{|u|=1} du \left[\int\limits_{-\infty}^{\infty} s^2 F_R(su) e^{is(<x,u>)} \right] ds \\
&= \frac{1}{2} \int\limits_{|u|=1} \mathcal{F}^{-1} \left[\frac{su}{|su|} s^2 F(su) e^{is(<x,u>)} \right] du \\
&= \frac{1}{2} \int\limits_{|u|=1} \mathcal{F}^{-1} \left[u\, sgn(u) s^2 F(su) e^{is(<x,u>)} \right] du \\
&= \frac{1}{2} \int\limits_{|u|=1} u\, \mathcal{F}^{-1} \left[sgn(u) s^2 F(su) e^{is(<x,u>)} \right] du \\
&= \frac{1}{2} \int\limits_{|u|=1} u\, \mathcal{H} \left[\mathcal{F}^{-1} \left[s^2 F(su) e^{is(<x,u>)} \right] \right] du \\
&= -\frac{1}{2} \int\limits_{|u|=1} u\, \mathcal{H} \left[\frac{\partial^2}{\partial t^2} \mathcal{R}[f](u,t) \right]_{t=<x,u>} du \\
&= -\frac{1}{2} \Delta \int\limits_{|u|=1} u\, \mathcal{H} \left[\mathcal{R}[f](u,t) \right]_{t=<x,u>} du
\end{aligned}$$

Using the inverse Radon transform formula

$$f(x) = -\frac{1}{2} \Delta \int\limits_{|u|=1} \mathcal{R}[f](u, < x, u >) du \tag{5.9}$$

which may be found in [10] it follows that

$$-\frac{1}{2} \Delta \int\limits_{|u|=1} u\, \mathcal{H} \left[\mathcal{R}[f](u,t) \right]_{t=<x,u>} du \tag{5.10}$$

$$= \mathcal{R}^{-1}[u \mathcal{H}[\mathcal{R}[f](u,t)]_{t=<x,u>}](x) \tag{5.11}$$

$$= \begin{pmatrix} \mathcal{R}^{-1}[\cos(\theta)\sin(\varphi)\mathcal{H}[\mathcal{R}[f]]_{t=<x,u>}](x) \\ \mathcal{R}^{-1}[\sin(\theta)\sin(\varphi)\mathcal{H}[\mathcal{R}[f]]_{t=<x,u>}](x) \\ \mathcal{R}^{-1}[\cos(\varphi)\mathcal{H}[\mathcal{R}[f]]_{t=<x,u>}](x) \end{pmatrix} \tag{5.12}$$

$$= (R_{x_1}[f](x), R_{x_2}[f](x), R_{x_3}[f](x))^T. \tag{5.13}$$

□

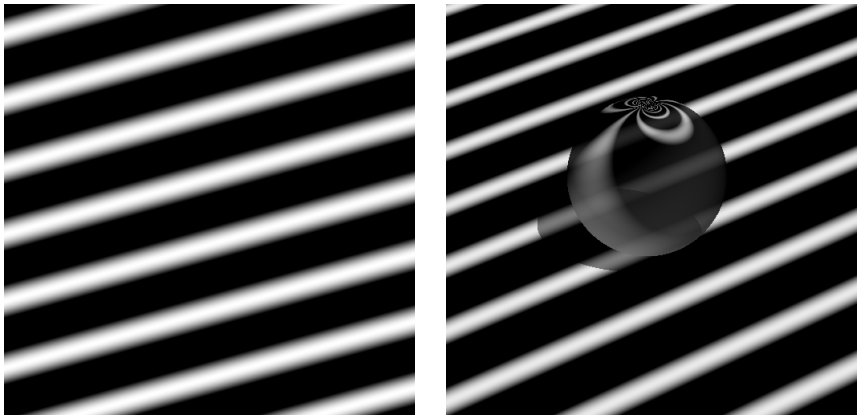

Figure 5.1: Left: i1D signal. Right: Its projection to the sphere $\mathbb{S}_R$

According to the two dimensional case, the Riesz transform performs a one-dimensional Hilbert transform in the Radon domain along each orientation described by the two angles θ and φ. Since the Radon space has also increased in its dimension, the orientation is described by two orientation angles instead of one in the two dimensional case. The additional angle is the key feature of the conformal monogenic signal. Together with the inverse stereographic projection to the sphere it provides the information to determine the isophote curvature of signals. In the following certain signal models will be studied in terms of the conformal monogenic signal to show that it is able to determine all the properties the monogenic signal does and in addition the isophote curvature a given signal.

5.1 Analysis of i1D signals

The analysis of signals with the conformal monogenic signal is governed by the geometric entities the investigated signal models represent after their projection to the sphere $\mathbb{S}_R$. Instrinsically one dimensional signals have been defined as signals which are constant along an orientation angle θ_{Main}. Hence they can be considered as a set of straight lines with constant function values along these lines with orientation θ_{Main}. As the underlying geometric model the single straight line passing through the origin $(0,0)$ with orientation angle θ_{Main} is chosen. Let L be the straight line described by the set of points p

$$L = \{p :< n, p >= 0\} \tag{5.14}$$

where $n = (\cos(\theta_{Main}), \sin(\theta_{Main}))^T$ is the normal of the line with angle θ_{Main}. Projecting this line to the sphere $\mathbb{S}_R$ as $\mathcal{S}^{-1}(L)$ results in a great circle passing through the north- and the southpole, with azimuthal angle θ_{Main} [26] (see Figure 5.2).
It is known from geometry that a circle on a sphere in $\mathbb{R}^3$ can be described by the intersection of a plane and the sphere (see e.g. [26]). This relationship establishes the

link to the Radon transform in $\mathbb{R}^3$ since planes in $\mathbb{R}^3$ are the entities the Radon transform integrates over. Let P_L be the plane with

$$\mathcal{S}^{-1}(L) = P_L \cap \mathbb{S}_R. \tag{5.15}$$

The plane can be written in Hessian normal form as:

$$P_L = \{p :< n, p >= 0\}. \tag{5.16}$$

Since the plane describes a great circle passing through the north- and the southpole the zenithal angle φ of the normal n is equal to $\frac{\pi}{4}$ resulting in the explicit form:

$$P_L = \left\{ p : \quad < \begin{pmatrix} \cos(\theta)\sin(\varphi) \\ \sin(\theta)\sin(\varphi) \\ \cos(\varphi) \end{pmatrix}, p >= 0 \right\} \tag{5.17}$$

$$= \left\{ p : \quad < \begin{pmatrix} \cos(\theta_{Main}) \\ \sin(\theta_{Main}) \\ 0 \end{pmatrix}, p >= 0 \right\}. \tag{5.18}$$

The signal model can be described by the intersection of one single plane in $\mathbb{R}^3$ with the sphere $\mathbb{S}_R$. Hence the Radon transform of the projected signal has, according the two dimensional case, only one single non-constant slice function at

$$(\theta, \varphi, d)^T = (\theta_{Main}, \frac{\pi}{4}, 0)^T \tag{5.19}$$

in the three dimensional Radon space. The situation is the three dimensional analogue of the already introduced interpretation of the two dimensional Riesz transform in the Radon domain for i1D signals. Since the Riesz transform in $\mathbb{R}^3$ can be represented in terms of the Radon transform and its inverse (see (5.6)), the sine and cosine terms can be moved out of inverse Radon transform integral due to the existence of just one single non-constant slice at $(\theta_{Main}, \frac{\pi}{4}, 0)^T$. The angle θ_{Main} is then obtained as

$$\theta_{Main} = \frac{R_{x_2}[f_S](0,0,0)}{R_{x_1}[f_S](0,0,0)}. \tag{5.20}$$

just as it was the case in $\mathbb{R}^2$.

5.2 Analysis of superposed i1D signals

The concept can be extended to two superposed i1D signals $f_{i12D} = f_{i1D_1} + f_{i1D_2}$ with orientations θ_1, θ_2, main orientation θ_{Main}, and apex angle α. The underlying geometric entities are two straight lines L_1, L_2 with the above orientations passing through the

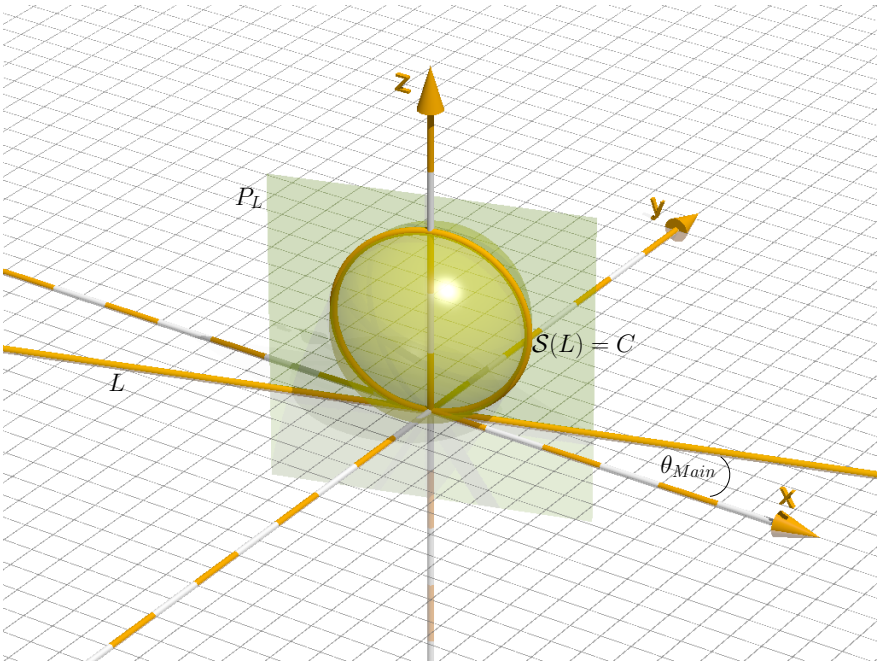

Figure 5.2: Geometric model of a line L projected to $\mathbb{S}_R$ resulting in the circle C

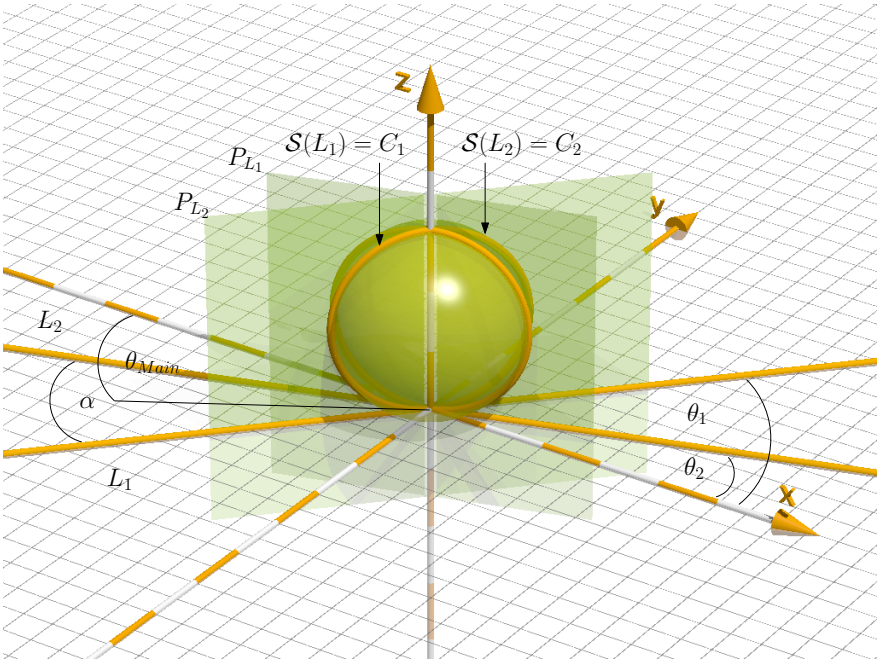

Figure 5.3: Geometric model of two lines L_1, L_2 projected to $\mathbb{S}_R$ resulting in the circles C_1, C_2

origin $(0,0)$ in $\mathbb{R}^2$. Projecting them to $\mathbb{S}_R$ as $\mathcal{S}^{-1}(L_1)$ and $\mathcal{S}^{-1}(L_2)$ results in two great circles passing through the north- and the southpole with azimuthal angles θ_1, θ_2, zenithal angle $\frac{\pi}{4}$, and apex angle α (see Figure 5.3). Characterizing the circles as intersections of planes with $\mathbb{S}_R$ leads to the two planes P_{L_1} and P_{L_2} with

$$P_{L_1} = \left\{ p : \quad < \begin{pmatrix} \cos(\theta_1) \\ \sin(\theta_1) \\ 0 \end{pmatrix}, p >= 0 \right\}. \tag{5.21}$$

and

$$P_{L_2} = \left\{ p : \quad < \begin{pmatrix} \cos(\theta_2) \\ \sin(\theta_2) \\ 0 \end{pmatrix}, p >= 0 \right\}. \tag{5.22}$$

Considering the Radon transform, integrating over all planes in $\mathbb{R}^3$ applied to the target function, which has only non-zero function values along the two circles, results in *two* non-constant slice functions in the Radon domain. Using the Riesz transform in $\mathbb{R}^3$ and its interpretation in terms of the Radon transform and its inverse one obtains:

$$R_{x_1} = \cos(\theta_1)\mathcal{R}^{-1}[\mathcal{H}[\mathcal{R}[f_S]]](0,0,0) + \cos(\theta_2)\mathcal{R}^{-1}[\mathcal{H}[\mathcal{R}[f_S]]](0,0,0) \tag{5.23}$$

$$R_{x_2} = \sin(\theta_1)\mathcal{R}^{-1}[\mathcal{H}[\mathcal{R}[f_S]]](0,0,0) + \sin(\theta_2)\mathcal{R}^{-1}[\mathcal{H}[\mathcal{R}[f_S]]](0,0,0) \tag{5.24}$$

which allows the calculation of θ_{Main} and α according to (3.44) and (3.3.3).

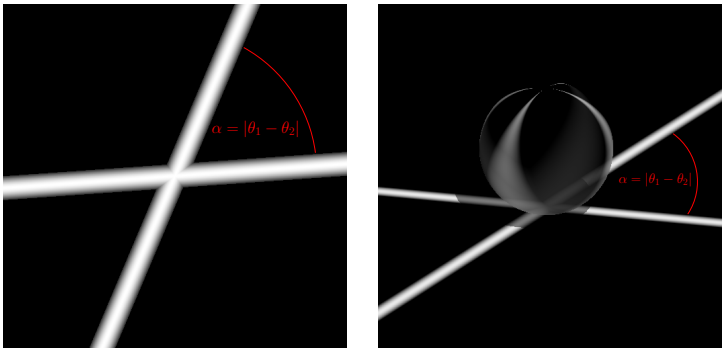

Figure 5.4: Left: Superposition of two i1D signals. Right: Superposition of of two i1D signals and its projection to the sphere $\mathbb{S}_R$

5.3 Analysis of circular signals

In addition to the already studied signal types the conformal monogenic signal is able to analyze circular signals whose underlying signal model is a circle passing through the origin. It is possible to exactly calculate the radius of such a circle. Let C be a circle through the origin $(0,0)$ in $\mathbb{R}^2$ with center $m = (m_{x_1}, m_{x_2})$ and radius r described by the set

$$C = \{p : p = (r\cos(\theta) + m_{x_1}, r\sin(\theta) + m_{x_2})^T, \sqrt{m_{x_1}^2 + m_{x_2}^2} = r\} \tag{5.25}$$

The orientation of the circle is then given by

$$\begin{pmatrix} \frac{m_{x_1}}{\sqrt{m_{x_1}^2+m_{x_2}^2}} \\ \frac{m_{x_2}}{\sqrt{m_{x_1}^2+m_{x_2}^2}} \end{pmatrix} = \begin{pmatrix} \cos(\theta_{Main}) \\ \sin(\theta_{Main}) \end{pmatrix} \tag{5.26}$$

and the signal model in $\mathbb{R}^2$ is defined as

$$f(x) = \begin{cases} c, & x \in C \\ 0, & else \end{cases} \tag{5.27}$$

The inverse stereographic projection $\mathcal{S}^{-1}(C)$ maps C to the circle C_S on $\mathbb{S}_R$ with center m_S and radius r_S which passes through the southpole (see 5.3). Accordingly, the inverse stereographic projection of the signal f is denoted by f_S with

$$f_S(x) = \begin{cases} c, & x \in \mathcal{S}^{-1}(C) \\ 0, & else \end{cases} \tag{5.28}$$

C_S can be described by the intersection of a plane P_C and $\mathbb{S}_R$. In contrast to the planes that represented the projections of i1D signals, the plane P_C describing the circle of the projected circular signal has a zenithal angle φ different from $\frac{\pi}{4}$. Its zenithal angle depends on the radius of the projected circle. If the radius r of the circle increases, φ increases according to the relation

$$\tan(\varphi) = 2r \tag{5.29}$$

which is illustrated in Figure 5.3 for different radii. P_C can be written in Hessian normal form as

$$P_C = \left\{ p : \quad < \begin{pmatrix} \cos(\theta_{Main})\sin(\varphi) \\ \sin(\theta_{Main})\sin(\varphi) \\ \cos(\varphi) \end{pmatrix}, p >= -d \right\}. \tag{5.30}$$

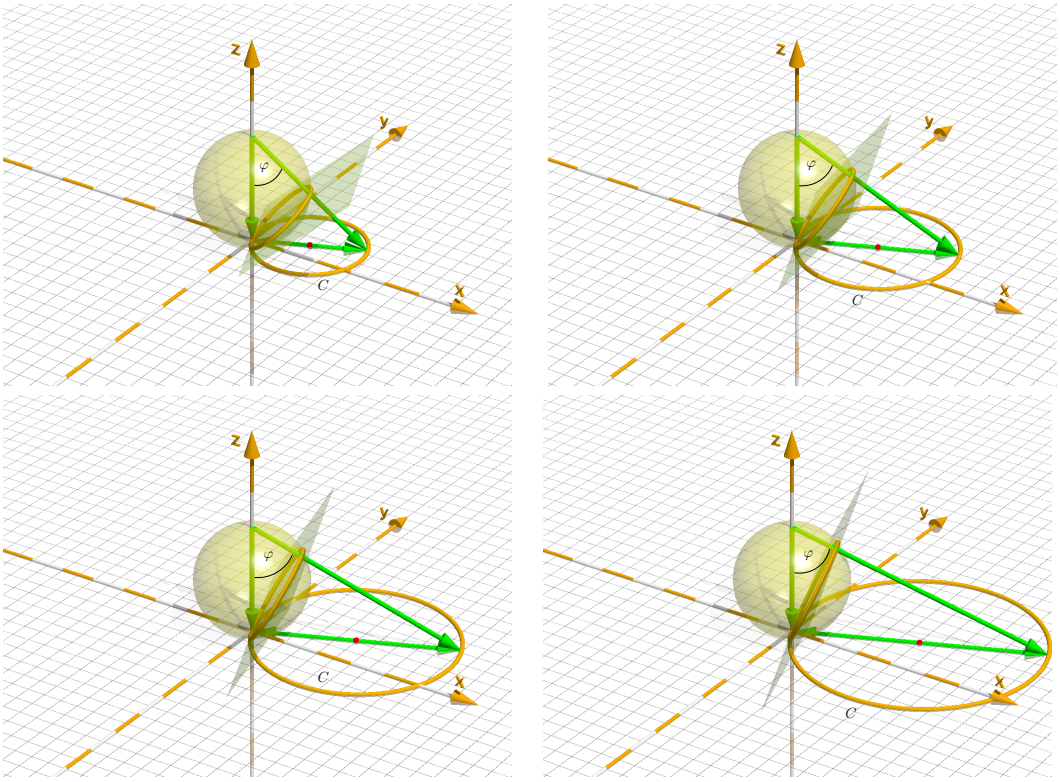

Figure 5.5: Circles with increasing radii sterographically projected to $\mathbb{S}_R$. The angle φ of the plane intersecting $\mathbb{S}_R$ which describes the projected circle is obtained as $\varphi = \arctan(\frac{2r}{1})$, hence $r = \frac{\tan(\varphi)}{2}$.

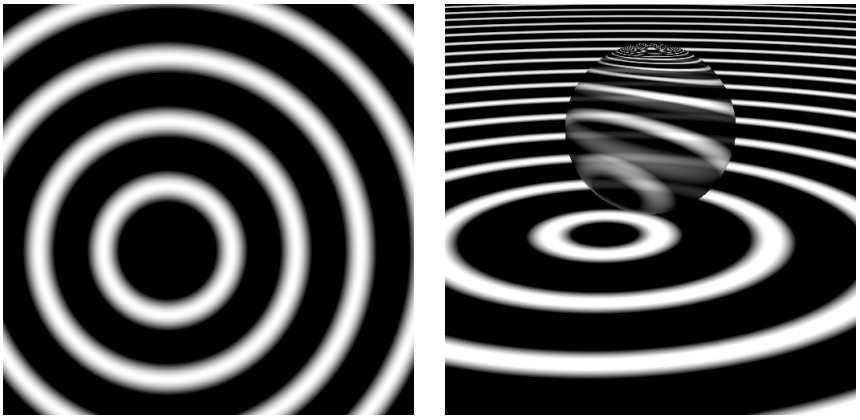

Figure 5.6: Left: Circular signal Right: Its projection to the sphere $\mathbb{S}_R$

The Radon transform results again in one single non-constant slice function located at $(\theta, \varphi, d)^T$. It is characterized by the angles of its normal vector above and the distance d from the origin. Hence the Riesz transform written in terms of the Radon transform allows again to move the sine and cosine terms out of the invers eRadon transform integral resulting in the three components:

$$R_{x_1} = \cos(\theta_{Main}) \sin(\varphi) \mathcal{R}^{-1}[\mathcal{H}[\mathcal{R}[f_S]]](0,0,0) \tag{5.31}$$

$$R_{x_2} = \sin(\theta_{Main}) \sin(\varphi) \mathcal{R}^{-1}[\mathcal{H}[\mathcal{R}[f_S]]](0,0,0) \tag{5.32}$$

$$R_{x_3} = \cos(\varphi) \mathcal{R}^{-1}[\mathcal{H}[\mathcal{R}[f_S]]](0,0,0) \tag{5.33}$$

Using the Riesz transform components it is possible to determine several properties of the circular signal which are discussed in the following.

Theorem 5.3.1. *The orientation θ_{Main} of C is obtained by*

$$\theta_{Main} = \frac{R_{x_2}[f_S](0,0,0)}{R_{x_1}[f_S](0,0,0)}. \tag{5.34}$$

In addition to the main orientation it is possible to obtain the radius of the circle C from the Riesz transform components as:

Theorem 5.3.2.

$$r = \frac{1}{2}\tan(\varphi) = \frac{1}{2}\tan\left(\frac{\sqrt{R_{x_1}[f_S](0,0,0)^2 + R_{x_2}[f_S](0,0,0)^2}}{R_{x_3}[f_S](0,0,0)}\right). \tag{5.35}$$

The same theorem can be formulated working in the Poisson scale space where it stays valid and is independent from the interpretation in the Radon domain. The vectors in $\mathbb{R}^3$ will be denoted by $\underline{x}$ and the Poisson transformed vectors in $\mathbb{R}^4$ are denoted by $x = (x_0, \underline{x})$ where x_0 is the new coordinate in $\mathbb{R}^4$. Furthermore one should recall that

the conjugate Poisson kernel obtained by the Poisson transform of the Riesz kernels in $\mathbb{R}^{n+1}_+$ reads

$$\begin{aligned} \mathcal{Q}(\underline{x}) &:= \sum_{i=1}^{n} e_i \mathcal{Q}_{x_0,i}(\underline{x}) && (5.36) \\ &= \sum_{i=1}^{n} e_i (\mathcal{P}_{x_0,i}(\underline{x}) * R_i(\underline{x})) && (5.37) \end{aligned}$$

with the Riesz Kernels

$$r_j(\underline{x}) = \frac{x_j}{|\underline{x}|^{n+1}}, \quad j = 1, 2, 3. \tag{5.38}$$

With these preliminaries the following theorem is stated:

Theorem 5.3.3. *The radius r of C is obtained by:*

$$r = \frac{1}{2} \tan \left(\frac{\sqrt{(\mathcal{Q}_{x_0,1}(\underline{x}) * f_S(\underline{x}))(0)^2 + (\mathcal{Q}_{x_0,2}(\underline{x}) * f_S(\underline{x}))(0)^2}}{(\mathcal{Q}_{x_0,3}(\underline{x}) * f_S(\underline{x}))(0)} \right). \tag{5.39}$$

Proof. Consider the convolution

$$\begin{aligned} (\mathcal{Q}(\underline{x}) * f_S(\underline{x}))(x_0, 0, 0, 0) &= \int_{\mathbb{R}^3_+} \mathcal{Q}(\underline{x} - 0) f_S(\underline{x}) d\underline{x} \\ &= \int_{\mathbb{R}^3_+} \mathcal{Q}(\underline{x}) f_S(\underline{x}) d\underline{x} && (5.40) \\ &= \int_{\mathbb{R}^3_+} (\frac{\underline{x}}{|\underline{x}|^4} * \mathcal{P}_{x_0}(\underline{x})) f_S(\underline{x}) d\underline{x}. && (5.41) \end{aligned}$$

Since the values of $f_S(\underline{x})$ are only non-zero for $\underline{x} \in C_S$ the integration can be restricted to the integration over the volume of the ball $\mathbb{B}(\underline{m_S}, r_S)$.

$$\int_{\mathbb{R}^3_+} \mathcal{Q}(\underline{x}) f_S(\underline{x}) d\underline{x} = \int_{\mathbb{B}(\underline{m_S}, r_S)} \mathcal{Q}(\underline{x}) f_S(\underline{x}) d\underline{x}. \tag{5.42}$$

Let $\mathbb{S}(\underline{m}, r)$ be the sphere whose intersection with $\mathbb{S}(\underline{m_S}, r_S)$ results in C_S. Then C_S is a circle on the surface of $\mathbb{S}(\underline{m_S}, r_S)$ and $\mathbb{S}(m, r)$. The integration over the volumes of $\mathbb{B}(\underline{m}, r)$ and $\mathbb{B}(\underline{m_S}, r_S)$ will be the same:

$$\int\limits_{\mathbb{B}(\underline{m_S},r_S)} \mathcal{Q}(\underline{x}) f_S(\underline{x}) d\underline{x} \;=\; \int\limits_{\mathbb{B}(\underline{m},r)} \mathcal{Q}(\underline{x}) f_S(\underline{x}) d\underline{x}. \tag{5.43}$$

According to well known results from harmonic analysis (see e.g. [2]), the convolution of a function in $\mathbb{R}^n$ with the Poisson kernel $\mathcal{P}_{x_0}$ in upper the half space $\mathbb{R}^{n+1}_+$ results in a harmonic function in $\mathbb{R}^{n+1}_+$. Therefore $\mathcal{Q}(\underline{x}) = (\frac{\underline{x}}{|\underline{x}|^4} * \mathcal{P}(\underline{x}))$ is harmonic in $\mathbb{R}^{3+1}_+$. Using the mean value theorem for harmonic functions it follows that

$$\int\limits_{\mathbb{B}(\underline{m},r)} \mathcal{Q}(\underline{x}) d\underline{x} \;=\; k\; \mathcal{Q}(\underline{m}) \tag{5.44}$$

with

$$\mathcal{Q}_{x_0,1} = \frac{\cos(\theta_{Main})\sin(\varphi)}{|\underline{m} + x_0 e_0|^4}, \mathcal{Q}_{x_0,2} = \frac{\sin(\theta_{Main})\sin(\varphi)}{|\underline{m} + x_0 e_0|^4}, \mathcal{Q}_{x_0,3} = \frac{\cos(\varphi)}{|\underline{m} + x_0 e_0|^4}. \tag{5.45}$$

Since $f_S(\underline{x})$ is constant for $\underline{x} \in C_S$ per definition, one obtains:

$$\int\limits_{\mathbb{B}^{(m,r)}} \mathcal{Q}(\underline{x}) f_S(\underline{x}) d\underline{x} \;=\; c \int\limits_{\mathbb{B}^{(m,r)}} \mathcal{Q}(\underline{x}) d\underline{x} \tag{5.46}$$

$$=\; c\; k\; \mathcal{Q}(\underline{m}). \tag{5.47}$$

With Eq. (5.39) it is now possible to determine $\frac{\sin(\varphi)}{\cos(\varphi)}$. Figure (5.7) illustrates that this is exactly $\frac{2r}{2r_S}$. Since $r_S = \frac{1}{2}$, it follows that $\frac{1}{2}\frac{\sin(\varphi)}{\cos(\varphi)} = r$.

□

The above method provides the possibility of determining the radius of a circle passing through the origin. It is known from differential geometry that the curvature of a plane curve $\gamma(t)$ at some point x is determined by the radius of the osculating circle touching the curve at x (see Figure 5.8). Therefore given a plane curve $\gamma(t)$ and applying the above method for an infinitely small neighbourhood at some point x will result in the radius of the osculating circle at that point. Being able to determine the curvature of a plane curve turns out to be extremely useful in the field of image processing, since it allows the analysis of the curvature for so called isophotes. Isophotes in images are defined as curves consisting of a a set of points with the same height which is in the

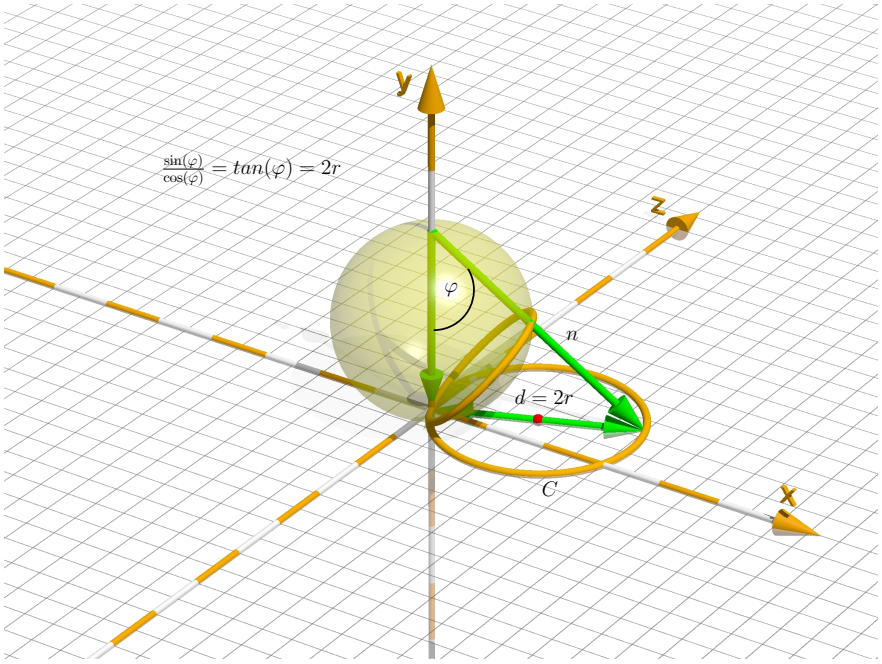

Figure 5.7: Relation between the angle φ describing the zenithal orientation of plane intersecting $\mathbb{S}_R$ resulting in the projected circle $\mathcal{S}^{-1}(S)$ and the radius of the original circle C in $\mathbb{R}^2$

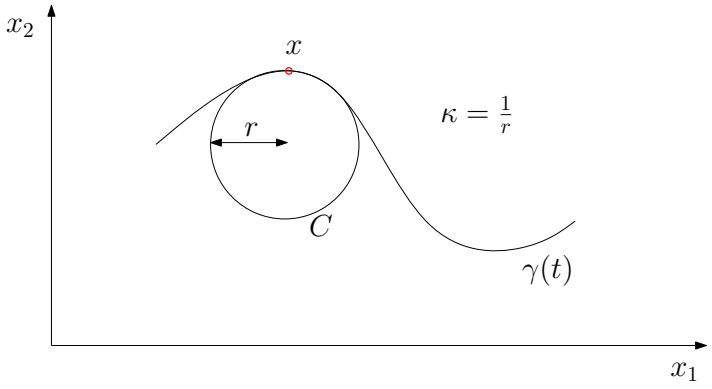

Figure 5.8: Osculating circle with radius r of the curve $\gamma(t)$ at the point x. The curvature of $\gamma(t)$ at x is equal to $\frac{1}{r}$

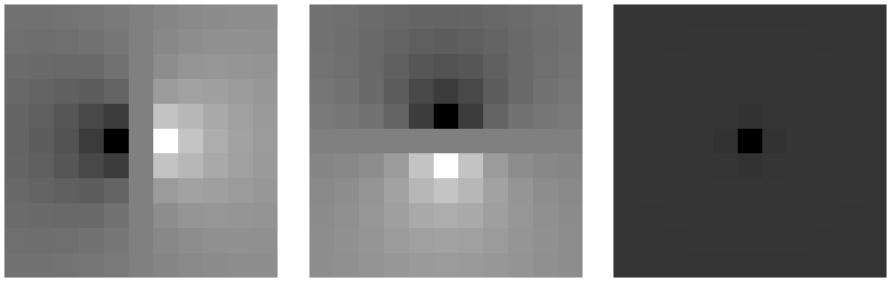

Figure 5.9: Three 11x11 convolution kernels used to obtain the Riesz transforms along the x_1, x_2 and x_3 directions.

language of image processing the same pixel value. The classical method to calculate the isophote curvature for a signal $f : \mathbb{R}^2 \to \mathbb{R}$ is given in terms of first and second order derivatives as (see for example [28]):

$$\kappa = \frac{2f_{x_1}f_{x_2}f_{x_1x_2} - f_{x_1}^2 f_{x_2x_2} - f_{x_2}f_{x_1x_1}}{(f_{x_1}^2 + f_{x_2}^2)^{(3/2)}} \tag{5.48}$$

which is sensitive to noise and illumination changes due to the nature of the first and second order derivatives. Although most of these drawbacks arising from the derivatives can be overcome working in the Gaussian scale space and using Gaussian derivatives (see e.g. [28]), the conformal monogenic signal provides an innovative way to calculate the isophote curvature without using derivatives at all. Furthermore, the calculation is as efficient as the Gaussian derivative analogue. It is implemented as a two dimensional convolution in the spatial domain. Although the operation carried out is a Riesz transform in $\mathbb{R}^3$, the manifold which is the target of the integration is the sphere $\mathbb{S}_R$ which is a two dimensional manifold. Hence one can discretize the plane $\mathbb{R}^2$, inverse stereographically project the discretized points to $\mathbb{S}_R$, and convolute the two dimensional filter masks with the input signal. Since the Riesz transform is applied in the x_1, x_2 and x_3 directions three convolutions with the appropriate filter masks have to be calculated (see figure 5.3). These operations have the same complexity as the convolutions with the three Gaussian derivative filter masks.

5.4 Phase analysis

The conformal monogenic signal is supposed to extend the monogenic signal and provide additional information such as the radius of a circular signal which can be used to obtain the isophote curvature of signals. But in order to serve as an extension it has to be able to determine the same features as the monogenic signal does. So far only orientation and curvature information has been covered by the conformal monogenic signal. The

Figure 5.10: Left: Original input signals. Right: Curvature output of the conformal monogenic signal with convolution mask size 5x5 pixels and scale space parameters fine= 1.3, coarse= 1.5.

phase analysis and calculation has not been covered up to this section since there exists a link between the radius of a circular signal and therefore the isophote curvature and the phase of an i1D signal.

i1D Signals

The monogenic signal is able to determine the phase of i1D signals. The phase of an i1D signal represents the phase of the one dimensional function obtained by restricting the signal to a one-dimensional slice perpendicular to its orientation and calculating the argument of its Hilbert transform pair. Furthermore, the phase of a i1D function can be described as the translation $\varphi \in [0, 2\pi]$ of a cosine function obtained by the one-dimensional restriction perpendicular to its orientation. Figure 5.11 shows an i1D signal with different phases. The phase equals the distance of the cosine peak which can be modeled as the distance of the straight line L with orientation θ from the origin. In order to establish the link between the phase of an i1D signal and the radius of a circular signal passing through the origin, the inversion at the unit circle S_1 is used to map circles through the origin into straight lines not passing through the origin and vice versa. The inversion of a point $x = (x_1, x_2)^T = r(\cos(\theta), \sin(\theta))^T \in \mathbb{R}^2$ at the unit circle in $\mathbb{R}^2$ is given by

$$\mathcal{I}(x) = \frac{x}{|x|^2} = \frac{(\cos(\theta), \sin(\theta))^T}{r}. \tag{5.49}$$

A straight line L with distance p from the origin is mapped to a circle C passing through the origin with radius $r = \frac{1}{2p}$. Since the conformal monogenic signal is able to determine the radius r of a circle passing through the origin, it follows that the phase is obtained as $p = \frac{1}{2r}$ (see Figure 5.11). Hence, in the case of i1D signals the conformal monogenic signal additionally encodes the phase information in the curvature.

3D plane waves

In addition to the phase of i1D signals in $\mathbb{R}^2$ the conformal monogenic signal is able to analyze the phase of plane waves in $\mathbb{R}^3$ restricted to $\mathbb{S}_R$:

$$\begin{aligned} f_p(x) &= Re[A\, e^{i(k<x,u>+\phi)}] && (5.50)\\ &= A\cos(k < x, u > +\phi) && (5.51)\\ &= A\cos(\cos(k(\theta)\sin(\varphi) + \sin(\theta)\sin(\varphi) + \cos(\varphi)) + \phi) && (5.52) \end{aligned}$$

where $A, k \in \mathbb{R}, k > 0$ and $x \in \mathbb{S}_R, u \in \mathbb{S}^2$.
According to the the two dimensional case, it is achieved by a one dimensional Hilbert transform along the one-dimensional non constant slice function in the Radon domain:

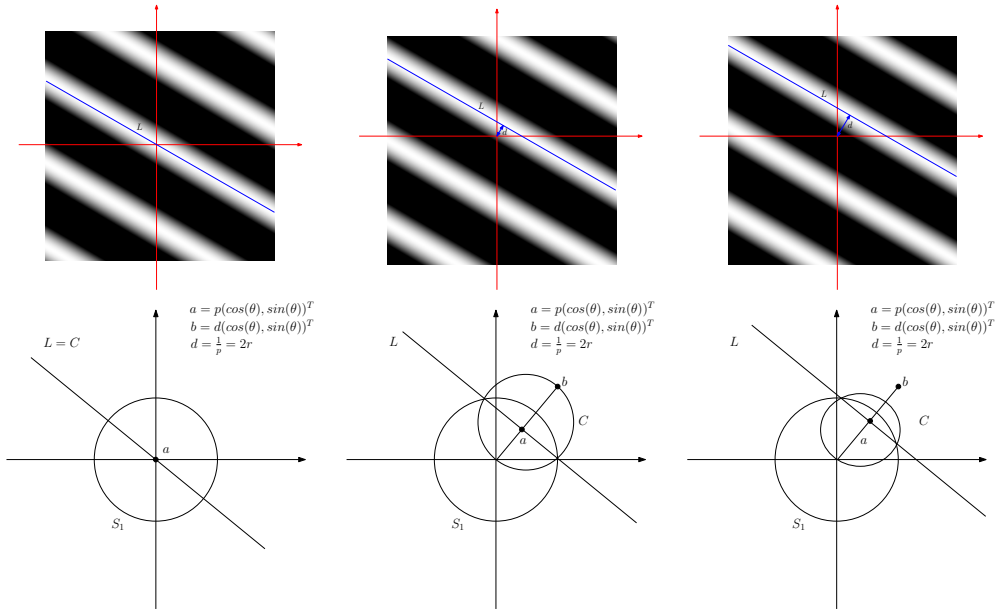

Figure 5.11: Upper row: i1D signal with increasing phase. Lower row: Relation between the distance of the straight line described by the peak of the i1D signal and the radius of its inversion at the unit circle.

Theorem 5.4.1. *Phase of three dimensional plane waves*

$$\phi = \arg(f_S(0,0,0)) = \arg(Re[A\, e^{i(k<(0,0,0)^T,u>+\phi)}] \tag{5.53}$$

$$= \arctan\left(\frac{\sqrt{R_{x_1}[f_S](0,0,0)^2 + R_{x_2}[f_S](0,0,0)^2 + R_{x_3}[f_S](0,0,0)^2}}{f_S(0,0,0)}\right) \tag{5.54}$$

$$= \arctan\left(\frac{\mathcal{R}^{-1}[\mathcal{H}[\mathcal{R}[f_S]]](0,0,0)}{f_S(0,0,0)}\right) \tag{5.55}$$

In contrast to two-dimensional plane waves, the orientation of the three dimensional analogue is determined by an additional orientation angle φ. Its phase is, as it is also the case for the phase of two dimensional plane waves, invariant against rotations in $\mathbb{R}^3$ and therefore all rotations of $\mathbb{S}_R$. Hence different rotated version of the same plane wave may have the same phase. Since the signals of intereset are two-dimensional signals projected to S_R, it is of interest which functions in $\mathbb{R}^2$ correspond to these rotated versions. These different rotated versions correspond to various structures in $\mathbb{R}^2$ if they are back-projected to $\mathbb{R}^3$ with the inverse stereographic projection . The azimuthal rotation angle θ controls the rotation in the x_1, x_2 plane of the backprojected signal in $\mathbb{R}^2$ whereas the angle φ controls the structure of the backprojection as it can bee seen in figure 5.13. Hence the two angles θ, φ completely characterize the image structure, that is being analyzed in terms of the phase. Consequently, the conformal monogenic signal extends the phase determination from straight lines to all structures of the kind

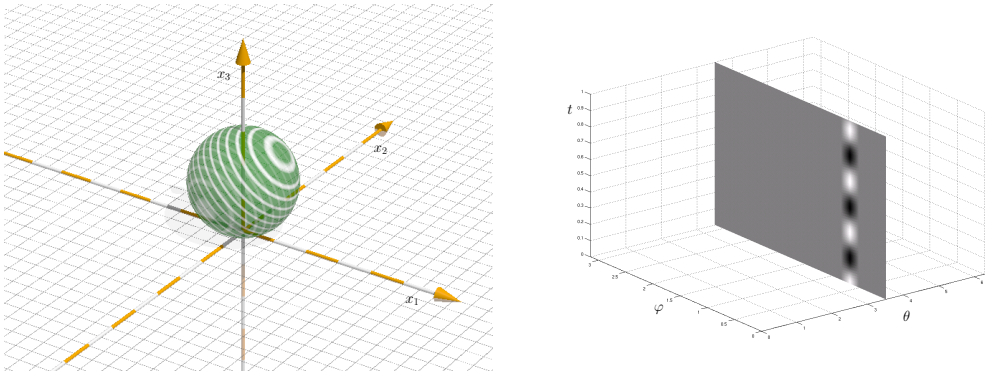

Figure 5.12: Left: Real part of a three dimensional plane wave restricted to $\mathbb{S}_R$ with orientation $(\theta, \phi) = (3.5, 0.8)$. Right: Cut through the three-dimensional Radon space to obtain a view of the transformed plane wave.

$$\cos\left(k\left(\frac{x_1u_1}{1+x_1^2+x_2^2}+\frac{x_2u_2}{1+x_1^2+x_2^2}+\frac{(x_1^2+x_2^2)u_3}{1+x_1^2+x_2^2}\right)+\phi\right) \tag{5.56}$$

$$=\cos\left(k\left(\frac{x_1\cos(\theta)\sin(\varphi)}{1+x_1^2+x_2^2}+\frac{x_2\sin(\theta)\sin(\varphi)}{1+x_1^2+x_2^2}+\frac{(x_1^2+x_2^2)\cos(\varphi)}{1+x_1^2+x_2^2}\right)+\phi\right) \tag{5.57}$$

where $u = (u_1, u_2, u_3)$ is the orientation vector of the plane wave in $\mathbb{R}^3$.

5.5 The Hilbert transform on $\mathbb{S}^n$

The Riesz transform has been introduced as the generalized Hilbert transform for the upper half space $G = \mathbb{R}^{n+1}_+$ with the boundary $\partial G = \mathbb{R}^n$. The conformal monogenic signal uses the Riesz transform for signals projected to the sphere $\mathbb{S}_R$. In this setting the question arises if the generalized Hilbert transform (2.21) with $\partial G = \mathbb{S}^n$ leads to equivalent results. The Hilbert transform on the unit sphere in the Clifford analysis setting has for example been introduced in [12]. In this section, the Hilbert transforms on $\mathbb{S}^2$ and $\mathbb{S}^3$ are investigated and the equivalence between them and the Riesz transforms in $\mathbb{R}^2$ and $\mathbb{R}^3$ for certain signal models is shown.
Starting from the generalized Hilbert transform (2.21) with $G = \mathbb{B}^n$ and $\partial G = \mathbb{S}^n$ the definition of the Hilbert transform on the unit sphere in $\mathbb{R}^{n+1}$ is obtained.

Definition 5.5.1. *Hilbert transform on* $\mathbb{S}^n$
Let ω, ξ be points on $\mathbb{S}^n$. The Hilbert transform on $\mathbb{S}^n$ reads:

$$Hf(\xi) = \frac{2}{A_{n+1}} P.V. \int_{\mathbb{S}^n} \frac{\xi - \omega}{|\xi - \omega|^{n+1}} \omega f(\omega) dS(\omega) \tag{5.58}$$

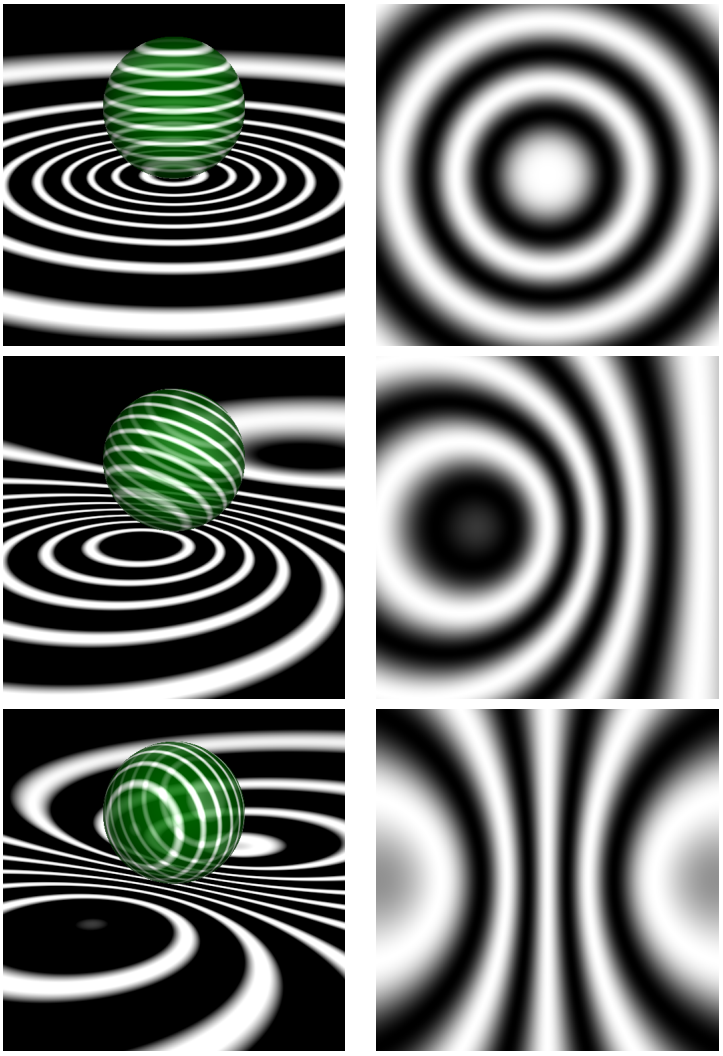

Figure 5.13: Left: Real part of a plane wave in $\mathbb{R}^3$ restricted to $\mathbb{S}_R$ with zenithal angles $\varphi = 0$, $\varphi = \frac{\pi}{2}$, $\varphi = \frac{\pi}{2}$. Right: The corresponding stereographic projections to $\mathbb{R}^2$.

where A_{n+1} is the surface area and dS is the surface element of $\mathbb{S}^n$.

5.6 Application of the Hilbert transform on $\mathbb{S}^2$

It has already been shown that the orientation of i1D signals and the main orientation of two superposed i1D signals with same but arbitrary phase can be obtained by the monogenic signal and hence the conformal monogenic signal. The monogenic signal uses the two dimensional Riesz transform in the plane $\mathbb{R}^2$ to determine these features. An illustrative interpretation in the Radon domain has been given in previous section. In the following, the same features are determined by the Hilbert transform on $\mathbb{S}^2$.
Let $\xi, \omega, \xi_0 \in \mathbb{S}^2$ with $\xi_0 = (0, 0, -1)$. To interpret the singular integral (5.58) in a geometric way, the geometric product $(\xi - \omega)\omega$ is rewritten as:

$$\begin{aligned}(\xi - \omega)\omega = &-(\xi_1 - \omega_1)\omega_1 - (\xi_2 - \omega_2)\omega_2 - (\xi_3 - \omega_3)\omega_3 \\ &+ (\xi_1\omega_2 - \xi_2\omega_1)e_1e_2 \\ &+ (\xi_1\omega_3 - \xi_3\omega_1)e_1e_3 \\ &+ (\xi_2\omega_3 - \xi_3\omega_2)e_2e_3\end{aligned}$$

As the evaluation point ξ_0 the south pole of $\mathbb{S}^2$ is used. Since the Hilbert transform on the unit sphere $\mathbb{S}^2$ and not on $\mathbb{S}_R$ the southpole is not the origin $(0, 0, 0)$, as it was the case in the conformal monogenic signal setting, but $(0, 0, -1)$. Evaluating at that point, the above expressions shorten to:

$$\begin{aligned}(\xi_0 - \omega)\omega &= \omega_1^2 + \omega_2^2 + \omega_3^2 + \omega_3 + \omega_1e_1e_3 + \omega_2e_2e_3 && (5.59)\\ &= 1 + \omega_3 + \omega_1e_1e_3 + \omega_2e_2e_3 && (5.60)\end{aligned}$$

In addition, the evaluation of $|\xi - \omega|^3$ at ξ_0 results in:

$$\begin{aligned}|\xi_0 - \omega|^3 &= \left(\sqrt{(-\omega_1)^2 + (-\omega_2)^2 + (-1 - \omega_3)^2}\right)^3 && (5.61)\\ &= \left(\sqrt{\omega_1^2 + \omega_2^2 + \omega_3^2 + 2\omega_3 + 1}\right)^3 && (5.62)\\ &= \left(\sqrt{2 + 2\omega_3}\right)^3 && (5.63)\end{aligned}$$

With these results definition 5.58 evaluated at ξ_0 reads:

$$
\begin{aligned}
H[f](\xi_0) &= \frac{2}{A_3} P.V. \int_{\mathbb{S}^2} \frac{f(\omega)}{\sqrt{2+2\omega}^3} dS(\omega) \\
&+ \frac{2}{A_3} P.V. \int_{\mathbb{S}^2} \frac{\omega_1}{\sqrt{2+2\omega}^3} f(\omega) dS(\omega) e_1 e_3 \\
&+ \frac{2}{A_3} P.V. \int_{\mathbb{S}^2} \frac{\omega_2}{\sqrt{2+2\omega}^3} f(\omega) dS(\omega) e_2 e_3 \\
&+ \frac{2}{A_3} P.V. \int_{\mathbb{S}^2} \frac{\omega_3}{\sqrt{2+2\omega}^3} f(\omega) dS(\omega) \\
&= H_0[f](\xi_0) + H_1[f](\xi_0) e_1 e_3 + H_2[f](\xi_0) e_2 e_3 + H_3[f](\xi_0)
\end{aligned}
$$

where dS is the surface element of $\mathbb{S}^2$. Switching to spherical coordinates for ω

$$
\begin{aligned}
\omega &= \omega_1 e_1 + \omega_2 e_2 + \omega_3 e_3 \\
&= \cos(\theta)\sin(\varphi) e_1 + \sin(\theta)\sin(\varphi) e_2 + \cos(\varphi) e_3
\end{aligned}
$$

where φ is the zenith and θ is the azimuth yields to:

$$
\begin{aligned}
H[f](\xi_0) &= \frac{2}{A_3} P.V. \int_{\mathbb{S}^2} \frac{f(\omega)}{\sqrt{2+2\omega}^3} dS(\omega) \\
&+ \frac{2}{A_3} P.V. \int_{\mathbb{S}^2} \frac{\cos(\theta)\sin(\varphi)}{\sqrt{2+2\omega}^3} f(\omega) dS(\omega) e_1 e_3 \\
&+ \frac{2}{A_3} P.V. \int_{\mathbb{S}^2} \frac{\sin(\theta)\sin(\varphi)}{\sqrt{2+2\omega}^3} f(\omega) dS(\omega) e_2 e_3 \\
&+ \frac{2}{A_3} P.V. \int_{\mathbb{S}^2} \frac{\cos(\varphi)}{\sqrt{2+2\omega}^3} f(\omega) dS(\omega) \\
&= H_0[f](\xi_0) + H_1[f](\xi_0) e_1 e_3 + H_2[f](\xi_0) e_2 e_3 + H_3[f](\xi_0)
\end{aligned} \tag{5.64}
$$

In order to apply the Hilbert transform on $\mathbb{S}^2$ to a signal, it is again projected with the inverse stereographic projection. In contrast to the steregraphic projection used in the previous section, the projection in this case maps to the unit sphere $\mathbb{S}^n$ instead of $\mathbb{S}_R$ which results in a slightly different definition which may be found in [26]:

Definition 5.6.1 (Stereographic projection on $\mathbb{S}^2$)**.** The stereographic projection $\mathcal{S}^{-1}$: $\mathbb{R}^2 \to \mathbb{S}^2$ and its inverse mapping $\mathcal{S} : \mathbb{S}^2 \to \mathbb{R}^2$ are defined as:

$$
\mathcal{S} : (x, y, z) \mapsto \left(\frac{x}{1-z}, \frac{y}{1-z}\right) \tag{5.65}
$$

and

$$\mathcal{S}^{-1} : (x, y) \mapsto (\frac{2x}{1+x^2+y^2}, \frac{2y}{1+x^2+y^2}, \frac{-1+x^2+y^2}{1+x^2+y^2}) \tag{5.66}$$

Proceeding analogously to the previous section i1D signals are studied first. Let f be a i1D signal and f_S the inverse stereographic projection to $\mathbb{S}^2$. The underlying geometric model is again a straight line with orientation θ_{Main} with an inverse stereographic projection resulting in a great circle C_S on $\mathbb{S}^2$ passing through the north- and the southpole at the azimuthal angle θ_{Main} (see Figure 5.14). The projected signal f_S has constant function values along C_S and is zero for all other points. Hence the integration over the sphere reduces to the integration over φ for $\theta = \theta_{Main}$ which allows to move the expressions depending on θ out of the integral. The evaluation of the integrals $H_1[f_S](\xi_0)$ and $H_2[f_S](\xi_0)$ in (5.64) for f_S at ξ_0 simplifies to:

$$\begin{aligned}
H_1[f_S](\xi_0) &= \frac{2}{A_3} P.V. \int_{\mathbb{S}^2} \frac{\cos(\theta)\sin(\varphi)c}{\sqrt{2+2\omega}^3} dS(\omega) e_1 e_3 \\
&= \frac{2}{A_3} \cos(\theta_{Main}) P.V. \int_{\mathbb{S}^2} \frac{\sin(\varphi)c}{\sqrt{2+2\omega}^3} dS(\omega) e_1 e_3 \\
&= \cos(\theta_{Main})\ k\ s(\xi_0) \qquad (5.67) \\
H_2[f_S](\xi_0) &= \frac{2}{A_3} P.V. \int_{\mathbb{S}^2} \frac{\sin(\theta)\sin(\varphi)c}{\sqrt{2+2\omega}^3} dS(\omega) e_1 e_3 \\
&= \frac{2}{A_3} \sin(\theta_{Main}) P.V. \int_{\mathbb{S}^2} \frac{\sin(\varphi)c}{\sqrt{2+2\omega}^3} dS(\omega) e_1 e_3 \\
&= \sin(\theta_{Main})\ k\ s(\xi_0) \qquad (5.68)
\end{aligned}$$

From (5.67) and (5.68) it follows that θ_{Main} can be determined as:

$$\theta_{Main} = \arctan\left(\frac{H_2[f_S](\xi_0)}{H_1[f_S](\xi_0)}\right) \tag{5.69}$$

The same idea is used to study superpositions of i1D signals with same but arbitrary phase. Let $f = f_{i1D_1} + f_{i1D_2}$ be a superposition of two i1D signals with same but arbitrary phase and let f_S be its stereographic projection. The underlying geometric model are two straight lines L_1, L_2 passing through the origin with angles θ_1, θ_2, main orientation θ_{Main}, and apex angle α. Projecting L_1 and L_2 to $\mathbb{S}^2$ results in the two circles C_1, C_2 with the azimuthal angles θ_1, θ_2 on the sphere. Figure (5.15) illustrates the superposition case. The projected function f_S has constant function values for points on the circles C_1, C_2 and is zero elsewhere. Hence the integration over the sphere is reduced to the integration over φ for θ_1 and θ_2. The integrals $H_1[f_S](\xi_0)$ and $H_2[f_S](\xi_0)$ from (5.64) simplify to:

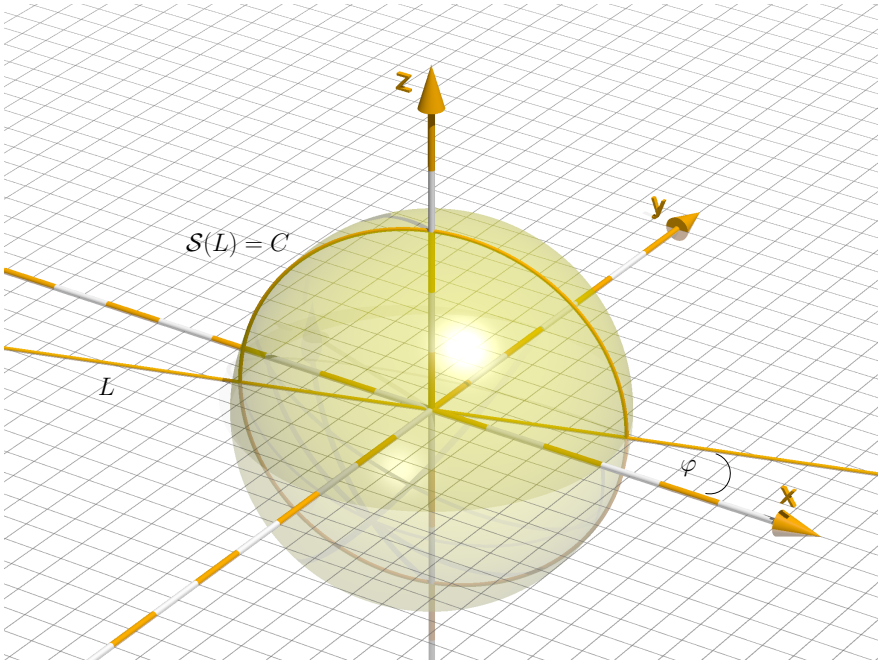

Figure 5.14: Geometric model of the straight line L projected to $\mathbb{S}^2$ resulting in the circle C

$$
\begin{aligned}
H_1[f_S](\xi_0) &= \frac{2}{A_3} P.V. \int_{\mathbb{S}^2} \frac{\cos(\theta)\sin(\varphi)c}{\sqrt{2+2\omega}^3} dS(\omega) e_1 e_3 \\
&= \frac{2}{A_3} \cos(\theta_1) P.V. \int_{\mathbb{S}^2} \frac{\sin(\varphi)c}{\sqrt{2+2\omega}^3} dS(\omega) e_1 e_3 \\
&+ \frac{2}{A_3} \cos(\theta_2) P.V. \int_{\mathbb{S}^2} \frac{\sin(\varphi)c}{\sqrt{2+2\omega}^3} dS(\omega) e_1 e_3 \\
&= \cos(\theta_{Main_1})\ c\ s(\xi_0) + \cos(\theta_{Main_2})\ c\ s(\xi_0) \qquad (5.70) \\
H_2[f_S](\xi_0) &= \frac{2}{A_3} P.V. \int_{\mathbb{S}^2} \frac{\sin(\theta)\sin(\varphi)c}{\sqrt{2+2\omega}^3} dS(\omega) e_1 e_3 \\
&= \frac{2}{A_3} \sin(\theta_1) P.V. \int_{\mathbb{S}^2} \frac{\sin(\varphi)c}{\sqrt{2+2\omega}^3} dS(\omega) e_1 e_3 \\
&+ \frac{2}{A_3} \sin(\theta_2) P.V. \int_{\mathbb{S}^2} \frac{\sin(\theta_\varphi)c}{\sqrt{2+2\omega}^3} dS(\omega) e_1 e_3 \\
&= \sin(\theta_1)\ c\ s(\xi_0) + \sin(\theta_2)\ c\ s(\xi_0) \qquad (5.71)
\end{aligned}
$$

It follows that θ_{Main} can be written as:

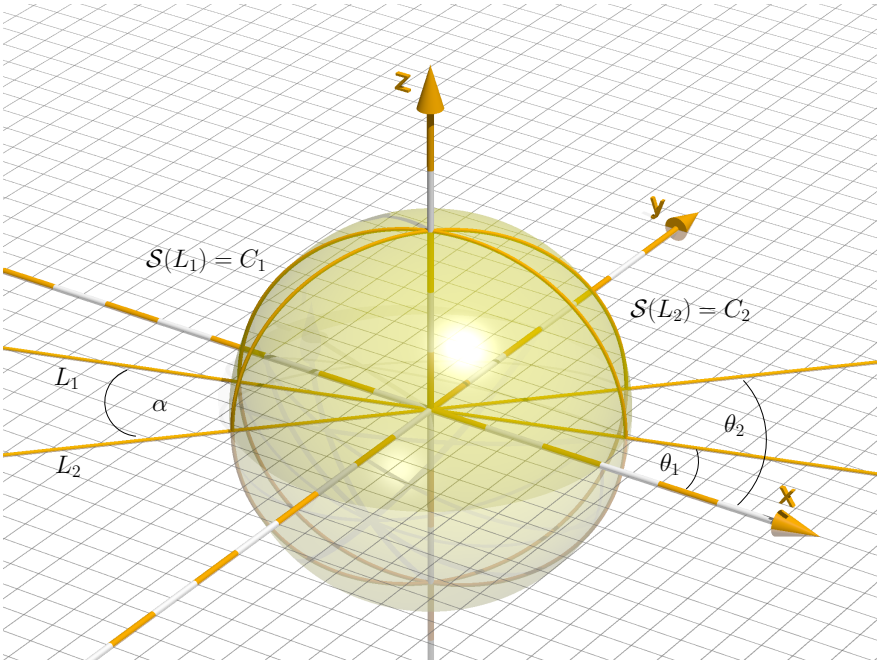

Figure 5.15: Straight lines L_1 L_2 with orientation angles θ_1, θ_2 projected to the sphere resulting two circles C_1, C_2 with azimuthal angles θ_1, θ_2

$$\theta_{Main} = \frac{\theta_1 + \theta_2}{2} = \arctan\left(\frac{H_2[f_S](\xi_0)}{H_1[f_S](\xi_0)}\right) \tag{5.72}$$

According to theorem 3.3.3, the apex angle α can be determined with the now known values for $H_1[f_S](\xi_0), H_2[f_S](\xi_0)$ and θ_{Main}.
The conformal monogenic signal extended the monogenic signal and provided the possibility to extract the isophote curvature from the given signal in addition to the classical monogenic signal features. The curvature which corresponds to the radius of the underlying circular signal model has been determined by the additional angle characterized by the normal of the plane intersecting the sphere which results in the projected circle. Using the interpretation of the Riesz transform in terms of the Radon transform and its inverse, the additional angle has been determined. In the case of the Hilbert transform on $\mathbb{S}^n$ the relation to the Radon transform and therefore a suitable interpretation of the Hilbert transform on $\mathbb{S}n$ is lost. Nonetheless, theorem 5.3.3 has been formulated in terms of the Poisson and conjugate Poisson transform without involving the Radon transform at all. The Hilbert transform has been defined as the non-tangential boundary value of the conjugate Poisson transform. In the case of the unit ball the Poisson integral has been given in (2.18). Therefore by just switching the domain from the upper half space $\mathbb{R}^{3+1}$ to the unit ball $\mathbb{S}^2$ the proof of 5.3.3 remains valid if the Riesz transforms are replaced by the components of the Hilbert transform on the unit sphere.

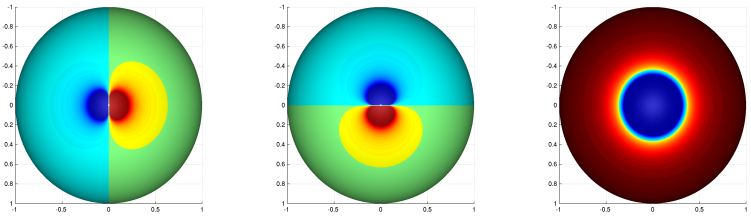

Figure 5.16: The three convolution kernels of the Riesz transforms in $\mathbb{R}^3$ inverse stereographically projected to the sphere.

5.7 The Hilbert transform on $\mathbb{S}^3$

The Hilbert transform on $\mathbb{S}^2$ is able to determine all the features that have also been determined by the Riesz transform in $\mathbb{R}^3$. Although it is possible to extract the same information from signals with the Hilbert transform on $\mathbb{S}^2$, it is not the same as the Riesz transform in $\mathbb{R}^3$ applied to a inverse stereographically projected function restricted to the unit sphere. A comparison of the components R_j of the Riesz transform with the components H_j of the Hilbert transform on the sphere will show the differences.
Recalling from the previous sections, the components evaluated at ξ_0 read:

$$R_j = P.V.\frac{1}{2\pi}\int_{\mathbb{R}^3}\frac{x_j}{|x|^4}f_S(x)dx$$
$$H_j = P.V.\frac{1}{2\pi}\int_{\mathbb{S}^2}\frac{\omega_j}{\sqrt{(2(1+\omega_3))}^3}f_S(\omega)dS(\omega)$$

$f_S(x)$ has only non-zero function values values for $x \in \mathbb{S}^2$. Hence $f_S(x)$ can be restricted to the set $\{x : 0 \leq |x| \leq 1\}$ (see [3]) resulting in the Riesz transform components :

$$\begin{aligned} R_j[f_S](\xi_0) &= P.V.\frac{1}{2\pi}\int_{0\leq|x|\leq 1}\frac{x_j}{|x|^4}f_S(x)dx \\ &= P.V.\frac{1}{2\pi}\int_0^1 r^2\left(\int_{\mathbb{S}^2}\frac{\omega_j}{\sqrt{(2(1+\omega_3))}^4}f_S(r\omega)dS(\omega)\right)dr \\ &= P.V.\frac{1}{2\pi}\int_{\mathbb{S}^2}\frac{\omega_j}{\sqrt{(2(1+\omega_3))}^4}f_S(w)dS(\omega) \end{aligned} \tag{5.73}$$

The only difference between the two transforms for the circular signal model is the factor $1/\sqrt{2(1+\omega_3)}$ under the integral sign. As a consequence a faster decay and rise of the R_j kernels toward the southpole can be noticed (Figure 5.7). In order to obtain the same results as the Riesz transform in $\mathbb{R}^3$ the Hilbert transform on $\mathbb{S}^3$ is considered. Since $\mathbb{S}^2 \subset \mathbb{S}^3$, the embedding $\tilde{\omega} = (\omega, 0)^T$ with $\omega \in \mathbb{S}^2$ is used. The signal f_S is then embedded as

$$\tilde{f}_S(\omega') = \begin{cases} f_S(\omega) & \text{if } \omega' = (\omega, 0), \omega \in \mathbb{S}^2 \\ 0 & \text{else} \end{cases} \tag{5.74}$$

Using definition (5.58) with $n = 3$ and the calculations from the previous section yields to the Hilbert transform on $\mathbb{S}^3$ evaluated at $\tilde{\xi_0} = (0, 0, -1, 0)$ as

$$\begin{aligned} H[\tilde{f}_S](\tilde{\xi_0}) &= \frac{2}{A_3} P.V. \int_{\mathbb{S}^3} \frac{\tilde{f}(\omega)}{(\sqrt{2+2\omega_3})^4} dS(\omega) \\ &+ \frac{2}{A_3} P.V. \int_{\mathbb{S}^3} \frac{\omega_1}{(\sqrt{2+2\omega_3})^4} \tilde{f}(\omega) dS(\omega) e_1 e_4 \\ &+ \frac{2}{A_3} P.V. \int_{\mathbb{S}^3} \frac{\omega_2}{(\sqrt{2+2\omega_3})^4} \tilde{f}(\omega) dS(\omega) e_2 e_4 \\ &+ \frac{2}{A_3} P.V. \int_{\mathbb{S}^3} \frac{\omega_3}{(\sqrt{2+2\omega_3})^4} \tilde{f}(\omega) dS(\omega) \\ &+ \frac{2}{A_3} P.V. \int_{\mathbb{S}^3} \frac{\omega_4}{(\sqrt{2+2\omega_3})^4} \tilde{f}(\omega) dS(\omega) e_3 e_4 \\ &= H_0[\tilde{f}_S](\tilde{\xi_0}) + H_1[\tilde{f}_S](\tilde{\xi_0}) e_1 e_4 + H_2[\tilde{f}_S](\tilde{\xi_0}) e_2 e_4 \\ &+ H_3[\tilde{f}_S](\tilde{\xi_0}) + H_4[\tilde{f}_S](\tilde{\xi_0}) e_3 e_4 \end{aligned} \tag{5.75}$$

Since $\omega_4 = 0$ for all $\omega \in \mathbb{S}^3$ with $\tilde{f}(\omega) \neq 0$ due to the nature of the embedding, it follows that $H_4[\tilde{f}_S](\tilde{\xi_0}) = 0$. Furthermore, considering spherical coordinates in $\mathbb{S}^3$

$$\begin{aligned} \omega &= \omega_1 e_1 + \omega_2 e_2 + \omega_3 e_3 + \omega_4 e_4 \\ &= \sin(\theta)\cos(\varphi) e_1 + \sin(\theta)\sin(\varphi)\cos(\gamma) e_2 \\ &+ \cos(\theta) e_3 + \sin(\theta)\sin(\varphi)\sin(\gamma) e_4 \end{aligned}$$

and using $\omega_4 = 0$ where $\tilde{f}_S(\omega) \neq 0$ yields to $\gamma = 0$. But then the components $H_j[\tilde{f}_S](\tilde{\xi_0})$ are exactly the same components as the components $R_j[f_S]$ in $\mathbb{R}^3$. As a conclusion it has been shown that the Riesz transform in $\mathbb{R}^3$ restricted to the sphere and the Hilbert transform on $\mathbb{S}^3$ are equivalent for the discussed signal models.

Now why is the link between the generalized Hilbert transform on the unit sphere and the conformal monogenic signal of importance? If it is as powerful as the conformal monogenic signal, would it not be sufficient to deal with the conformal monogenic signal if one is only interested in working with signals arising in $\mathbb{R}^2$? The answer would be yes. But from a theoretical point of view, generalized Hilbert transforms arising in the context of Clifford analysis open up the possibility to work with Hilbert transforms on arbitrary closed surfaces in $\mathbb{R}^n$. These include for example signals arising on the unit sphere such as geophysical data captured on the earth or images captured with catadioptric cameras. In these cases a projection on the sphere is not necessary since the signals are already defined on this manifold in the higher dimensional space. Furthermore since the Hilbert transform arises from Cauchy transform, a scale space concept for arbitrary closed surfaces in $\mathbb{R}^n$ is already provided. Therefore the introduction of the usage and equivalence between the generalized Hilbert transforms and the conformal monogenic signal for certain signal types was only the first step in the application of generalized Hilbert transforms in the field of image processing.

5.8 Application: Normal and Gaussian curvature

The conformal monogenic signal is able to extract the isophote curvature at a given point of a signal without using derivatives. To establish an alternative to the monogenic curvature tensor, the conformal monogenic signal will be used to calculate the normal curvature and the Gaussian curvature at a point of a signal interpreted as a Monge patch. Consider the Monge patch embedding $S : (x, y) \to (x, y, f(x, y))^T$ of a signal f in Euclidean space and let k_n denote the normal curvature at a point $P = (x_0, y_0, f(x_0, y_0))^T$ along a direction n. Furthermore, let c be the contour curve that is obtained by the orthogonal projection Λ of the patch to the plane with normal vector vector n (see Fig. 5.17). The curvature of the contour c at the orthogonal projection $\Lambda(P)$ is denoted by k_c. For this setting Koenderink formulated the following theorem in [24]:

Theorem 5.8.1 (Shape from contour)**.** *The Gaussian curvature at P is given by*

$$K = k_n k_c. \tag{5.76}$$

Instead of determining the maximum and minimum normal curvatures at P to calculate the Gaussian curvature, it is possible to use the normal curvature along any direction and the contour curvature of the surface. This idea is now applied to a point P of the Monge patch embedding and combined with the conformal monogenic signal which is used to obtain the single curvatures k_n and k_c.
Foremost a normal curvature direction has to be chosen. Since theorem 5.8.1 holds for any normal curvature direction, n is defined as $n = (0, 1, 0)^T$. This decision will be useful in the concrete implementation since the normal curvature along n will just be the curvature of the curve described by the pixels along the y axis in a local neighbourhood.

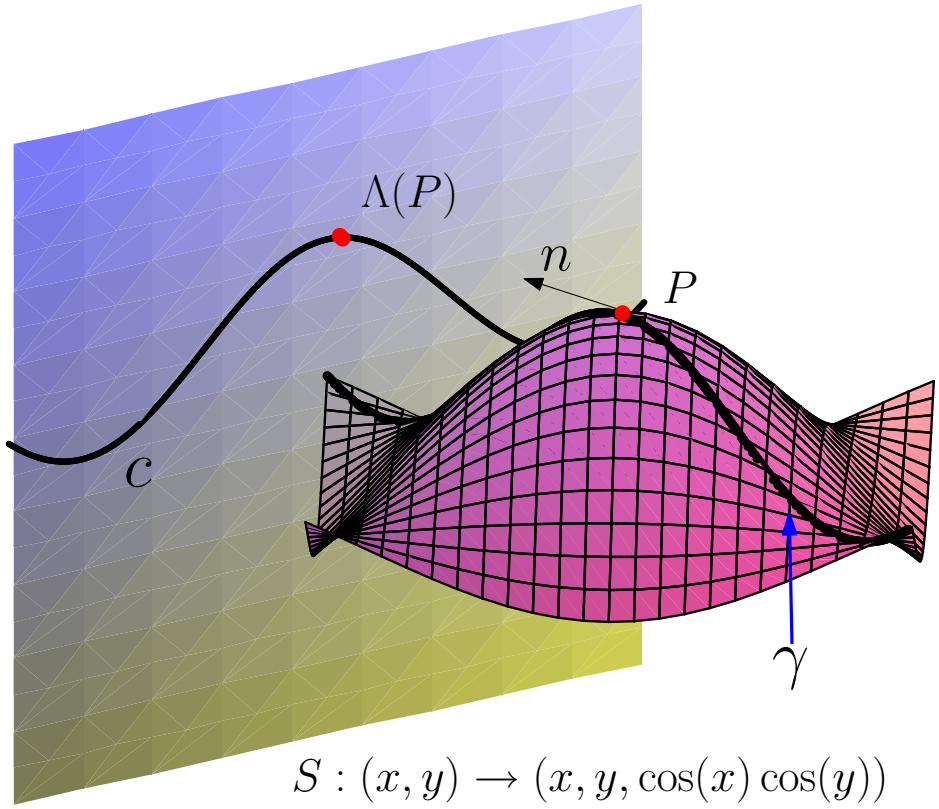

Figure 5.17: The Gaussian curvature K at P is determined by the curvature k_c of c at $\Lambda(P)$ the curvature k_n of γ at P

The decision is justified as follows: Let Π_1 be the plane spanned by the normal vector at P and the tangent vector v in the direction n. The normal curvature along n is then described by the curvature of the curve obtained by the intersection of the S and Π_1. According to Meusnier's theorem [13] the normal curvatures along n at a point P of all curves with tangent v at P are equal. Let Π_2 be the plane spanned be $(0,0,1)^T$ and the tangent at P along n. Then Π_1 and Π_2 contain the same tangent v at P along n and therefore their intersection curves with S have the same curvature.
The projection plane characterized by the normal vector $n = (0,1,0)^T$ is a plane parallel to the xz plane. The points of the patch along n describe the space curve γ in the yz plane with curvature k_n at P. It has been shown that the conformal monogenic signal is able to determine the curvature of curves in a plane. Since γ is a curve residing in a plane, it can be interpreted as a new input signal f_γ. Projecting f_γ to the sphere and convolving with the 3-dimensional Riesz kernel results in the conformal monogenic signal representation of f_γ. The evaluation of (5.35) for the conformal monogenic signal representation of f_γ provides the curvature of γ at P which is denoted by k_n. Additionally, the orthogonal projection of the patch to the xz plane results in the contour c of the patch. In the same manner as above k_c is obtained by interpreting c as a new input signal f_c and evaluating (5.35) for the conformal monogenic signal representation f_c.
The concept described can be transferred to the discrete case. For each pixel in the input signal f a local neighbourhood M of $k \times l$ pixels describes a surface in Monge patch form. Without loss of generality n is again the direction $(0,1,0)^T$ pointing along the y-axis. The pixels along the middle column of the neighbourhood described by the set

$$\gamma = \{M(\lfloor k/2 \rfloor, i) | i = 1 \dots l\} \tag{5.77}$$

with $\lfloor x \rfloor := max\{z \in \mathbb{Z} | z <= x\}$ constitute the curve γ. The orthogonal projection c to the xz plane is determined by the set

$$c = \{L_i | L_i = \max_j(M(i,j)), i = 1 \dots l\} \tag{5.78}$$

which are the pixels with the maximum height in each column (see Fig. 5.18). Both curves γ and c are now interpreted as two new separate $k \times l$ pixels wide input signals f_γ and f_c. They are projected to the sphere and convolved with the 3D Riesz kernel according to the previous section in order to obtain the conformal monogenic signal representation. Using Eq. (5.35) the curvatures k_c and k_n are obtained. The Gaussian curvature then reads $K = k_c k_n$.
In addition to the Gaussian curvature the normal curvature along an arbitrary direction can be obtained by applying a subset of the steps above. n is then defined as the normal curvature direction of interest. The pixels along this direction describe again a space curve with curvature k_n that can be determined by the conformal monogenic signal.
Figure 5.19 demonstrates the results of the proposed method in contrast to the standard method based on first and second order derivatives. The images have been convolved with a Poisson kernel and scaling parameter 2.0 before the two methods were applied. It turns out that the new method is less noisy and more accurate along edges. At corners

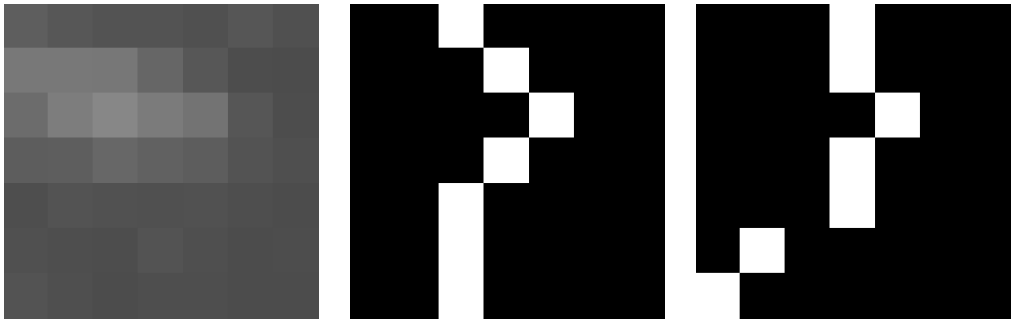

Figure 5.18: Left: 7x7 neighbourhood M taken from the Lena test image Middle: γ obtained by the pixels in the middle column $\{M(i,4)|i = 1..7\}$ Right: Contour c of the projection described by the maximum pixel values of each column $\{L_i|L_i = \max_j(M(i,j))\}$

and junctions a higher curvature output is established which can be used for the detection of these features. Nonetheless the new method is far more complex than the standard one. For each pixel the maximum of the the columns in the neighbourhood M has to be calculated for the contour c. Furthermore two Riesz transforms involved in the conformal monogenic signal have to be calculated for γ and c in order to obtain the curvatures k_n and k_c.

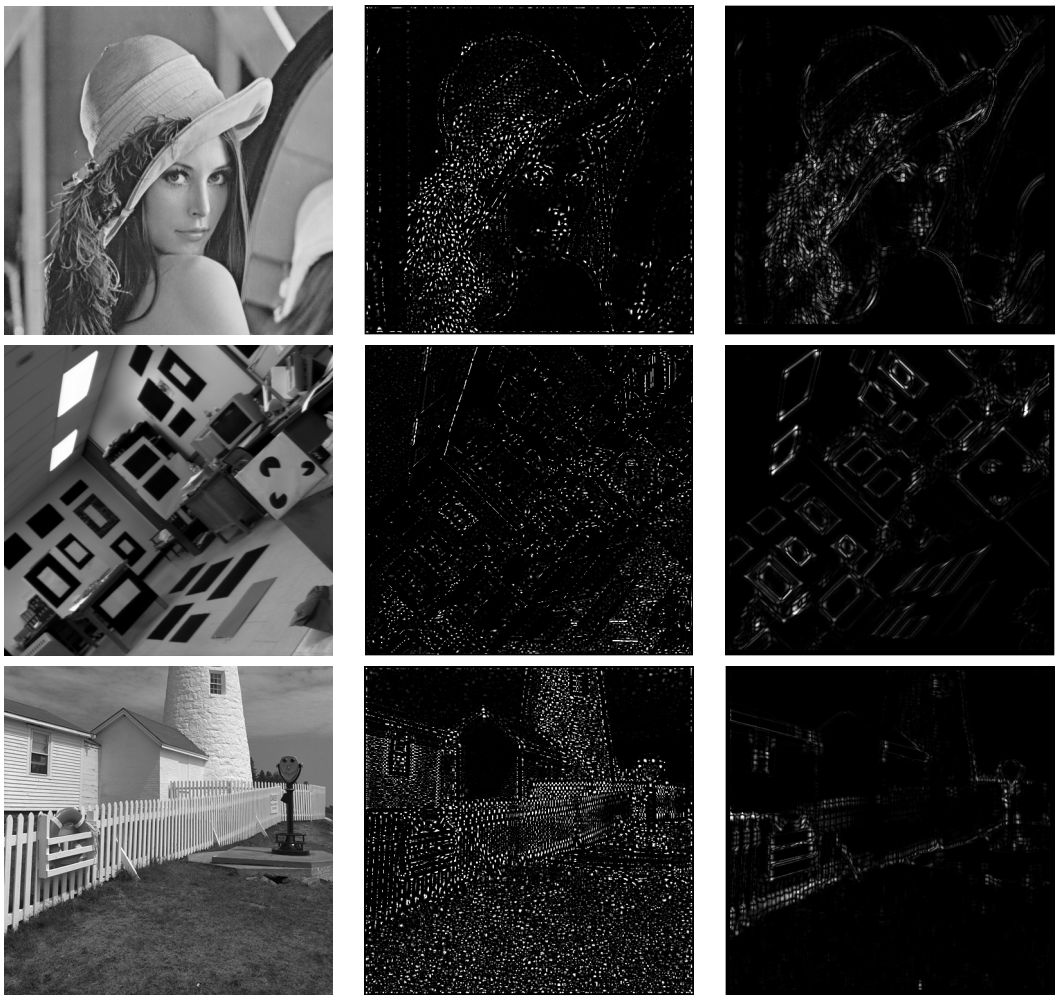

Figure 5.19: Left: Original test images Middle: Gaussian curvature calculated with finite differences in Poisson scale space (s=2.0) Right: Gaussian curvature calculated with the conformal monogenic signal method and filter mask size 15 pixel(s=2.0)

6 Conclusion and outlook

This thesis introduced generalized Hilbert transforms known from Clifford analysis which arise as boundary values of the Cauchy transform. They can be applied to arbitrary closed surfaces with sufficiently smooth boundary in $\mathbb{R}^n$. The Hilbert transforms on the sets $\mathbb{R}^n$ with the boundaries $\mathbb{R}^{n+1}_+$ have been identified with the Riesz transforms where the case $n = 1$ turned out the be the classical Hilbert transform on the real line. As a consequence the generalized Hilbert transform turned out to be the next step following the Riesz transform in the idea of further generalizing the classical Hilbert transform to higher dimensions and manifolds different from the upper half spaces.

Emphasis has been put on the link between the Riesz transform and the Radon transform in order to interpret the Riesz transform in an innovative and descriptive way. This strategy allowed the determination of signal features such as orientation, local phase and the apex angle of i1D signals and their superposition with same but arbitrary phase and amplitude.

Furthermore, higher order Riesz transforms in $\mathbb{R}^2$ have been studied in conjunction with the monogenic curvature tensor to justify that the monogenic curvature tensor is in general not able to extract differential geometric properties such as the Gaussian and the mean curvature. It turned out that only for special signal models such as i1D signals and the superposition of two i1D signals the entities of the monogenic curvature tensor, which were supposed to represent the mean and Gaussian curvature, coincided with the actual mean and Gaussian curvature due to vanishing first order derivatives at the origin.

To compute the second and third order Riesz transforms in $\mathbb{R}^2$, exact convolution kernels have been determined for the spatial domain. They have been calculated in the Poisson scale space. These kernels circumvent the calculation of the higher order Riesz transforms in the Fourier domain.

Following the idea of lifting up a signal to a higher dimension, the conformal monogenic signal has been introduced. By inverse stereographically projecting the signal to the sphere $\mathbb{S}_R$ the Riesz transform in $\mathbb{R}^3$ has been used to extend the monogenic signal. It is able to obtain all the features the monogenic signal does plus an additional information. A formal proof has been given that this additional information is equal to the isophote curvature of a two-dimensional signal. Hence the conformal monogenic signal turned out to calculate the isophote curvature in a completely new way using no derivatives at all. As an application the ability to calculate the isophote curvature was used to obtain the mean and Gaussian curvature.

To establish the link to the generalized Hilbert transforms on arbitrary closed surfaces with sufficiently smooth boundary in $\mathbb{R}^3$ the Hilbert transform on the unit sphere has been studied and compared with the conformal monogenic signal for i1D signals, superpositions of two i1D signals and circular signals. For these signal types they turned out to be equivalent.

Future work might split into two directions. One possibility is the modification of the conformal monogenic signal. Instead of projecting the two-dimensional signal to the sphere other manifolds are possible which might reveal new kinds of features. Furthermore, the conformal monogenic signal can be extended to $\mathbb{R}^4$ in order to analyze image sequences or volumetric image data. Due to the increasing dimension the geometric entities turn from circles to spheres.
Another possibility is the study of the generalized Hilbert transform on manifolds such as the unit sphere. Yet there is no link to a Radon-like transform for generalized Hilbert transforms different from the Riesz transform in $\mathbb{R}^n$. Nonetheless, in the case of the unit sphere the recently introduced Radon transform on SO(3) which may be found in [19] is of interest. The authors establish a Fourier slice theorem for the Radon transform on SO(3) which might be useful in relating the Hilbert transform on $\mathbb{S}^2$ to the Radon transform on SO(3). Motivations for a detailed study of the Hilbert transform on $\mathbb{S}^2$ are given by signals naturally arising on $\mathbb{S}^2$ such as geophysical data captured around the earth or catadioptric cameras.

List of symbols

$C_r(\mathbb{R}^n, \mathbb{R}^m)$	space continuous functions which are $r-$times differentiable
$L_r(\mathbb{R}^n, \mathbb{R}^m)$	space continuous functions which are $r-$times integrable
$\mathbb{S}^n$	unit sphere in $\mathbb{R}^n$
$\mathbb{S}_R$	sphere with center $(0, 0, \frac{1}{2})$ and radius $\frac{1}{2}$ in $\mathbb{R}^3$
$\mathbb{R}^{0,n}$	vector space $\mathbb{R}^n$ of signature $(0, n)$
$\mathbb{R}_{0,n}$	Universal clifford algebra over the vector space n
$\mathcal{F}[f]$	Fourier transform
$\mathcal{R}[f]$	Radon transform
$R[f]$	Riesz transform
$\mathcal{P}[f]$	Poisson transform
$\mathcal{Q}[f]$	Conjugate Poisson transform
$H[f]$	generalized Hilbert transform in the Clifford analysis setting
$\mathcal{H}[f]$	classical one-dimensional Hilbert transform
r	Riesz transform convolution kernel
h	One-dimensional Hilbert transform convolution kernel
$\mathcal{P}_{x_0}$	Poisson kernel
$\mathcal{Q}_{x_0}$	conjugate Poisson kernel
$\mathcal{S}^{-1}$	stereographic projection
f_{x_i}	first order derivative along the x_i direction
$f_{x_i x_j}$	second order derivative along the x_i and x_j direction
θ_{Main}	main orientation of a signal
A_n	surface area of the unit sphere $\mathbb{S}^n$

Bibliography

[1] L. Ahlfors. *Complex Analysis.* McGraw-Hill Science/Engineering/Math, 1979.

[2] S. Axler, P. Bourdon, and W. Ramey. *Harmonic Function Theory (Graduate Texts in Mathematics, Vol 137).* Springer, 2002.

[3] J. A. Baker. Integration over spheres and the divergence theorem for balls. *The American Mathematical Monthly*, 104(1):36–47, 1997.

[4] R. Banuelos and A. Lindeman. A martingale study of the Beurling-Ahlfors transform. *Journal of Functional Analysis*, pages 224–265, 1997.

[5] F. Brackx, R. Delanghe, and F. C. Sommen. On conjugate harmonic functions in Euclidean space. *Mathematical Methods in the Applied Sciences*, 25(16-18):1553–1562, 2002.

[6] F. Brackx, B. De Knock, and H. De Schepper. Generalized multidimensional Hilbert transforms in Clifford analysis. *International Journal of Mathematics and Mathematical Sciences*, 2006, 2006.

[7] F. Brackx, B. De Knock, and H. De Schepper. On generalized Hilbert transforms and their interaction with the Radon transform in Clifford analysis. *Mathematical Methods in the Applied Sciences*, 30(9):1071–1092, 2007.

[8] F. Brackx, B. De Knock, H. De Schepper, and D. Eelbode. On the interplay between the Hilbert transform and conjugate harmonic functions. *Mathematical Methods in the Applied Sciences*, 29(12):1435–1450, 2006.

[9] A. P. Calderon and A. Zygmund. Singular integral operators and differential equations. *American Journal of Mathematics*, 79(4):901–921, 1957.

[10] L. Debnath and D. Bhatta. *Integral Transforms and Their Applications, Second Edition.* Chapman & Hall/CRC, 2006.

[11] R. Delanghe. Clifford analysis: History and perspective. *Computational Methods and Function Theory*, 1(1):107–153, 2001.

[12] R. Delanghe. On some properties of the Hilbert transform in Euclidean space. *Bull. Belg. Math. Soc. Simon Stevin*, 11(2):163–180, 2004.

[13] M. P. do Carmo. *Differential Geometry of Curves and Surfaces.* Prentice-Hall, Englewood Cliffs, NJ, 1976.

[14] M. Felsberg. *Low-Level Image Processing with the Structure Multivector*. PhD thesis, Inst. f. Informatik u. Prakt. Math. der Christian-Albrechts-Universität zu Kiel, 2002.

[15] M. Felsberg and G. Sommer. The monogenic signal. *Signal Processing, IEEE Transactions on*, 49(12):3136–3144, 2001.

[16] M. Felsberg and G. Sommer. The monogenic scale-space: A unifying approach to phase-based image processing in scale-space, 2003.

[17] D. Gabor. Theory of communication. *Journal of the IEE (London)*, 93:429–457, 1946.

[18] K. Gürlebeck, K. Habetha, and W. Sprössig. *Funktionentheorie in der Ebene und im Raum (Grundstudium Mathematik)*. Birkhäuser Basel, 2006.

[19] R. Hielscher, D. Potts, J. Prestin, H. Schaeben, and M. Schmalz. The Radon transform on SO(3): A Fourier slice theorem and numerical inversion. *Inverse Problems*, 24(2):025011+, 2008.

[20] J. Horvath. Singular integral operators and spherical harmonics. *Transactions of the American Mathematical Society*, 82(1):52–63, 1956.

[21] T. Iwaniec and G. Martin. *Geometric Function Theory and Non-linear Analysis*. Oxford University Press, USA, 1st edition, 2002.

[22] B. Jähne. *Digital Image Processing*. Springer, 6th revised and extended ed. edition, 1997.

[23] A. Jeffrey and D. Zwillinger. *Table of Integrals, Series, and Products, Seventh Edition*. Academic Press, 7 edition, 2007.

[24] J. J. Koenderink. What does the occluding contour tell us about solid shape? *Perception*, 13(3):321–330, 1984.

[25] U. Köthe and M. Felsberg. Riesz-transforms versus derivatives: On the relationship between the boundary tensor and the energy tensor. pages 179–191. 2005.

[26] T. Needham. *Visual Complex Analysis*. Oxford University Press, Oxford, 1997.

[27] M. Riesz. L'intégrale de Riemann-Liouville et le problème de Cauchy. *Acta Mathematica*, 81(1):1–222, 1949.

[28] M. B. Romeny. *Geometry-Driven Diffusion in Computer Vision*. Kluwer Academic Publishers, Norwell, MA, USA, 1994.

[29] E. M. Stein. *Singular Integrals and Differentiability Properties of Functions. (PMS-30)*. Princeton University Press, 1971.

[30] L. Wietzke, O. Fleischmann, and G. Sommer. 2d image analysis by generalized hilbert transforms in conformal space. In *ECCV*, 2008.

[31] L. Wietzke, G. Sommer, C. Schmaltz, and J. Weickert. Differential geometry of monogenic signal representations. In *RobVis08*, pages 454–465, 2008.

[32] D. Zang, L. Wietzke, C. Schmaltz, and G. Sommer. Dense optical flow estimation from the monogenic curvature tensor. In Fiorella Sgallari, Almerico Murli, and Nikos Paragios, editors, *Scale Space and Variational Methods in Computer Vision*, volume 4485, pages 239–250. SSVM 2007, Springer-Verlag, 2007.

[33] D. Ziou and S. Tabbone. Edge detection techniques - an overview. Technical report, International Journal of Pattern Recognition and Image Analysis, 1997.